153

UNIVERSITY OF SOUTHAMPTON

PLANAR WAVEGUIDE DEVICES FABRICATED BY PULSED LASER DEPOSITION

Stephen John Barrington

Submitted for the degree of Doctor of Philosophy

Faculty of Science

Department of Physics

August 2001

UNIVERSITY OF SOUTHAMPTON

ABSTRACT

Faculty of Science
Department of Physics

Doctor of Philosophy

PLANAR WAVEGUIDE DEVICES FABRICATED BY PULSED LASER DEPOSITION

By Stephen John Barrington

This thesis is intended to be a comprehensive study on the use of pulsed laser deposition to fabricate planar waveguide devices. As such, a thorough review into the state of the art of current activities in this area is initially presented.

A versatile technique has been developed to efficiently and homogeneously heat substrates using a raster scanned CO_2 laser. Use of this device has virtually eliminated the occurrence of substrate fracture and has greatly reduced the turn-around time for depositions of crystalline films. The heating homogeneity achievable with this system is ultimately limited to the speed at which it is able to scan the substrate.

Growth of photosensitive lead germanate glass layers by pulsed laser deposition is reported. The photosensitivity has been investigated with a wide variety of UV sources and is found to be capable of exhibiting both positive and negative refractive index changes. The maximum index difference observed in this system was also the highest reported for a germanium based glass at -1.06×10^{-2}.

The effect of particulates on the lasing threshold of waveguide lasers has been investigated. This was achieved by growing Nd:GGG waveguide lasers with a range of particulate densities modulated by a pulsed gas valve. It is found that particulates generate a detrimental effect and that the threshold is seen to increase as the particulate density increases. This detrimental effect becomes less pronounced in thicker ($\sim$8μm) films.

A buried Nd:GGG waveguide laser has been fabricated for the first time by PLD and has achieved lasing action at a threshold of 14.8 mW of absorbed power. Comparison of the lasing threshold to that of similar uncapped devices demonstrate that the capped layer has a highly beneficial effect on the lasing threshold when the particulate density in the film is high.

Can you help me, occupy my brain?

Ozzy Osbourne, from the song *Paranoid.*

Acknowledgements

There are not enough pints of beer in the world with which I could thank my supervisor Rob Eason for his continued support, motivation, free rounds and good humoured nature despite what I've thrown at him over the past few years.....Cheers Prof.

I've also enjoyed the collaborations with the BAS in Bulgaria and FORTH in Greece so thanks there to Peter Atanassov and Nikos Vainos. Top marks to Christos Grivas for film growth in FORTH. Thanks also due to the EU copernicus for the 'Impulsenet' contract that supports this kind of collaboration.

Thanks to the ORC and EPSRC for financial support and making the whole PhD thing possible.

Big up large to the bOyz (and regular guests) of office 2071 'babylon'..... you'd better keep that place a fleapit you hear? And a special mention to Joycie for keeping me sane in the first year. Cheers also to 'fatboy' Stu for the kung fu, and Taj for the artwork.

Much love to Catherine for being probably the best girlfriend in the world ..... I must have done something right in a previous life.

A big shout out to the London posse: Alison, Piers, Jo, Dr.Eggs, Jane, Quilt, Mr. A. Freak, The Boy Riley, Sooze, Shani, Thom, and Broose is also necessary. Special mention for Steve and Joss for the many many things they've done for me over the past few years.

Last but not least a big thanks to my folks for being generally great and my big old smelly hound Sam.

Contents

Chapter 1

Introduction

1.1 Overview

This thesis will discuss the growth of optical waveguide devices by pulsed laser deposition (PLD). Chapters 1 to 4 review the background of PLD including history, apparatus, theory, and the various analytical techniques used. There is currently no comprehensive review of PLD of thin films for use as active optical waveguides, therefore chapter 3 looks in depth at the current work in this field. This also establishes the context for work presented in this thesis. Chapter 5 discusses the growth and analysis of photosensitive lead germanate films. Chapter 6 presents a new and efficient homogeneous substrate heating system and other minor mechanical improvements to the PLD apparatus. Chapter 7 describes the theory underlining active optical waveguides that is relevant to the the proceeding chapters. Nd:GGG waveguide lasers were grown to study the effect of particulates on lasing performance and this work is presented in chapter 8. Chapter 9 presents work on fabrication and results of a buried Nd:GGG waveguide laser, which is the first reported capped laser grown by PLD.

1.2 Optical Waveguides

The sudden explosive development of the internet has sparked worldwide interest in optical technology and in particular optical waveguides. Optical fibres are a proven waveguide technology which are now used routinely in high bandwidth and long distance data transmission. Optical waveguides, however, have far more to offer than just high bandwidth transmission of data. Confinement of light inside a waveguide generates a higher intensity-length product that yields several advantages when compared to bulk media counterparts. Lasing power thresholds become lower in waveguides due to the dependence on the pump and lasing mode size (see chapter 7). This enables lasing to be achieved in transitions that possess an impractically high lasing power threshold in bulk materials [1]. The efficiency of many non-linear optical effects are dependent on intensity and so can be greatly increased in waveguides. This leads to efficient harmonic generation, four wave mixing and many other effects, all of which have applications that are potentially desirable in the market place.

The holy grail of thin film waveguide technology exists in the form of optical integrated circuits. The possibility of combining many of the above mentioned effects into a single monolithic waveguide device is the ultimate goal of research in this area. There many established technologies for fabricating optical thin films and section 1.3 briefly details many of these techniques. Section 2.2 of the next chapter explains the basics of PLD; its advantages and disadvantages.

1.3 Summary of thin film fabrication methods

1.3.1 Evaporation

Evaporation or thermal vapour deposition is the simple method of heating materials to melting point in a vacuum chamber. Heating is often achieved with a resistive component for temperatures up to 1200°C . Where much higher temperatures are required electron beam evaporation (EBV) can be employed. Different constituents within multicomponent materials, however, can possess different vapour pressures which can cause differential rates of evaporation. This can lead to production of films of a composition different to that of the target. This process is mainly suitable for simple amorphous materials and is most commonly used in optics for manufacturing antireflection coatings (e.g MgF_2 and MgO). The highly isotropic distribution of the evaporants from the target can lead to poor deposition rates and may require multiple chambers for different targets if contamination is an issue.

1.3.2 Sputtering

Sputtering is used in industry largely as an alternative to EBV. Material ejection in a sputtering system is achieved by high energy ions (up to 2keV) colliding with a negatively biased target in a vacuum chamber. Inert gases flow into the chamber and are ionised and accelerated into the target by a high electric field (~kV) . DC sputtering is generally used to sputter conductive materials, while radio frequency (RF sputtering) is often used for insulators. RF sputtering also reduces deposition of insulator materials on the electrodes and helps to reduce surface charge build-up on the substrate. Epitaxial growth of crystalline materials is possible by using heated substrates. Reactive deposition is achievable by use of reactive gases. The angular distribution of the plume in sputtering is larger

than in PLD allowing the production of evenly distributed large area films. Chamber contamination, however, is more of an issue with highly divergent plumes. Currently the main use of sputtering is to coat optics, but many active films have been produced [2]. Magnetron sputtering is often used for fabrication of optical films as this further excites the deposition species allowing a lower substrate temperature than is usually required for epitaxial growth of dielectrics.

1.3.3 Chemical vapour deposition (CVD)

CVD is a method of thin film fabrication by the decomposition of high vapour pressure gases or *precursors*. Triggering of the reaction is usually achieved by a heated substrate after the gaseous reactants initially adsorb onto its surface. Subsequently, surface chemical reactions occur involving the decomposition of the precursor. These reactions are often catalysed by the substrate surface. The resultant film also includes unwanted by-products of the reaction which must be desorbed from the surface and removed.

Plasma enhanced chemical vapour deposition (PECVD) enables deposition at lower temperatures than conventional CVD. These temperatures are sometimes essential to prevent diffusion of lighter elements and undesirable reactions of the film with the substrate. Energy is transferred into the reactants via a glow discharge, which ionises the mixture to form radicals and other reactive species. The reactants are excited whilst in a gaseous phase, which permits initiation of the reaction at a lower substrate temperature.

Deposition rates are limited in CVD systems to as little as 400 - 500 nm per hour [3]. The range of materials that can be deposited is also limited by the difficulty of establishing suitable precursors. Due to contamination CVD systems often require individual chambers for different fabricated materials.

1.3.4 Sol-gel proccessing

Sol-gel processes are based on the hydrolysis and condensation of molecular precursors. A sol can be defined as a colloidal suspension of solid particles in a liquid. Gellation of this sol creates a continuous suspension (gel). Thin films are usually formed by dipping appropriate substrates into the liquid sol and removing. Subsequent heating and spinning is usually required in order to improve thickness uniformity and the composition of the resultant film. The sol usually requires far lower temperatures for formation of epitaxial films than conventional deposition processes. This versatile technique is often used to solidify laser dyes to allow easier management [4] and can also be used to pull unusual optical fibres [5]. Sol-gel can be used to fabricate a variety of oxides but like CVD, formation of the correct film is dependent on finding appropriate precursors and the films are often polycrystalline. Due to the dipping process required for film formation it is difficult to fabricate films thin enough for single mode propagation of light ($< 10\mu m$). Sol-gel waveguide lasers have been reported [6].

1.3.5 Molecular beam epitaxy (MBE)

MBE is used to produce ultra pure high quality epitaxial growth of single crystal structures. MBE is most commonly used in the semiconductor industry where high crystal quality is required for devices.

The constituent components of the desired film are heated to vapour phase in separate effusion cells. The cells are isothermal cavities with an aperture to allow effusion of the vapour in a forward directional plume or so-called molecular beam. The beam is incident on a heated substrate where epitaxial growth can occur. With partial or complete shuttering of the vapour sources the final composition of the developing film can be precisely controlled. Heterostructures can be engineered on the substrate or alternately

the crystal composition can be gradually altered throughout the film. MBE waveguides are almost exclusively semiconductor devices [7], however rare-earth doped devices have been fabricated [8].

The main disadvantage of MBE is the high cost of the fabrication equipment as an ultra-high vacuum ($\sim 10^{-10}$ mbar) is required to maintain the film purity. For industrial applications, MBE is only practical for mass produced devices such as LEDs, ICs, laser diodes and fast transistors. The molecular beams also possess low thermal energies compared to some deposition processes and so require high substrate temperatures for epitaxial growth.

1.3.6 Liquid-phase epitaxy (LPE)

LPE thin films are fabricated by dipping of an appropriate substrate into a suitable, supersaturated, melt of oxides. For example Nd:YAG can be fabricated by a melt of $PbO/B_2O_3/Al_2O_3/Y_2O_3/Nd_2O_3$ in various concentrations. The substrate is dipped into the melt, its crystal structure precipitates, and is a template for, epitaxial growth. When growth of the desired thickness is achieved, the substrate is removed from the melt. To enhance flatness and to achieve thinner films, spinning of the molten layer is sometimes required after dipping and before solidification. If the melt temperature does not exceed the melting temperature of the resultant solidified film then re-dipping in different solutions can achieve multilayer films. LPE is capable of achieving very low-loss films ($\leq$0.05dBcm^{-1}) [9] and is a very inexpensive fabrication technique. Deducing the initial concentrations of the melt constituents, however, can be a difficult process. The type of films that can be fabricated are also limited by the availability of suitable melt constituents. Currently, it is difficult to fabricate very thin layers for single mode devices with LPE.

1.3.7 Direct and thermal bonding

It has been known since the advent of suitable polishing techniques that highly polished surfaces can bond on contact but it is only recently [10] that this effect has been used for waveguide applications.

With direct bonding, the substrate and active layer begin as separate pieces of bulk material. The active layer and one side of the substrate are polished to optical flatness. Both layers are then subject to rigorous cleaning techniques whereupon joining, the Van der Waals forces are sufficient to permanently bond the two layers (although depending on the material the exact bonding mechanism may be complicated). Heating of the structure is often used to further strengthen the bond, resulting in the process also having the name thermal bonding. Once bonded the active layer can be polished down to waveguide dimensions.

Direct bondng can achieve very low loss waveguides ($\leq 0.4 dBcm^{-1}$) which by definition possess the exact composition of the bulk material. It can also fabricate high numerical aperture guides as there are no lattice matching constraints as required for epitaxial growth. The only constraint is that the two layers possess a similar thermal expansion co-efficient so as to prevent fracture upon cooling.

Recently it has also been found [11] that during the heat treating phase, ion-exchange can take place between two suitable layers, thus creating a buried waveguide structure. Previously this could only be achieved in a two step process.

The process is very time consuming, however, and prone to low yield due to breakages. In structures where the interjoin is not used as a waveguide (i.e unclad waveguides) the active layer is difficult to polish below 50μm thickness.

1.4 Other waveguide fabrication techniques

Rather than creating a waveguide by formation of a thin material layer, the techniques described in this section directly modify the refractive index of bulk material. Such techniques should not necessarily be considered as alternatives to thin film deposition as they can often be used in conjunction with thin films to create channel waveguides in the planar structure.

1.4.1 Indiffusion

Indiffusion of an element into a lattice can create a refractive index change sufficient to provide a waveguide structure. The bulk material is coated with the element to be indiffused in a thermal evaporator. This structure is then held in a oven at high temperatures (~1000°C) for a period of time that can be as long as several days. For active films the lasing dopant would be the ideal choice for indiffusion but it is usually unable to create a large enough refractive index change. For this reason titanium is often indiffused to create the refractive index boundary and further indiffusion of the dopant (Yb, Nd, Er) is then used to create an active layer [12, 13]. Lasing from the Ti atom itself, though, has been reported after indiffusion into sapphire [14, 15]. By using masking techniques in the initial coating phase this technique can also produce channel waveguide devices [16]. Indiffusion cannot produce a sharp index step in waveguides and so the confinement of light is limited. The fabrication process is also very time consuming for a single waveguide although multiple guides can be fabricated simultaneously.

1.4.2 Ion exchange

This simple technique involves immersion of a substrate into a molten salt bath. The bath provides a source of alkali ions which slowly exchange with

ions in the substrate material. The Application of heat or an electric field to the bath can control the rate of ion exchange. Secondary processing in different solutions can achieve buried waveguide devices [17] and channel devices can be fabricated by use of masking techniques [18]. Like indiffusion it is difficult to achieve a sharp index step in these guides therefore limiting the confinement of light.

1.4.3 Ion implantation and etching

Bombardment of a material with high energy (~MeV) ions can create localised damage and thus a refractive index change within the material. The material modification is caused by atomic displacement in the lattice by incoming ions. At high energies the lattice is relatively unaffected, and it is only at lower energies that the majority of damage take place. This allows the ions to pass through the surface layer down to a depth of a few microns before losing enough energy to modify the lattice. This can result in a damage layer with a lower refractive index, enabling the surface layer to act as a waveguide. With different materials however it is possible for high refractive index damage layers to form, creating buried structures. This led to the fabrication of planar laser devices [19] but has also been used in conjunction with masking techniques to produce channel structures [20]. In addition to bulk materials this channel fabrication technique has been shown to work with PLD grown films [21]. Ion beams can also be used, with appropriate masking, to etch away material to create ridge waveguides [22, 23]. As with ion exchange, creating a sharp index step to fabricate a high numerical aperture guide is difficult. Furthermore, the damage to the material that is inherent to the process leads to losses of around 1-2dBcm^{-1} [19, 20]. By using very low loss planar guides, however, and ion beam etching, raised channel (rib) waveguides have been produced with losses down to 0.25dBcm^{-1} [23].

1.4.4 Direct writing

High peak powers obtainable in femtosecond laser pulses can be used to efficiently access a host of multi-photon effects in optical materials. This allows modification of the bulk material, by multi-photon absorption, even if the material is transparent to the writing wavelength (see section 2.3.1). By careful focussing, the beam can propagate into a bulk medium remaining just below the damage threshold until the focal point. At the focal point, damage of the material can induce a refractive index change. Using this technique the refractive index of the bulk material can be altered at a specific point within its structure to create three dimensional waveguides [24].

1.5 Conclusions

This chapter has mentioned some of the desirable qualities of waveguide devices and the potential of planar waveguides to produce monolithic integrated optical circuits which would be of great benefit to the photonics industry. The various methods of planar and channel waveguide fabrication have been presented and some of the advantages and disadvantages of each system along with some recent results in most cases. In chapter 2 PLD will be discussed as an alternative fabrication process for optical planar waveguides.

1.6 References

[1] D.C. Hanna, A.C. Large, D.P. Shepherd, A.C. Tropper, I. Chartier, B. Ferrand, and D. Pelenc. Low-threshold quasi-3-level 946 nm laser operation of an epitaxially grown Nd:$Y_3Al_5O_{12}$ waveguide. *Applied Physics Letters*, 63(1):7–9, 1993.

[2] M. Wada and Y. Miyazaki. Amplification characteristics of waveguide type optical amplifier using Nd doped garnet thin-film. *Ieice Transactions on Electronics*, E77C(7):1138–1145, 1994.

[3] D.B. Studebaker, G.T. Stauf, T.H. Baum, T.J. Marks, H. Zhou, and G.K. Wong. Second harmonic generation from beta barium borate (beta-BaB_2O_4) thin films grown by metalorganic chemical vapor deposition. *Applied Physics Letters*, 70(5):565–567, 1997.

[4] M. Fukuda, K. Takeshita, and K. Mito. Analysis of the laser action of a solid-state dye laser with a thin film ring resonator. *Japanese Journal of Applied Physics Part 1-Regular Papers Short Notes & Review Papers*, 38(11):6347–6350, 1999.

[5] R. Gvishi, G. Ruland, and P. N. Prasad. New laser medium: Dye-doped sol-gel fiber. *Optics Communications*, 126(1-3):66–72, 1996.

[6] I. Finkelstein, S. Ruschin, Y. Sorek, and R. Reisfeld. Waveguided visible lasing effects in a dye-doped sol-gel glass film. *Optical Materials*, 7(1-2):9–13, 1997.

[7] W. T. Tsang. Extremely low threshold (AlGa)As graded-index waveguide separate confinement heterostructure lasers grown by molecular- beam epitaxy. *Applied Physics Letters*, 40(3):217–219, 1982.

[8] R. A. McFarlane, M. Lui, and D. Yap. Rare-earth-doped fluoride wave-guides fabricated using molecular-beam epitaxy. *IEEE Journal of Selected Topics in Quantum Electronics*, 1(1):82–91, 1995.

[9] I. Chartier, B. Ferrand, D. Pelenc, S.J. Field, D.C. Hanna, A.C. Large, D.P. Shepherd, and A.C. Tropper. Growth and low-threshold laser oscillation of an epitaxially grown Nd :YAG waveguide. *Optics Letters*, 17(11):810–812, 1992.

[10] C.T.A. Brown, C.L. Bonner, T.J. Warburton, D.P. Shepherd, A.C. Tropper, D.C. Hanna, and H.E. Meissner. Thermally bonded planar waveguide lasers. *Applied Physics Letters*, 71(9):1139–1141, 1997.

[11] C. B. E. Gawith, T. Bhutta, D. P. Shepherd, P. Hua, J. Wang, G. W. Ross, and P. G. R. Smith. Buried laser waveguides in neodymium-doped BK-7 by K^+-Na^+ ion- exchange across a direct-bonded interface. *Applied Physics Letters*, 75(24):3757–3759, 1999.

[12] R. Brinkmann, W. Sohler, H. Suche, and C. Wersig. Fluorescence and laser operation in single-mode Ti-Diffused Nd-Mgo-$LiNbO_3$ waveguide structures. *IEEE Journal of Quantum Electronics*, 28(2):466–470, 1992.

[13] C. H. Huang and L. McCaughan. Er-indiffused Ti:$LiNbO_3$ channel waveguide optical amplifiers pumped at 980 nm. *Electronics Letters*, 32(3):215–216, 1996.

[14] L. M. B. Hickey and J. S. Wilkinson. Titanium diffused waveguides in sapphire. *Electronics Letters*, 32(24):2238–2239, 1996.

[15] L. M. B. Hickey. *Ti:sapphire waveguide laser by thermal diffusion of titanium into sapphire*. PhD thesis, University of Southampton, 1998.

[16] J. K. Jones, J. P. Desandro, M. Hempstead, D. P. Shepherd, A. C. Large, A. C. Tropper, and J. S. Wilkinson. Channel wave-guide laser at 1μm in Yb-indiffused $LiNbO_3$. *Optics Letters*, 20(13):1477–1479, 1995.

[17] R. V. Ramaswamy and S. I. Najafi. Planar, buried, ion-exchanged glass wave-guides - diffusion characteristics. *IEEE Journal of Quantum Electronics*, 22(6):883–891, 1986.

[18] S. J. Hettrick, J. I. Mackenzie, R. D. Harris, J. S. Wilkinson, D. P. Shepherd, and A. C. Tropper. Ion-exchanged tapered-waveguide laser in neodymium-doped BK7 glass. *Optics Letters*, 25(19):1433–1435, 2000.

[19] S.J. Field, D.C. Hanna, A.C. Large, D.P. Shepherd, A.C. Tropper, P.J. Chandler, P.D. Townsend, and L. Zhang. An efficient, diode-pumped, ion-implanted Nd-GGG planar waveguide laser. *Optics Communications*, 86(2):161–166, 1991.

[20] S.J. Field, D.C. Hanna, A.C. Large, D.P. Shepherd, A.C. Tropper, P.J. Chandler, P.D. Townsend, and L. Zhang. Low threshold ion-implanted Nd-YAG channel waveguide laser. *Electronics Letters*, 27(25):2375–2376, 1991.

[21] L. Beckers, C. Buchal, D. Fluck, T. Pliska, and P. Gunter. Potassium niobate waveguides: He^+ implantation in bulk single crystals and pulsed laser deposition of thin films. *Materials Science and Engineering A-Structural Materials Properties Microstructure and Processing*, 253(1-2):292–295, 1998.

[22] Y. Katoh, N. Sugimoto, and A. Shibukawa. Formation of ridges on $Gd_3Ga_5O_{12}$ by ion-beam etching and subsequent phosphoric-acid treatment utilizing tri-layered etching mask. *Japanese Journal of Applied Physics Part 1-Regular Papers Short Notes & Review Papers*, 31(12A):3888–3894, 1992.

[23] R. Gerhardt, J. Kleine-Borger, L. Beilschmidt, M. Frommeyer, H. Dotsch, and B. Gather. Efficient channel-waveguide laser in Nd:GGG at 1.062μm wavelength. *Applied Physics Letters*, 75(9):1210–1212, 1999.

[24] A. M. Streltsov and N. F. Borrelli. Fabrication and analysis of a directional coupler written in glass by nanojoule femtosecond laser pulses. *Optics Letters*, 26(1):42–43, 2001.

Chapter 2

Pulsed laser deposition: Practice and Theory

2.1 Introduction

PLD is a very versatile technique for thin film fabrication and this chapter outlines the basic apparatus and principles involved in the process. A brief description of PLD is presented and some of the main advantages and disadvantages of the system are listed. A more detailed description of the three most important interactions, namely; laser-target interactions, plasma dynamics and film nucleation and growth are presented in the following sections.

2.2 Fabrication by PLD

The basic experimental apparatus for PLD is shown in figure 2.1. A suitable target is situated inside the vacuum chamber and it usually rotated during the deposition process. The ablation laser beam is focussed down onto the target where it is absorbed, causing rapid evaporation and ejection of a small volume of target. The constituents of the evaporated ma-

terial consist of neutral and ionic atoms, molecules and macroscopic particles or *particulates*[1]. This mixture of ionic and neutral species, termed the plasma plume, adiabatically expands in a narrow angular distribution towards a substrate. A photograph of the plasma plume can be seen in fig 2.2. The process of simultaneous evaporation of all the constituents of the target material is known as congruent evaporation, which is discussed further in section 2.3.1.

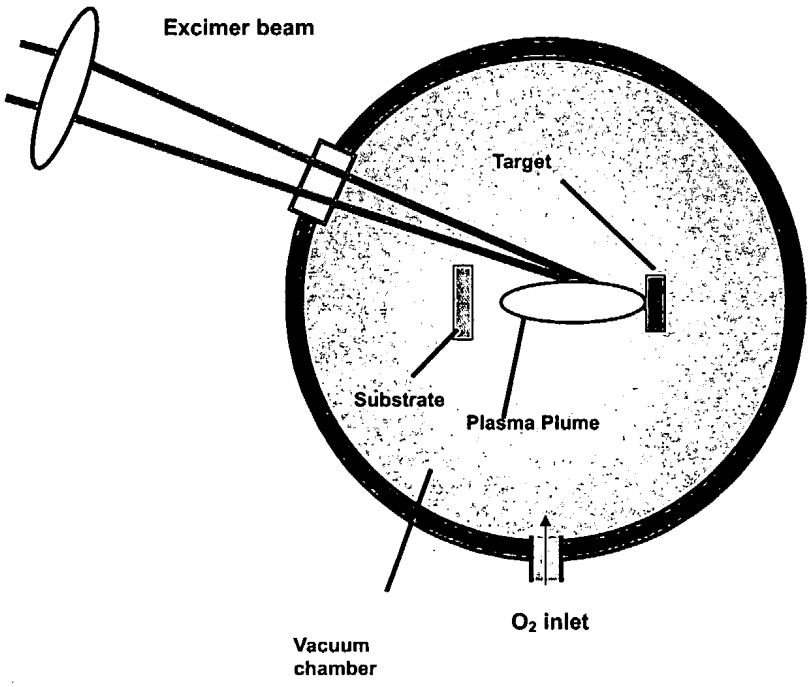

Figure 2.1: Simple PLD Set-up

The ejected matter that arrives on the substrate forms the film for which

[1]In this thesis *Particulates* refer to macroscopic particles of target material that are deposited on the substrate during the deposition process. Some reports will distinguish between particulates (irregular shaped particles resulting from removal of cone-like features present on the target surface or *exfoliation*) and droplets (molten globules resulting from sub surface boiling of the target followed by explosive ejection or *splashing*). In this report however, no such distinction will be made as the mechanism by which the particulates (or droplets) are produced is by no means clear. Mostly the term *particulates* will be used but this is to be taken as the equivalent of droplets or particles.

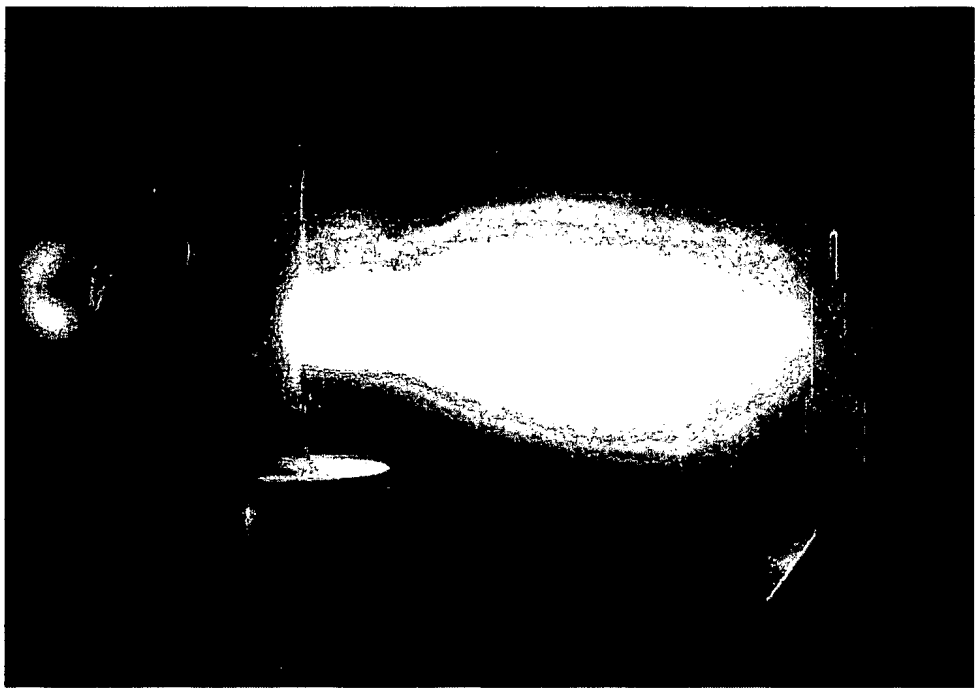

Figure 2.2: Expulsion of the energetic plume onto a heated substrate

the growth mechanisms are discussed in section 2.3.3.

For crystalline growth the substrate will need to be heated to provide additional energy to the arriving species. This allows orientation and migration of the species to the correct crystallographic plane as dictated by either the crystal substrate or by preferential orientation of the developing crystal (See section 2.3.3.1). If crystallinity is not required, (i.e for glasses or other amorphous materials) the substrate may be left at room temperature.

Congruent evaporation is often achieved from the target surface; however lighter elements can be lost in transit between the target and substrate due to scattering processes. For many oxide films this would mean a reduction in their oxygen content if grown in vacuum. For this reason the chamber is usually backed-filled with oxygen typically up to pressures of $\sim 10^{-2}$ mbar. Back-filling also serves to expand the angular distribution of the plume (see section 2.3.2) leading to a more homogeneous distribution of film thickness across the substrate. Reactive background gases can have

a dramatic effect on both the chemical and physical properties of the resultant film, therefore the pressure of the gas during growth is a critical parameter in optimising growth conditions.

With high power pulsed lasers becoming ever more reliable, compact and cheaper there are few other deposition systems that can compete in terms of the initial financial outlay required to install a PLD system. The external nature of the laser as the energy source for ablation allows multiple chambers to be used from one laser. This enables pooling of resources from research groups in very different fields e.g. superconductivity [1], diamond like coatings [2], tribology [3], optical waveguides [4], polymers [5] and many more. Since actual deposition times can be short, time sharing is easily achievable. The versatility of the excimer laser has also been demonstrated by its use in irradiation of as-grown films *in situ* to allow polycrystallisation of amorphous films or even single crystal production from polycrystalline films. The high substrate temperatures often required for epitaxial growth can occasionally lead to undesirable reactions with the film. Providing additional adatom surface mobility by UV irradiation instead is a method of avoiding these reactions. Excimer radiation at low fluences (below that required for ablation) has also been used a method of cleaning the substrate prior to film deposition [6].

Some of the main advantages of PLD are generally thought to include:

- Congruent evaporation of the target material allows complex stoichiometries to be successfully transferred to the substrate [7].
- The high energies of the ablated species often allow much lower substrate temperatures than for other deposition processes.
- Almost any material can be grown, including some that cannot be fabricated by other thin film techniques [8,9], extending the usefulness of PLD to many areas of science and engineering.
- Multiple target switching coupled with the pulsed laser source al-

lows very fine control of heterostructure growth or dopant concentration [10,11].

- External nature of the laser ablation source allows high flexibility of experimental configurations.
- Extreme non-equilibria in PLD can result in meta-stable formation of new compounds and phases of materials with unusual characteristics [12].

The main disadvantages of PLD include:

- High particulate densities present on the deposited films.
- Inhomogeneous thickness profile of the deposited films.
- Difficulty in achieving atomic flatness and 'perfect' crystal structures due to the occasional impact by high energy (< 100eV) plasma constituents with the film. However, this is more relevant to semiconductor and superconductor growth as such perfection is not usually required for optical devices.

2.3 Theory of PLD

Laser ablation and deposition of materials is a process that takes place far from equilibrium and involves a large number of highly complex mechanisms. As such it is extremely difficult to formulate a theoretical model [13] and to date there is no model that can successfully account for the experimental results seen in PLD. This is unfortunate as there are a high number of variables (not all of which are independent) to characterise during PLD growth which makes for laborious work when trying to optimise growth conditions by empirical methods. This section looks at three important steps in PLD; The laser-target interaction, the dynamics of the resultant plasma plume and the growth mechanisms at the substrate surface.

2.3.1 Laser-target interactions

High power, short pulse, laser-target interactions are notoriously difficult to model analytically due to there being at least 3 mechanisms operating in the process of absorption of radiation into the material. These mechanisms are commonly thought to be:

- Phonon and electron excitation within the lattice.
- Free carrier excitation.
- Excitation of the resulting plasma and subsequent transfer of energy to the material.

Although clearly some mechanisms dominate over others, depending on the target material and the wavelength of the ablation laser and its fluence.

Much of the theoretical work in this area has led to models that are unsatisfactory as they depend on constants or variables that are not well known. To illustrate this with a well cited example, Singh *et al* [14] have developed a simplified, one dimensional model to determine the temperature at a point within the irradiated target from the following heat flow equation:

$$\rho_i(T)C_{Pi}(T)\frac{\partial T_i(x,t)}{\partial t} = \frac{\partial}{\partial x}\left(K_i(T)\frac{\partial T_i(x,t)}{\partial x}\right) + I_0(t)\{1-R(T)\}e^{-\alpha(T)x} \tag{2.1}$$

Here T is temperature, t is time, $I_0(t)$ is intensity, $\rho(T)$ is the density, $C_p(T)$ is the thermal heat capacity per unit mass, K is the thermal conductivity and $R(T)$ and $\alpha(T)$ are the respective reflection and absorption coefficients of the material at the incident radiation wavelength. The position at which the temperature is to be determined is given by x which is measured along a vector normal to the target surface. The subscript i takes on the value 1 or 2 and represents the solid or liquid phase respectively.

Simplification of equation 2.1 by assuming constant intensity (I_0) over nanosecond timescales and calculating the temperature at the material surface yields:

$$\rho(T)C_P(T)(T - T_0) = I_0(1 - R)\alpha(T)\tau \tag{2.2}$$

Where T_0 is the initial temperature and τ is the laser pulse duration.

Even this very simplified equation still retains the values $\rho(T)$, $C_p(T)$, and $\alpha(T)$ which are functions of temperature and as such are not easily determined.

It is more useful at this stage, therefore, to give a more qualitative description of this interaction.

The predominant mechanism for radiation absorption in dielectrics at typical PLD irradiances (i.e <100MWcm^{-2}) is phonon and electron excitation in the lattice [15] (though direct phonon excitation is only significant in long wavelength (CO_2) lasers. Low optical absorption is usually desirable in materials deposited for optical applications as this typically leads to low losses. However, high absorption is desired in the target at the ablation wavelength for reasons outlined below. The majority of optical devices fabricated by PLD, therefore, utilise excimer lasers at either 248nm or 193nm to increase the absorption of radiation by the target. The short pulse radiation of excimer lasers also enables rapid heating of the target thus facilitating congruent evaporation.

The volume heated by the laser pulse is dictated by the larger value of either the thermal diffusion length L or the absorption depth $1/\alpha$. The diffusion length L, is given by [16].

$$L = 2\sqrt{(D \cdot \tau)} \tag{2.3}$$

Where D is the thermal diffusivity of the material and τ is the pulse duration .

For ablation of materials where the absorption depth is much smaller than the diffusion length, heat is very rapidly transported away from the ablation area thus preventing congruent evaporation. For this reason short pulse lasers are desirable to decrease the thermal diffusion length.

Generally, for the ablation of dielectrics, where both the absorption and the thermal conductivity are low, the absorption length is usually greater than the diffusion length. In this case the depth removed d (cm) by ablation at fluence F (Jcm^{-2}) is found to follow [17]:

$$d = \frac{1}{\alpha} \ln \left| \frac{F}{F_T} \right| \tag{2.4}$$

Where F_T and α are respectively, the ablation threshold (Jcm^{-2})and the absorption co-efficient (cm^{-1}) for the incident wavelength.

Large absorption depths, however, result in superheating of a large volume of material which upon transformation into a melt phase causes rapid expansion and subsequent explosive ejection from the target. This can result in molten droplets being ejected from the target followed by droplet formation or *particulates* on the substrate. This is often the case in ablation of optical materials by nanosecond 1.06µm YAG lasers (for irradiances typically < 100MWcm^{-2}) where the absorption depths can be 100s of microns. The production of particulates is discussed further in chapter 8.

It is possible, however, to achieve high absorption in materials that are (under low fluences) completely transparent to the incident ablation radiation. This is fortunate for PLD of optical materials as fabrication of materials with a broad range of transparency is often required. The process which allows absorption, termed optical breakdown, occurs as a result of high irradiance (>GWcm^{-2}) of the target [18]. Free electrons present on the surface during ablation undergo rapid acceleration due to the high

electric field of the incident radiation. These high energy electrons ionise atoms within the lattice thus creating further free electrons which also undergo rapid acceleration. A cascade effect is thus initiated giving rise to metal-like qualities, including high absorption, at the target surface. Impurities and defects in the crystal can result in free electron production by multiphoton absorption and subsequent ionisation. Therefore free carrier absorption can occur even in dielectrics where there are no free carriers present initially. There is a threshold to this process though, which depends heavily on defect densities, initial free-electron concentrations, ionisation energy and the radiation wavelength. Typically, this absorption occurs predominantly with picosecond or femtosecond ablation sources.

2.3.2 The plasma plume

Radiation absorption by the target results in rapid, localised, heating and then melting and evaporation which produces a hot vapour above the target area. Optical breakdown also occurs in the hot vapour emitted from the surface, creating a plasma that strongly absorbs the incident radiation through an inverse Bremsstrahlung process. The Bremsstrahlung absorption co-efficient α in cm^{-1} of the laser radiation within the plasma plume at a frequency ν is given by [19]:

$$\alpha = (3.69 \times 10^8)\frac{Z^3 n_i^2}{T^{1/2}\nu^3}(1 - e^{-h\nu/kT}) \tag{2.5}$$

Where Z is the average charge, T is temperature (K), n_i is the ion density (cm^{-3}) and k is the Boltzmann constant (SI units).

At typical ion densities of 10^{-19} cm^{-3} and temperatures of 5000K this would imply an absorption length of 33mm for 248nm radiation. This long absorption length is in contradiction to the high opacities observed experimentally in the initial ablation plasma. The plasma will also expand in the order of 100µm during the ablation pulse, thus further increasing the

predicted absorption length. This is another example that illustrates how the complex behaviour of the laser-target interaction in PLD can not easily be modelled. The time and temperature dependence of each variable must be considered when such an equation is utilised.

In practice, the high opacity of the plasma enables further absorption and acceleration of the constituent species up to the high energies that have been observed, corresponding to temperatures up to ~15,000K.

Due to the high energies within the plasma, Bremsstrahlung radiation can occur at shorter wavelengths than that of the ablation laser. This acts as another method of energy transfer to the material surface.

The Saha equation gives the ratio of single charged ions n_i to neutrals n_n within a plasma and shows that the majority of the plume consists of charged ions at this stage.

$$\frac{n_i}{n_n} = 2.4 \times 10^{15} \frac{T^{3/2}}{n_i} e^{-U_i/kT} \tag{2.6}$$

Where units and variables are as given in equation 2.6 and U_i is the first ionisation potential in Joules. Using typical parameters this predicts over 80% ionisation at 10,000K.

This high thermal energy is transferred to kinetic energy during the initial adiabatic expansion of the plume which gives rise to high velocities v of the plasma constituents as given by:

$$v = \left(\frac{2}{\gamma - 1}\right)\left(\frac{\gamma kT}{m}\right)^{1/2} \tag{2.7}$$

Where γ is the ratio of specific heats (C_p/C_v) for the plume m is the atomic mass and all units are SI. This predicts maximum velocities of $\sim 1 \times 10^6$ cm s^{-1} for temperatures around 10,000K and has been verified experimentally by Murakami and Geohegan [19,20].

The narrow angular distribution of the ejected plume towards the sub-

strate is a principal feature of PLD (and not always a desired one). Although it can lead to fast deposition rates and prevents extensive chamber contamination it can also result in inhomogeneous stoichiometries over large deposition areas.

The characteristics of the expanding plume are highly dependent on the presence of a background gas. Expansion through reactive oxygen (as is the case with all depositions presented in this thesis) can cause molecular formation of oxides within the plasma and will also alter the kinetic energy of the species incident on the substrate. These effects can cause a remarkable change in the characteristics of the film.

Figure 2.3 shows long exposure photographs of a single plume expansion at three different background pressures of oxygen.

It can be seen that at 1mbar the mean free path within the plasma is drastically reduced which leads to strong confinement of the plasma. Deposition at such high pressures generally leads to vastly reduced deposition rates and films with low adhesion to the substrate. At $\sim 5 \times 10^{-2}$ mbar (typical deposition background pressure) the plume is highly luminescent due to collisions within the plasma and with the background gas. At this pressure the narrow angular distribution is very evident. Pressures down to $\sim 1 \times 10^{-4}$ mbar often result in the plume having a much lower luminescence as there are less collisional processes occuring. Additionally, the elevated expansion speed acts to spread out the plume which makes it much more difficult to see with the naked eye (or a 35mm camera). Deposition of oxides at this pressure often result in oxygen deficient films.

The plume shape has been compared to an adiabatic expansion of a supersonic gaseous jet [21]. The expansion front of the plume is initially a supersonic shockwave that travels towards the substrate but is rapidly slowed by the background gas. This rapid deceleration can generate reflections of the wavefront which can undergo collisions with secondary shockwaves before dissipation. This can account for the high number of

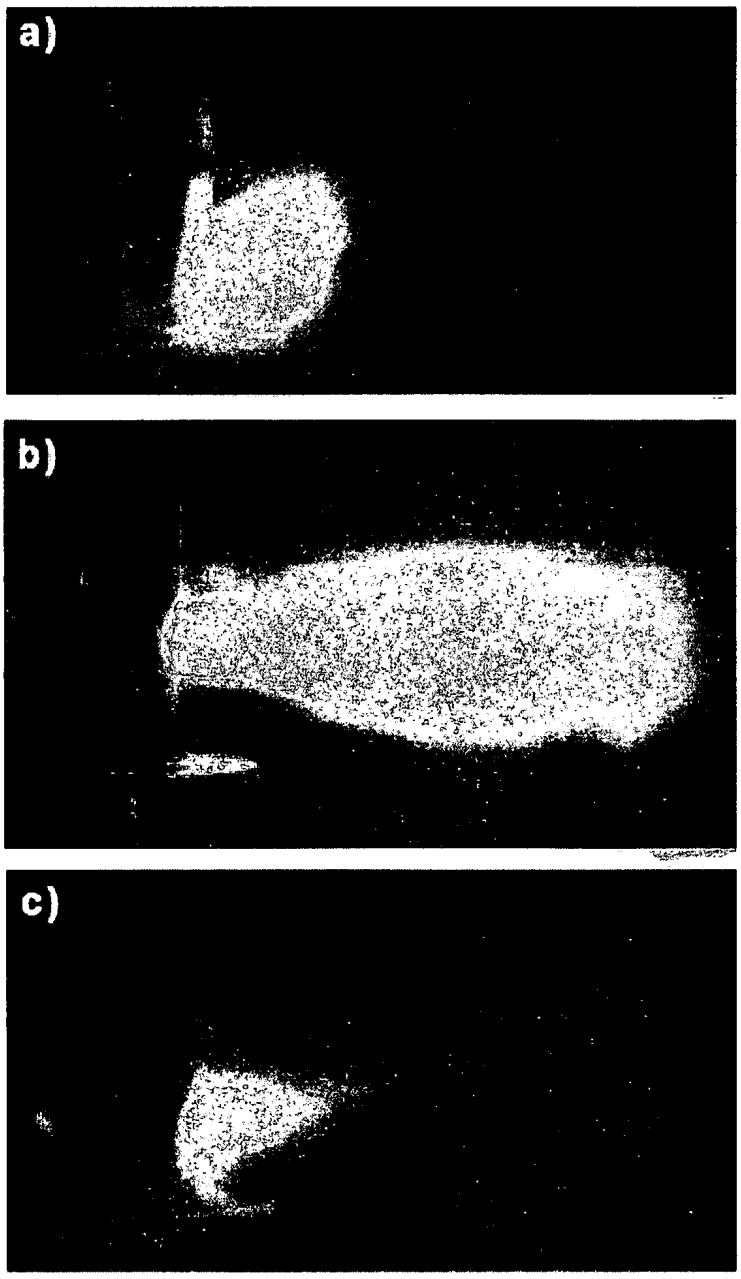

Figure 2.3: Plasma plume viewed at a) 1mbar b) 5×10^{-2} mbar and c) 1×10^{-4} mbar through a long exposure (~4 secs) shot of a single plume expansion

collisional processes seen within the plume (i.e. strong luminescence) [21]. The shockwaves are not always present when the background gas is at a lower pressure [22], hence the lack of luminescence in figure 2.3c.

The angular distribution of the ablated species in the plume has been successfully fitted to a $\cos\theta^n$ or a $\cos\theta + \cos\theta^n$ curve where n can range from 2 to 200 [23,24]. The forward directional nature of the plume is believed to arise due to inter-plasma collisions of the species.

Given the shape of the expansion front $X(t)$,$Y(t)$,$Z(t)$ at a time t the number density $n(z,t)$ of the species within the plume can be estimated at a point z measured back from the expansion front [25]:

$$n(z,t) = \frac{N_t}{\pi^{3/2}\sqrt{2}X(t)Y(t)Z(t)} \exp^{\frac{-z^2}{2Z(t)^2}} \tag{2.8}$$

Where N_t is the total number density of all species.

The maximum propagation length of the plume from the target R_m in a background gas of mass density ρ_b and at pressure p_b is given by [26].

$$R_m \sim \left(\frac{ME}{\pi\rho_b p_b}\right)^{1/6} \tag{2.9}$$

Where M is the ejected mass and E is the laser energy absorbed.

2.3.3 Growth mechanisms

The atomic and molecular species within the plasma plume can initially possess energies of over 100eV. Collisions within the plasma and with the background gas will typically reduce these energies to thermal levels upon impact with the substrate (usually a few cm from the target). Therefore, the adatoms on the surface of the substrate do not always possess sufficient mobility to migrate to the correct lattice site. In this case substrate heating is required to increase adatom mobility. In general, higher tem-

peratures lead to better crystal structures until a point is reached where re-evaporation of the more volatile elements in the film will lead to non-stoichiometric growth. In some cases these two regimes of amorphous growth and atom re-evaporation will overlap making it difficult to grow crystalline structures of a desired phase (see section 3.3.2.1 for growth of lithium niobate).

The mechanisms underlying nucleation and growth of films have been well documented and reviewed by Horwitz and Sprague [27]. The dominant factor governing the method of growth is the strength of the adatom bond to the substrate compared to the bond strength between its surrounding neighbours . Higher bond strength between the deposited atoms and molecules result in clustering of the arriving species leading to *island growth* or *Volmer-Weber growth*. Alternatively if there is a higher bond strength between the substrate and the film constituents then a 2-D *layer-by-layer growth* results also known as *Frank-Ven der Merwe growth*. A hybrid of the two mechanism is known as *Stranski-Krastinov* growth, whereby layer-by-layer growth is initiated on the substrate but after growth of a few monolayers, island growth predominates. This is thought to be due to a build up of strain due to a lattice mismatch between the film and substrate. These growth systems are depicted in figure 2.4.

2.3.3.1 Lattice matching

The quality of crystals grown by epitaxy is greatly affected by the choice of substrate and in general single crystal growth is usually only possible on substrates with a similar lattice spacing (see table 3.1 for a list of lattice constants). The lattice mismatch f between film and substrate is defined as:

$$f = \left(\frac{a_0(s) - a_0(f)}{a_0(f)} \right) \tag{2.10}$$

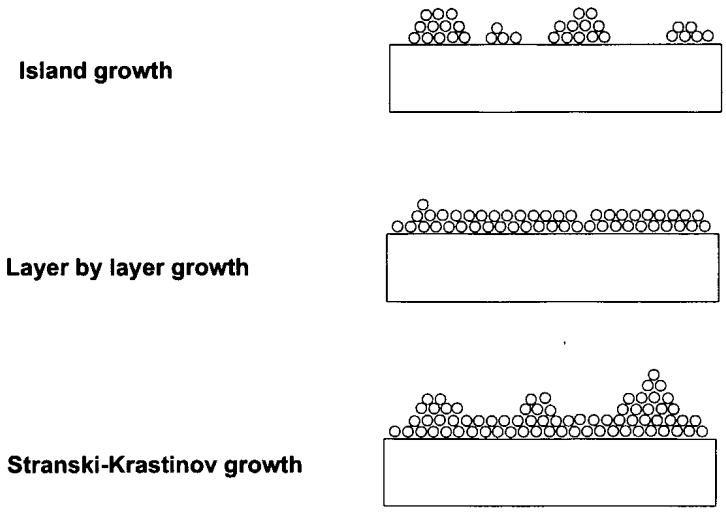

Figure 2.4: Three popular mechanisms of film growth

Where a_0 is the lattice spacing and subscripts f and s refer to the film and substrate respectively.

Lattice mismatches of up to ~7% can be accommodated by strain within the lattice for thin films of a few (1-5) monolayers. Thicker films will incur an increase in point defects and dislocations to relax the strain. Higher lattice mismatches will usually result in polycrystalline growth of the film or growth of small 'micro-crystallites' [28]. In some systems the growth of a certain crystalline phase is so energetically favourable that if given enough adatom mobility, polycrystalline growth [9] or even single crystal growth [29] can be possible on completely amorphous substrates.

2.4 Conclusions

The basic principles involved in PLD have been outlined with the main advantages and disadvantages presented. It should be noted at this point that the largest single disadvantage of PLD to date is the presence of particulates in the film. It is believed by some that until particulate free

growth can be routinely achieved without the need for complex mechanical shuttering or other impractical mechanisms then PLD will not be a viable deposition process for many application. Chapter 8 of this report looks more closely at the problem of particulates and assesses their actual impact on the device performance of waveguide lasers.

The basic phenomena involved in PLD interactions have also been discussed, which give a general idea of the highly complex PLD process. Formulation of a complete analytical model of the PLD process is an extremely difficult task and many phenomena observed in PLD have still to be fully explained.

2.5 References

[1] P. H. Hor, L. Gao, R. L. Meng, Z. J. Huang, Y. Q. Wang, K. Forster, J. Vassilious, C. W. Chu, M. K. Wu, J. R. Ashburn, and C. J. Torng. High-pressure study of the new Y-Ba-Cu-O superconducting compound system. *Physical Review Letters*, 58(9):911–912, 1987.

[2] A. A. Voevodin and M. S. Donley. Preparation of amorphous diamond-like carbon by pulsed laser deposition: A critical review. *Surface & Coatings Technology*, 82(3):199–213, 1996.

[3] G. Radhakrishnan and P. M. Adams. Pulsed-laser deposition of particulate-free TiC coatings for tribological applications. *Applied Physics A-Materials Science & Processing*, 69:S33–S38, 1999.

[4] K.E. Youden, R.W. Eason, M.C. Gower, and N.A. Vainos. Epitaxial-growth of $Bi_{12}GeO$ thin-film optical wave-guides using excimer laser ablation. *Applied Physics Letters*, 59(16):1929–1931, 1991.

[5] S. G. Hansen and T. E. Robitaille. Formation of polymer-films by pulsed laser evaporation. *Applied Physics Letters*, 52(1):81–83, 1988.

[6] Y. Y. Tsui and D. G. Redman. A laser ablation technique for improving the adhesion of laser- deposited diamond-like carbon coatings to metal substrates. *Surface & Coatings Technology*, 126(2-3):96–101, 2000.

[7] P. R. Willmott, P. Manoravi, and K. Holliday. Production and characterization of Nd,Cr : GSGG thin films on Si(001) grown by pulsed laser ablation. *Applied Physics A-Materials Science & Processing*, 70(4):425–429, 2000.

[8] A.A. Anderson, R.W. Eason, M. Jelinek, C. Grivas, D. Lane, K. Rogers, L.M.B. Hickey, and C. Fotakis. Growth of Ti:sapphire single crystal thin films by pulsed laser deposition. *Thin Solid Films*, 300(1-2):68–71, 1997.

[9] R. Chety, E. Millon, A. Boudrioua, J. C. Loulergue, A. Dahoun, and J. Perriere. Growth of $Ca_4GdO(BO_3)_3$ thin films by pulsed-laser deposition for nonlinear optical applications. *Journal of Materials Chemistry*, 11(2):657–659, 2001.

[10] J. T. Cheung and J. Madden. Growth of HgCdTe epilayers with any predesigned compositional profile by laser molecular-beam epitaxy. *Journal of Vacuum Science & Technology B*, 5(3):705–708, 1987.

[11] R. Serna and C. N. Afonso. In situ growth of optically active erbium doped Al_2O_3 thin films by pulsed laser deposition. *Applied Physics Letters*, 69(11):1541–1543, 1996.

[12] S. Mailis, A.A. Anderson, S.J. Barrington, W.S. Brocklesby, R. Greef, H.N. Rutt, and R.W. Eason. Photosensitivity of lead germanate glass waveguides grown by pulsed laser deposition. *Optics Letters*, 23(22):1751–1753, 1998.

[13] M. E. Fajaro and M. Macler. Velocity selection of laser ablated metal atoms by a novel non-mechanical technique. In H. A. Atwater, J. T. Dickinson, D. H. Lowndes, and A. Polman, editors, *Film synthesis and*

growth using energetic beams, volume 388, pages 39–44. Materials Research Society, 1995.

[14] R. K. Singh and J. Narayan. A novel method for simulating laser-solid interactions in semiconductors and layered structures. *Materials Science and Engineering B -Solid State Materials for Advanced Technology*, 3(3):217–230, 1989.

[15] R. W. Dreyfus. Comparison of the ablation of dielectrics and metals at high and low laser powers. In E. Forgarassy and S. Lazare, editors, *Laser ablation of electronic materials: Basic mechanisms and applications*, volume 4 of *European Materials Research Soceity monographs*, pages 61–72. Elsevier Science, 1992.

[16] J. T. Cheung. History and fundamentals of pulsed laser deposition. In D. B. Chrisey and G. K. Hubler, editors, *Pulsed laser deposition of thin films*, pages 1–22. John Wiley and Sons, New York, 1994.

[17] S.R. Jackson, W.J. Metheringham, and P.E. Dyer. Excimer-laser ablation of Nd-YAG and Nd-Glass. *Applied Surface Science*, 86(1-4):223–227, 1995.

[18] M. Von Allmen. Laser ablation of solids : Basix principles and physical effects. In E. Forgarassy and S. Lazare, editors, *Laser ablation of electronic materials: Basic mechanisms and applications*, volume 4 of *European Materials Research Soceity monographs*, pages 55–61. Elsevier Science, 1992.

[19] D. B. Geohegan. Diagnostics and characteristics of pulsed laser deposition laser plasmas. In D. B. Chrisey and G. K. Hubler, editors, *Pulsed laser deposition of thin films*, pages 115–167. John Wiley and Sons, New York, 1994.

[20] K Murakami. Dynamics of laser ablation of high Tc superconductors and semiconductors, and a new method for growth of films. In E. Fogarassy and S. Lazare, editors, *Laser ablation of electronic materials:*

Basic mechanism and applications, volume 4 of *European research society monographs*, pages 125–140. Elsevier Science, The Netherlands, 1992.

[21] A.V. Bulgakov and N.M. Bulgakova. Gas-dynamic effects of the interaction between a pulsed laser- ablation plume and the ambient gas: analogy with an underexpanded jet. *Journal of Physics D-Applied Physics*, 31(6):693–703, 1998.

[22] D. B. Geohegan. Effects of ambient background gases on YBCO plume porpagation under film growth conditions: Spectroscopic, ion probe and fast photgraphic studies. In E. Forgarassy and S. Lazare, editors, *Laser ablation of electronic materials: Basic mechanisms and applications*, volume 4 of *European Materials Research Soceity monographs*, pages 73–88. Elsevier Science, 1992.

[23] P. R. Willmott and J. R. Huber. Pulsed laser vaporization and deposition. *Reviews of Modern Physics*, 72(1):315–328, 2000.

[24] A. Thum-Jager and K. Rohr. Angular emission distributions of neutrals and ions in laser ablated particle beams. *Journal of Physics D-Applied Physics*, 32(21):2827–2831, 1999.

[25] A.J. Paul, P.K. Schenck, D.W. Bonnell, and J.W. Hastie. *In situ* monitoring and and model simulation of $BaTiO_3$ pulsed laser deposition. In H. A. Atwater, J. T. Dickinson, D. H. Lowndes, and A. Polman, editors, *Film synthesis and growth using energetic beams*, volume 388, pages 45–51. Materials Research Society, 1995.

[26] A.V. Bulgakov and N.M. Bulgakova. Dynamics of laser-induced plume expansion into an ambient gas during film deposition. *Journal of Physics D-Applied Physics*, 28(8):1710–1718, 1995.

[27] J. S. Horwitz and J. A. Sprague. Film nucleation and film growth in pulsed laser deposition of ceramics. In D. B. Chrisey and G. K. Hubler, editors, *Pulsed laser deposition of thin films*, pages 229–253. John Wiley and Sons, New York, 1994.

[28] Z. K. Tang, G. K. L. Wong, P. Yu, M. Kawasaki, A. Ohtomo, H. Koinuma, and Y. Segawa. Room-temperature ultraviolet laser emission from self-assembled ZnO microcrystallite thin films. *Applied Physics Letters*, 72(25):3270–3272, 1998.

[29] W.S. Hu, Z.G. Liu, Y.Q. Lu, S.N. Zhu, and D. Feng. Pulsed-laser deposition and optical properties of completely (001) textured optical waveguiding $LiNbO_3$ films upon SiO_2/Si substrates. *Optics Letters*, 21(13):946–948, 1996.

Chapter 3

Pulsed Laser Deposition: History and Future

3.1 Introduction

This chapter details the history of PLD, and in particular examines the current work in the area of active optical waveguides grown by PLD. To contain the discussion only results of oxide films are presented, as only these are grown by our group (one exception is CdS which is discussed as lasing action has been demonstrated in this system). Some future directions PLD may take are also suggested.

3.2 History of PLD

A thorough review of the history of PLD has been presernted by Cheung [1]. This section briefly summarises the important stages in PLD history.

The possibility of PLD was investigated shortly after the availability of the first commercial ruby lasers. The first report was presented by Smith and Turner in 1965 [2]. The idea of a laser deposition process, however,

received very little attention over the next two decades. The preliminary investigations had not fully discovered the benefits of PLD over other deposition processes, only the drawbacks of high particulate densities on the film surface and the inhomogeneous stoichiometries over large deposition area.

The introduction of reliable Q-switched lasers in the mid 1970's enabled repeatable short pulse generation which fuelled more interest in PLD. Shorter ablation pulses provide a mechanism of achieving congruent evaporation as discussed in chapter 2. This was seen as a major potential advantage over other deposition systems at that time.

Development of efficient second harmonic generation (SHG) allowed production of shorter wavelength laser systems, which lead to higher absorption within the target thus reducing splashing (see section 2.3.1). SHG also allowed ablation of some materials which were transparent at the fundamental wavelength of the ablation laser.

Importantly, in 1978 Gapanov *et al* demonstrated a reactive deposition [3] which has become a major advantage of PLD, particularly in the fabrication of oxide films. Many other deposition systems which require open electrical components (i.e sputtering) are limited in the types of gases that can be present during deposition due to corrosion effects.

Semiconductors were grown with some success over the 1980's, however PLD suffered when compare to established deposition techniques due to the poor surface quality of the film. However in systems where splashing did not occur (eg. CdTe targets) it was shown that PLD could produce heterostructures of a much higher compositional resolution (on the order of 2 monolayers) than other processes at that time [4].

The 'killer application' (to use computer terminology) for PLD arrived with the discovery that it can be used for successful deposition of high temperature superconductors [5–7]. This discovery sparked off an explosion of interest in PLD largely due to the immense popularity of high tem-

perature superconductors at that time [8]. PLD has subsequently matured to enable growth of many material systems that cannot be reproduced as successfully with other depositions systems. Figure 3.1 shows a graph of number of papers published in the PLD field over the past 2 decades.

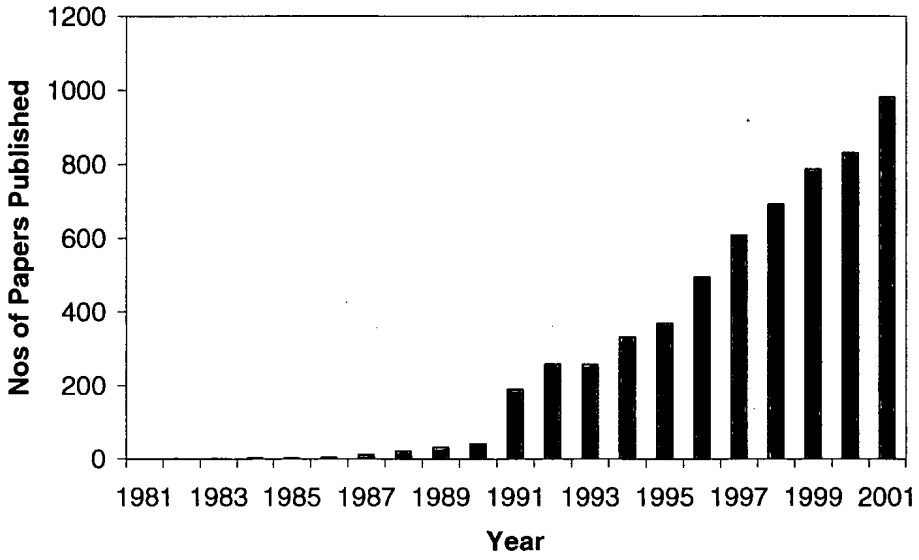

Figure 3.1: Number of papers published in PLD over the last two decades

This is compiled from the ISI Web of Science database using the keyword search term:

(deposit or film*) and ((laser molecular beam epitaxy) or (pulsed laser) or (laser excimer ablation) or(laser excimer reactive ablation) or (pulsed laser evaporation) or (excimer laser ablation) or (laser ablation deposition))*

This is obviously subject to some error and the value given for the number of papers published in 2001 is based upon those published within the first four months. It does however show the prolific rise of PLD over the past two decades.

3.3 Growth of active optical waveguides

After the discovery of reactive PLD [3], the focus of PLD shifted towards production of oxide films. Oxides constitute a large percentage of optical materials, many of which have complex stoichiometries. It would seem, therefore, that the congruent evaporation in an oxygen background that is achievable with PLD would be an ideal method of fabricating optical films.

The first oxides of optical interest were largely simple binary compounds like MgO [9] and Al_2O_3 [10], often used for optical coatings. The higher mobility of the ablated species means that improved crystalline growth is often achieved over other deposition processes but at the expense of poorer surface quality due to high particulate densities. The narrow angular distribution of the plume also makes it more difficult to scale up to the large deposition areas often required for optical coating applications.

Throughout this section material constants of laser hosts and substrates are referred to and compared. Table 3.1 gives a list of most of the material constants that are readily available and are mentioned in this section.

Material	Hardness (mohs)	Damage threshold ($GWcm^{-2}$)[a]	Thermal conductivity ($Wm^{-1}K^{-1}$)[b]	Transparency range (μm)	lattice constant ($\dot{A}$)	crystal structure	Refractive index (at 1.06μm)
Sapphire	9	10	x=y=30 z=35	0.17 - 5.5	a=b=4.76 c=12.99	hexagonal	1.75
YAG	8.5	1 - 3	14	0.25 - 5	12.01	cubic	1.82
Quartz	7	-	x=y=10.7 z=6.2	0.2 - 3	a=b=4.9 c=5.4	hexagonal	1.54(o) 1.53(e)
Silicon	8	-	163.3	1.2 - 7	5.43	cubic	3.4975 (at 1.35μm)
MgO	5	-	42	0.3 - 6	4.22	cubic	1.7
Lithium Niobate	5	0.05 - 0.1	5.6	0.4 - 5.0	a=b=5.14 c=13.78	hexagonal	2.2273(o) 2.1515(e)
KTP	5	1 - 3	x=20 y=33 z=30	0.35 - 4.5	a=12.81 b=6.40 c= 10.62	orthorhombic	n_x=1.738 n_y=1.746 n_z=1.830
GGG	7.5	0.3	6	0.3 -7	12.38	cubic	1.965
KGW	5	-	x=2.6 y=3.8 z=3.4	-	a=8.10 b=10.4 c=7.6	monoclinic	n_x=2.05 n_y=1.99 n_z=2.01
BBO	4	5 - 13.5	-	0.19 -3.5	a=b=12.53 c=12.72	hexagonal	1.65(o) 1.54(e)

Table 3.1: Material Constants of some common substrates and Laser hosts

[a]Discrepancies in values given are possibly due to different wavelengths used

[b]These values are typically taken around 300K

3.3.1 Semiconductors

3.3.1.1 ZnO

ZnO was one of the first optical films whose growth conditions and subsequent optical qualities received rigorous quantification [11, 12]. Much of this work stems from the semiconductor community[1] and has centred around growth of heterostructures for bandgap engineering [14, 15].

Lasing in PLD fabricated ZnO layers has been demonstrated [16, 17] but these devices do not have a simple waveguide cavity as fabricated for the work reported in this thesis. In the case of [16] the cavity is formed from the hexagonal crystal boundaries that are formed during growth. Lasing is seen at 387nm by optical pumping from a pulsed tripled YAG laser at 355nm. The pump laser is focused on the surface of the waveguide and laser output is observed from the waveguide edges. The pump laser changes the exciton concentration in the material and so changes the refractive index. This defines the cavity length of the laser with the end cavity mirrors formed by the crystal boundaries that occur just outside of the pump irradiated area. The crystal film in [17] however, is highly disordered and so this type of laser cavity is not possible. It is believed this cavity is formed from closed path scattering within the crystal.

[1]Interesting point to note: A large proportion of ZnO growth is published under the name of laser molecular beam epitaxy (LMBE or LAMBE) rather than PLD. LMBE, amongst many other names, was an alias PLD before PLD was voted as the official name at the first Material Research Society on Pulsed Laser Ablation (1989). LMBE, however, seemed to remain as a name mainly in the semiconductor community. There are some papers though that distinguish a difference between the two processes [13]. In LMBE the background pressures are more comparable with those of conventional molecular beam epitaxy. Where reactive depositions are performed, more reactive gases are used (O_3, NO_2) to keep the base pressure low. High vacuums are routinely used in work published under the name of PLD however, which creates a discrepancy over the naming issue. This thesis will use the term pulsed laser deposition or PLD regardless of the background pressure.

3.3.1.2 CdS

Similar hexagonal microcavity crystallite lasers have been fabricated by PLD in cadmium sulphide [18–20]. This material is of particular interest for high visible brightness devices as its bandgap lies around 2.49eV (498nm) which is close to the peak sensitivity of the human eye. Engineering of this material into a high power semiconductor laser would also provide a convenient source of pump power for Ti:sapphire lasers. This report is also a significant achievement for PLD as previously no deposition system had been able to fabricate thin film CdS that could achieve lasing at 498nm at room temperature.

3.3.2 Ferroelectrics

Ferroelectrics have also been fabricated by PLD for a relatively long time compared to other optical films. This is largely due to there being no satisfactory method of thin film production for many of these materials.

The alkali and alkali-earth tantalates and niobates represent a large group of ferroelectrics that have potential applications in laser radiation control via electro-optic, piezoelectric photorefractive or non-linear effects. Most of these compounds that have been successfully fabricated in bulk have also been fabricated in thin film form via PLD with varying degrees of success. Interest in many of these materials has declined over the years as their susceptibility to damage via the photorefractive effect limits both the wavelength and powers that can be used. The most notable exception to this waning interest has been lithium niobate ($LiNbO_3$).

3.3.2.1 Lithium niobate

Lithium niobate is ferroelectric below its Curie point of 1210 °C . It has a permanent dipole set up along the c axis enabling it to be photorefractive, piezoelectric, photoelastic, thermoelectric, acousto-optic and electro-optic [21]. It also possesses a relatively high non-linear co-efficient and damage threshold [22].

Due to this exceptional array of qualities it has become a material with huge potential for applications in optics and opto-electronics. The domain structure of lithium niobate can also be switched (poled) by application of high (up to ~22kV/mm) electric fields across the z-face of the crystal. By using this effect optical modulators and quasi-phase matched frequency doublers [23] can be fabricated. Poling has also been shown to have an effect on the etch rate of lithium niobate [24] making it suitable for potential application in MEMS (micro-electro-mechanical systems). The photorefractive effect will always limit its potential in high power applications, but the many other desirable properties of the crystal mean that there are unlikely to be a shortage of applications.

There have been almost a hundred papers published on PLD of lithium niobate so far. The interest in fabricating lithium niobate in thin film form is not just for the usual optical benefits of a high intensity-length product in the guided region of a waveguide. High electric fields are required for poling and switching lithium niobate electro-optic devices. In thin films the reduction in the distance between electrodes enables a reduction in the required voltage, which results in faster switching devices and also facilitates poling.

Successful fabrication of thin film lithium niobate is difficult due to the volatile nature of lithium. PLD fabrication of most of the ferroelectrics suffers a similar problem due to the presence of volatile elements such as potassium or lithium. Ablation from a stoichiometric target of lithium niobate usually results in growth of a lithium deficient phase, $LiNb_3O_8$.

Some reports indicate that the lighter elements suffer greater scattering and do not reach the substrate [25], other reports indicate that stoichiometric growth occurs at low substrate temperature and lithium deficiency increases with substrate temperature [26]. This would indicate that the deficiency occurs due to out-diffusion of the volatile element. It is however difficult to achieve crystalline growth at temperature lower than 400°C .

Deposition from a lithium rich source is a method of resolving the problem but this involves fabrication of a ceramic target. This is undesirable as single crystal lithium niobate is much easier to source and single crystal targets provide a higher quality film than ceramics [27]. Other methods of preventing lithium deficiency involve high pressure depositions [28], argon/oxygen mixtures [29], re-emission scattering or shadow mask techniques [30]. These usually result in an unacceptable reduction in deposition rate.

Literature on PLD of lithium niobate is confusing and many reports have conflicting accounts of how to achieve stoichiometric growth. A possible reason for this is the close similarity of the (006) plane of the desirable $LiNbO_3$ and the (602) plane of the undesirable $LiNb_3O_8$. Under X-ray diffraction (XRD) analysis (see section 4.2.2) the 2θ angle of these planes are at 38.1 degrees and 38.8 degrees respectively. Most XRD apparatus can resolve this difference but the 2θ offset often observed in PLD films (section 4.2.2) will always cast doubt over a report of stoichiometric growth if only XRD is used to validate the claim.

Lithium niobate also represents an interesting laser host as harmonic generation can be achieved *intra-cavity*. Waveguide lasers have been fabricated from Er^{3+}:Ti doped [31] and Yb^{3+}:Ti doped [32] lithium niobate by indiffusion, and Nd^{3+}:MgO [33] doped lithium niobate by ion implantation. A PLD fabricated lithium niobate laser, however, has not yet been reported, and the only doping attempt to date is by Alfonso [34,35] with a neodymium doped, lithium enriched target. Fluorescence observed in the waveguide was reported to be similar to that of bulk lithium niobate

doped with 3 at.% Nd, but with a broader linewidth as is often seen in PLD laser hosts. Rather unfortunately it appears that the inclusion of neodymium initiates growth of the lithium deficient phase and this has set an upper limit on the doping concentration.

3.3.2.2 KTP and BBO

Two ferroelectrics which are not alkali or alkali-earth tantalates or niobates but have achieved widespread use in optics are potassium titanyl phosphate (KTP), $KTiOPO_4$ and barium metaborate (also beta barium borate or BBO), BaB_2O_4.

These materials have a very high damage threshold (they are not photorefractives), very high nonlinear optical coefficients and have good transmission characteristics in the UV (BBO is transparent down to 190nm). These attributes make them ideal for harmonic generation. Typically KTP is used as a frequency doubler, commonly used to double the YAG fundamental at 1.06μm into the green. As well as frequency doubling, BBO is often utilised for sum-frequency generation, for example, mixing of the YAG fundamental and its second harmonic within BBO can generate the third harmonic in the UV. The conversion efficiency of harmonic generation is dependent on the intensity. Therefore realisation of these materials in a waveguide form would be useful due to generation of a large intensity-length product within the guide.

KTP has been fabricated by groups in Illinois, America [36–38] and a collaboration of groups in China and Hong Kong [39,40]. Both groups report an increase in titanium seen in the deposited layer and a potassium deficiency is reported in [40]. The Illinois group have concentrated largely on maximising the nonlinear coefficients of PLD grown KTP, and although SHG was observed its efficiency was not reported. They have also reported an instability in the films resulting in increasing optical loss over time. This effect has also been seen in bulk KTP crystals.

The Chinese groups have fabricated an optically active waveguide film of erbium doped KTP using multiple target rotation during deposition. KTP was also used as a substrate, with the erbium inclusion in the KTP matrix providing sufficient refractive index change to create a waveguide structure. Dopant levels were ~3% and optical pumping revealed photoluminescence at 1.54μm . This suggests a waveguide laser or amplifier could be successfully fabricated from Er:KTP in the future.

BBO has been fabricated by one group in Hong-Kong [41, 42], the best results being those films grown on a sapphire substrate with SHG being reported. These films were grown from a stoichiometric single crystal of BBO with a λ = 193nm ArF excimer laser.

3.3.3 Garnets

3.3.3.1 Nd:YAG

Yttrium aluminum garnet ($Y_3Al_5O_{12}$) or YAG is an isotropic cubic crystal. It is highly stable and possesses high thermal conductivity so efficient heat transfer for the crystal is possible. It has high damage threshold and is a physically hard crystal with high mechanical strength, so does not fracture easily. High optical quality crystals are relatively easily fabricated compared to other crystals and its hardness enables polishing to high optical quality. These qualities have made YAG possibly the most important solid state laser medium and certainly the most widespread. YAG lasers are utilised in applications in areas such as medicine , telecommunications, welding, laser cleaning, spectroscopy and many more.

YAG is most commonly doped with Nd^{3+} ions, substituting for the Y^{3+} ion. Typically lasing is achieved via the 1.06μm transition of the Nd^{3+} ion which is now commonly pumped via readily available diode lasers at 808nm. A 1.06μm Nd:YAG laser operates on a four level system (see section 7.6.1) and as such such does not suffer the problem of ground state

reabsorption.

Fabrication of Nd:YAG by PLD was first reported by the group at Keio University [43] on silicon and MgO substrates from a compressed ceramic target. Polycrystalline films were observed, although these grew as micro crystallites possibly due to the large (11%) mismatch between silicon, MgO and YAG, although there was no report on the presence of an oxide layer between the silicon and YAG film. Silicon is also an inappropriate choice of substrate as its high refractive index makes it unsuitable for waveguide devices. RBS data indicates the Nd^{3+} doping concentration at a rather high 8.3 at. %. Interestingly these films showed no lack of oxygen despite growth in a high vacuum of $\sim 10^{-7}$ torr. Further work by this group [44, 45] investigated Nd:YAG growth on different substrates. Curiously these included GGG (gadolinium gallium garnet) and GSGG (scandium substituted GGG) which again due to a high refractive ($\sim$1.96 compared to $\sim$1.81 for YAG) is unsuitable for waveguide fabrication. Growth on a YAG substrate was also investigated, the refractive index change induced by both the Nd dopant and the inherent strain induced during growth being sufficient to produce optical confinement within the 2.1µm thick film. Although only polycrystalline films were produced, photoluminescence spectra of the film was shown to be comparable to that of bulk Nd:YAG.

Further work was reported by the FORTH institute [46] on Nd:YAG growth on sapphire and YAG substrates from a single crystal target. Amorphous growth was observed even though substrate temperatures during fabrication were as high as $\sim$900°C . Annealing of these films for a further 5 hours at 1300°C produced polycrystalline films. No fluorescence or lasing action was reported.

3.3.3.2 Cr:YAG

Recently growth of Cr^{4+}:YAG by PLD was reported by the Keio university group [47]. This is a particularly interesting material as it has applications as a tunable source between 1.35μm and 1.45μm [48] but also can be used as a passive saturable absorber in the 1μm region making it an ideal candidate for Q-switching [49] and modelocking [50] Nd:YAG lasers. This is possibly the first attempt to fabricate such a device in planar waveguide format. PLD is suited to the fabrication of such a device as control of the reactive oxygen atmosphere is important for obtaining the correct valence state of the Cr ions. The Cr:YAG films were grown from a compressed ceramic target containing calcium ions to facilitate oxidation of the Cr ions. Films were grown at 300 °C and post annealed at 1000 °C which reportedly produced single crystal films. Fluorescence measurements and XPS confirm that the presence of Ca ions further oxidises the stable Cr^{3+} ion to Cr^{4+} but what fraction of each ion present in the film is not estimated in the report.

3.3.3.3 Nd:GGG

GGG is another garnet that is similar to YAG in most of its properties. It has a refractive index of ~1.97 which makes it an attractive material for high numerical aperture devices when fabricated on a YAG substrate (n ~1.83). GGG has a similar lattice spacing to YAG enabling epitaxial growth.

Nd:GGG waveguide lasers have been previously fabricated in planar structure by ion implantation [51] and in channel structure by LPE and ion beam etching [52]. The first report of growth of Nd:GGG by PLD and subsequent lasing was reported by Gill *et al* [53, 54]. Films were prepared from ceramic targets and showed relatively high losses at around 5.7 $dBcm^{-1}$. These were pumped by a Ti:sapphire laser at 808nm and lasing was achieved at 1.06μm with a high threshold of 91mW of absorbed input

power. The high lasing threshold was almost certainly due to high particulate density produced from the ceramic target. This was the first report of lasing from a PLD fabricated waveguide; subsequent reports by Anderson and Bonner [27, 55] describe growth of a low loss waveguide from a single crystal target and its lasing performance. Losses in the waveguide were confirmed to be as low as $0.5 dBcm^{-1}$ and lasing was achievable at thresholds as low as 2.2mW. This remains one of the lowest reported loss measurements and the lowest reported laser threshold in a PLD waveguide. Also demonstrated for the first time in Nd:GGG was lasing on the quasi-three-level 937nm transition. The slope efficiency of the device was measured to be 20% at both wavelengths.

The high damage threshold of Nd:GGG coupled with the large thickness (8μm) and high numerical aperture of the device, provided good evidence that PLD optical waveguides could be highly attractive for high power diode-pumped lasers.

Lasing from a PLD Nd:GGG waveguide pumped with a laser diode was reported by Keio University [56] in abstracts for CLEO 2000, though no details have subsequently been published on the performance of this device.

Further work by the Kieo University group includes growth of Nd, Cr co-doped GGG [57]. This has potential to act simultaneously as both a saturable absorber and a laser gain medium. Successful operation of a diode pumped monolithic self Q-switched laser in bulk [58, 59] has been reported for Nd,Cr co-doped YAG. The films were fabricated from simultaneous ablation of a Nd:GGG and Cr,Ca:GGG ceramic targets onto YAG substrates. Fluorescence measurements confirm the presence of Cr^{4+} and Nd^{3+} ions within the lattice. Studies have also been made on growth of Cr^{4+}:GGG on YAG [47] with similar results to those reported in Cr^{4+}:YAG fabrication.

3.3.3.4 Nd,Cr:GSGG

The Institute of Physical Chemistry in Switzerland recently reported the growth of crystalline Nd,Cr:GSGG thin films [60] on Si substrates. This work differs from that mentioned above [47] in that scandium substitute GGG is the host and Cr^{3+} is the desired ion incorporated along with the Nd^{3+} ion. Obviously lasing cannot be achieved in this film with a silicon substrate (unless a suitably thick SiO_2 buffer layer is present) but it is hoped that further work from both these groups will ultimately produce a monolithic self Q-switched waveguide laser.

3.3.4 Ti:sapphire

Sapphire is the crystalline alpha phase of alumina (Al_2O_3) and has a hexagonal structure. Sapphire has excellent optical and physical properties that make it a very desirable laser host. It has high transparency from the VUV through to the mid infra-red (~5μm). Sapphire also has good thermal conductivity, high mechanical strength and possesses almost diamond-like hardness[2]. Whilst this makes optical finishing a lengthy process it does enable good quality finishing.

Popular dopants in sapphire are Cr^{3+} (resulting in ruby) and Ti^{3+}, both of which substitute for the Al^{3+} in small percentages (0.01 - 0.4 at. %). This section will discuss only Ti:sapphire.

Ti:sapphire is a very attractive laser system that exhibits gain over a broad region of 650nm - 1100nm [61], making it one of the most widely tunable

[2]Note: These properties would also make sapphire an excellent substrate material (and it is often used as such) however its extreme hardness is a major drawback when end-polishing a waveguide device. Since sapphire is almost invariably much harder than the deposited film, finishing results in the film 'rounding off' during the lengthy final polishing phase (i.e the film end which would be the laser cavity edge is now bevelled). For this reason it is important to match the hardness of substrate and film if lasing is desired in a conventional parallel end-face-polished waveguide geometry

solid state laser sources and as such, very suitable for scientific applications. This high bandwidth is also attractive for modelocking devices as it allows generation of femtosecond pulses [62].

The main drawbacks of Ti:sapphire are that it has a small emission cross-section and short upper state lifetime compared to rare earth ions. This requires high power densities of optical pumping to achieve lasing, usually requiring bulky and expensive argon-ion lasers, although recently this can now achieved by diode pumped, frequency doubled, solid state lasers. High crystal quality is required for sapphire laser hosts as defects produce an absorption band at 750nm which is within the fluorescence region of Ti^{3+} [61]. The Ti:sapphire laser is also a three level laser system and so requires high pumping powers to overcome ground state absorption. The advantage of this is that losses due to scattering within the waveguide can be negligible compared to this absorption and so may not increase the input lasing power threshold significantly.

Alumina was one of the earliest optical films grown by PLD [10,63] and the UV laser ablation characteristics of sapphire were first reported by Dreyfus [64]. Growth of Ti:sapphire was first reported by Dyer [65,66]. This report studied film fabrication using a variety of ceramic and crystalline targets and both UV (193nm) and IR (10μm) wavelengths. Continuation of this work was performed by a collaboration of three groups from Southampton University, FORTH and the Institute of Physics in Prague. This resulted in both successful growth of the correct phase of Ti:sapphire [67] and lasing [68]. The Ti:sapphire layers were grown from a single crystal target on sapphire substrates in an oxygen atmosphere. Substitution of Al^{3+} for Ti^{3+} induced a sufficient refractive index change in the deposited layer to enable optical confinement between the film and substrate. Lasing was achieved at 0.56W input power threshold with a slope efficiency of 26%, giving quasi-cw output powers of ~350mW.

This is a particularly important result for PLD as it remains to date the only reported efficient planar waveguide Ti:sapphire laser. The only other

reported Ti:sapphire planar waveguide is by Ti indiffusion into sapphire [69,70], but lasing performance in this system is poor.

A subsequent report by the same collaboration detailed growth of Ti:sapphire on a quartz substrate [71]. Quartz would make an attractive substrate for Ti:sapphire as it has a much lower refractive index (n ~1.55) than undoped sapphire. This would create a waveguide with a large numerical aperture that would allow optical pumping by a divergent source. A significant problem of growing sapphire on quartz substrates is that the low thermal conductivity and a phase change at 573°C usually results in fracture of the substrate upon heating. Losses in the film were relatively high at ~6.5 $dBcm^{-1}$ and lasing was not reported.

Recently work reported by Manoravi and Willmott [72, 73] has demonstrated successful deposition of Ti:sapphire by use of molten Ti-Al alloy ablation targets. The use of molten targets prevents the expulsion of particulates from the surface and hence allows the production of smooth films. It is also reported that this allows fabrication of films at much lower temperatures (670°C [73] as opposed to ~1000°C [68]). We await further reports detailing optical losses and lasing performance.

Work reported by Uetsuhara details growth of Ti:sapphire on silica substrates [74], but again these films show appreciably high losses at 8.7$dBcm^{-1}$ due to particulates. They have recently employed a fast rotating target to remove the particulates from the plume by centrifugal separation but no details of its success have been reported.

3.3.5 Er/Yb Glass waveguides

The telecommunications industry currently influences much of the work in planar waveguide fabrication. Er^{3+} ions are of most interest as they exhibit linear, low noise optical gain in the 1.5μm region. This is conveniently in the same waveband at which light can propagate through specially en-

gineered optical fibre at low loss and almost zero dispersion. Currently there exists no cheap optical pump source for Er^{3+}, the absorption line of which is at ~500nm. To overcome this problem, co-doping with Yb^{3+} allows pumping from ~800nm to 1.05μm and cross relaxation enables energy transfer to the Er^{3+} ion.

For reasons mentioned in section 1.2 there is much interest in developing planar waveguide amplifiers at this wavelength for monolithic integrated optical circuits that could potentially be of great use to the telecommunications industry.

A large collection of work has been reported from the Instituto de Optica, Madrid on Er doping and Er-Yb co-doping of PLD fabricated planar waveguides [75–79]. This work details growth of both Al_2O_3 and phosphate glass hosts on a variety of substrates. Photoluminescence studies have shown that the alternate target deposition system employed (i.e ablation from a two separate host and dopant targets) is successful in incorporating active Er^{3+} ions [77,79] and Er^{3+} - Yb^{3+} [78] dopants in their respective host materials.

This is one of the few PLD groups who have attempted growth of glass waveguides by PLD. There are few other reports apart from growth of GLS [80,81], which will not be discussed here and lead germanate [82–84], which will be discussed further in chapter 5. The lack of interest in growth of glass compounds is largely because they are difficult to grow with smooth surface morphology and so usually exhibit high scattering losses.

3.3.6 Yttrium oxide

Ytrrium oxide is used most commonly as a phosphor in displays when doped with europium and there have been many reports on PLD growth of Eu:Y_2O_3 [85,86] . Y_2O_3 also possesses high thermal conductivity and a

large transparency range (230nm - 8μm) which makes it an excellent laser host. Korzenski *et al* have reported growth of Er:Y_2O_3 [87], performed by alternate target PLD to precisely control the dopant levels within the host. Fluorescence measurements confirmed their active position within the host. Waveguide losses of < 1 dBcm^{-1} were also reported which is comparable to the best reported losses in PLD waveguides [27].

Similar work by Huignard *et al* [88] has also reported growth of Tm:Y_2O_3 films. The Tm^{3+} ion exhibits a laser transition at 1.95μm which is known as the 'eye safe' region of laser radiation (for obvious reasons) and has broad applications within the medical industry. The reported films were grown from prepared ceramic targets and luminescence studies show the films to be very similar, spectroscopically, to bulk material.

3.3.7 $Ca_4GdO(BO_3)_3$ (GdCOB)

Recently a report by Chety *et al* [89] has demonstrated for the first time growth of GdCOB by PLD. This is a relatively new laser lost [90] that has received much attention due to its high efficiency for frequency doubling (~50% for 1064nm Nd:YAG radiation). This enables simultaneous lasing and harmonic conversion in a monolithic system similar to KTP. To date there have been no other reports of thin film fabrication of GdCOB, only waveguide fabrication by modification of bulk material [91]. Growth was performed from a ceramic target using an ArF excimer laser (λ = 193nm). A polycrystalline film was produced after suitable annealing. It is interesting to note that the GdCOB system does not apparently suffer from droplet production under the growth conditions reported. The results presented so far are preliminary and it is hoped that a higher quality single crystal film can be fabricated for lasing devices.

3.3.8 $KGd(WO_4)_2$ (KGW)

The Bulgarian Academy of Science have recently reported work on the growth of Nd:$KGd(WO_4)_2$ [92]. KGW is a laser host material that also enables low threshold raman scattering, leading to the production of efficient lasing at a variety of wavelengths. Nd:KGW lasers generally have a better slope efficiency than equivalent Nd:YAG lasers. Polycrystalline films were grown on sapphire substrates with a slight reduction in the volatile element, potassium, compared to the bulk material. Work was also carried out with Peter Atanasov in collaboration with Southampton University during the course of this thesis on attempting to grow KGW on a more appropriate MgO substrate (as this has a similar hardness to KGW). We found that films were typically brown under the stated growth conditions [92], which is usually indicative of oxygen deficiency. Higher pressures would reduce this discolouration at the expense of poorer film surface quality when observed under SEM. It was also found that at growth temperatures required to avoid amorphous growth, the dominant phase was that of $Gd_2(WO_4)_3$, i.e no potassium was present in the film.

3.3.9 Summary of active optical films grown by PLD

Over the last decade there has been a marked increase in the fabrication of active optical thin films by PLD. Largely this is due to the realisation that PLD is capable of fabricating certain materials in thin film form that could not be fabricated by other deposition systems (e.g. Ti:sapphire, GdCOB and CdS). Another factor contributing to the rise in popularity of PLD is that despite the presence of particulates in certain materials systems, PLD waveguide lasers can be fabricated with good performance characteristics.

3.4 Future of PLD

As discussed in section 8.1 the single largest disadvantage in PLD is the presence of particulates in the deposited layer. Recently, use of femtosecond deposition systems [93, 94] has suggested that very high intensity pulses may provide a solution to this problem.

3.4.1 Short pulse ablation lasers

The ablation process in femtosecond lasers is a non-thermal process, and therefore it is hoped that the problems associated with melt expulsion should not occur. To date no multi-component optical materials (beyond simple oxides and nitrides [94, 95],have been deposited using femtosecond PLD and it is uncertain whether the stoichiometry of a complex target material can be reproduced in the film. Although some reports show very favourable results from femtosecond deposition [94] others have shown it to produce lower quality films than nanosecond deposition with no particulate density reduction [96]. Additionally, deposition rates appear to be very low, so growth of films of typical waveguide dimensions (few μm) within an acceptable time scale may be difficult.

A detailed study by Rode and Gamaly [97,98] into deposition by high repetition rate, Q-switched nanosecond and mode-locked picosecond YAG lasers show it is possible under certain conditions to produce completely particulate free films from picosecond laser sources.

An important paper recently released details growth of an α-gallium layer by picosecond deposition [99, 100]. This interesting phase of gallium exhibits an ultra-fast (~2ps) light induced change in reflectivity. In this system picosecond deposition produced particulate free films whereas nanosecond deposition produced high particulate densities which was of severe detriment to the desired qualities of the film.

As more reports emerge on the effect of short-pulsed ablation lasers, the PLD community wait to see if this will solve the problem of particulate production.

Femtosecond deposition does have one distinct advantages over nanosecond deposition. The high peak intensities generated allow materials that are transparent to the ablation wavelength to be deposited. Furthermore, by careful focussing, deposition can be achieved from the opposite side of the target to the incident laser radiation. This enables microdeposition of artifacts on of the order of the size of the beam waist [101, 102].

3.4.2 Other routes for PLD

Another route to circumvent the particulate problem in PLD is to either grow systems where particulates do not effect the device performance or concentrate studies on systems that produce little or no particulates (i.e CdS or Ti:sapphire from molten targets).

In waveguide optics it is hard to conceive of a system where the particulates will be of little detriment to the device. It is, however, believed that in capped, thick film, waveguide lasers the losses due to scattering within the guide from particulates may have an almost negligible effect on laser performance.

The two most successful waveguide lasers grown by PLD to date have been the Ti:sapphire [68] and Nd:GGG [55] lasers. These waveguides were 12μm and 8μm thick respectively which is much thicker than almost every other report of doped optical waveguides grown by PLD. We do not believe this is a coincidence and work detailed in chapter 8 (and reported in [103] helps to confirm this. It is believed that detrimental scattering from the particulates largely occurs at the surface of the waveguide. By growing thick waveguides this loss can be minimised as detailed in section 8.3. The fact that PLD can easily grow relatively thick (and high numer-

ical aperture) waveguides suggests that this would be an excellent route to take for fabrication of planar laser waveguides by PLD. It is hoped that more devices will be fabricated by PLD by moving to thicker dimensions. Currently work in Southampton is focussing on growth of thick (possibly $> 100\mu m$) multilayer devices for high power diode pumped sources.

A recent report by Pollnau details use of Ti:sapphire waveguide grown by PLD as a continuous-wave broadband emitter [104] for use in optical coherence tomography (OCT). The resolution of OCT and other similar imaging systems is restricted by the bandwidth of the illumination source. Bulk, modelocked Ti:sappphire lasers are commonly used but these are neither compact nor portable sources, which are common requirements for such imaging systems. The compact broadband source reported would appear to be a ideal solution to this problem (with the exception that it currently requires pumping by an Ar^+ ion laser). Lasing is not desired in the film and the particulates can actually be beneficial by preventing laser oscillation at higher pump powers.

3.5 Conclusions

A brief history of PLD has been given along with a review of recent reports in the field of active optical films grown by PLD. Conclusions have been drawn from those systems that were successful and a prediction of the future trends for PLD of optical waveguide devices has been suggested.

3.6 References

[1] J. T. Cheung. History and fundamentals of pulsed laser deposition. In D. B. Chrisey and G. K. Hubler, editors, *Pulsed laser deposition of thin films*, pages 1–22. John Wiley and Sons, New York, 1994.

[2] H. M. Smith and A. F. Tuner. Vacuum depositied thin films using a ruby laser. *Applied Optics*, 4:147–148, 1965.

[3] S. V. Gaponov, E. B. Klyuenkov, B. A. Nesterov, N. N. Salashchenko, and M. I. Kheifets. Low -temperature epitaxy of dielectrics in laser sputtering a low-density chemically active gas. *Sov. Tech. Phys. Lett*, 5:193–194, 1979.

[4] J. T. Cheung and J. Madden. Growth of HgCdTe epilayers with any predesigned compositional profile by laser molecular-beam epitaxy. *Journal of Vacuum Science & Technology B*, 5(3):705–708, 1987.

[5] P. H. Hor, L. Gao, R. L. Meng, Z. J. Huang, Y. Q. Wang, K. Forster, J. Vassilious, C. W. Chu, M. K. Wu, J. R. Ashburn, and C. J. Torng. High-pressure study of the new Y-Ba-Cu-O superconducting compound system. *Physical Review Letters*, 58(9):911–912, 1987.

[6] D. Dijkkamp, T. Venkatesan, X. D. Wu, S. A. Shaheen, N. Jisrawi, Y. H. Minlee, W. L. McLean, and M. Croft. Preparation of Y-Ba-Cu oxide superconductor thin-films using pulsed laser evaporation from high-tc bulk material. *Applied Physics Letters*, 51(8):619–621, 1987.

[7] X. D. Wu, D. Dijkkamp, S. B. Ogale, A. Inam, E. W. Chase, P. F. Miceli, C. C. Chang, J. M. Tarascon, and T. Venkatesan. Epitaxial ordering of oxide superconductor thin-films on (100) $SrTiO_3$ prepared by pulsed laser evaporation. *Applied Physics Letters*, 51(11):861–863, 1987.

[8] J. G. Bednorz and K. A. Muller. Possible high-Tc superconductivity in the Ba-La-Cu-O system. *Zeitschrift Fur Physik B-Condensed Matter*, 64(2):189–193, 1986.

[9] H. S. Kwok, P. Mattocks, L. Shi, X. W. Wang, S. Witanachchi, Q. Y. Ying, J. P. Zheng, and D. T. Shaw. Laser evaporation deposition of superconducting and dielectric thin-films. *Applied Physics Letters*, 52(21):1825–1827, 1988.

[10] Ya. A. Bykovskii, V. M. Boyakov, V. T. Galochkin, A. S. Molchanov, I. N. Nikolaev, and A. N. Oraevskii. Deposition of metal, semiconductor, and oxide films with a periodically pulsed CO_2 laser. *Sov. Phys. Tech. Phys*, 23:578–581, 1978.

[11] H. Sankur and J. T. Cheung. Highly oriented ZnO films grown by laser evaporation. *Journal of Vacuum Science & Technology A-Vacuum Surfaces and Films*, 1(4):1806–1809, 1983.

[12] N. J. Ianno, L. McConville, N. Shaikh, S. Pittal, and P. G. Snyder. Characterization of pulsed laser deposited zinc-oxide. *Thin Solid Films*, 220(1-2):92–99, 1992.

[13] H. Koinuma, N. Kanda, J. Nishino, A. Ohtomo, H. Kubota, M. Kawasaki, and M. Yoshimoto. Laser mbe of ceramic thin films for future electronics. *Applied Surface Science*, 110:514–519, 1997.

[14] A. Ohtomo, M. Kawasaki, T. Koida, H. Koinuma, Y. Sakurai, Y. Yoshida, M. Sumiya, S. Fuke, T. Yasuda, and Y. Segawa. Double heterostructure based on ZnO and $Mg_xZn_{1-x}O$. In *Silicon Carbide, III-Nitrides and Related Materials, Pts 1 and 2*, volume 264-2 of *MATERIALS SCIENCE FORUM*, pages 1463–1466. 1998.

[15] E. Millon, O. Albert, J. C. Loulergue, J. Etchepare, D. Hulin, W. Seiler, and J. Perriere. Growth of heteroepitaxial ZnO thin films by femtosecond pulsed- laser deposition. *Journal of Applied Physics*, 88(11):6937–6939, 2000.

[16] Z. K. Tang, G. K. L. Wong, P. Yu, M. Kawasaki, A. Ohtomo, H. Koinuma, and Y. Segawa. Room-temperature ultraviolet laser emission from self-assembled ZnO microcrystallite thin films. *Applied Physics Letters*, 72(25):3270–3272, 1998.

[17] H. Cao, Y. G. Zhao, H. C. Ong, S. T. Ho, J. Y. Dai, J. Y. Wu, and R. P. H. Chang. Ultraviolet lasing in resonators formed by scatter-

ing in semiconductor polycrystalline films. *Applied Physics Letters*, 73(25):3656–3658, 1998.

[18] D. M. Bagnall, B. Ullrich, X. G. Qiu, Y. Segawa, and H. Sakai. Micro-cavity lasing of optically excited cadmium sulfide thin films at room temperature. *Optics Letters*, 24(18):1278–1280, 1999.

[19] D. M. Bagnall, B. Ullrich, H. Sakai, and Y. Segawa. Micro-cavity lasing of optically excited CdS thin films at room temperature. *Journal of Crystal Growth*, 214:1015–1018, 2000.

[20] B. Ullrich, D. M. Bagnall, H. Sakai, and Y. Segawa. Photoluminescence and lasing of thin CdS films on glass formed by pulsed-laser-deposition. *Journal of Luminescence*, 87-9:1162–1164, 2000.

[21] R. S. Weis and T. K. Gaylord. Lithium-niobate - summary of physical properties and crystal structure. *Applied Physics A-Materials Science & Processing*, 37(4):191–203, 1985.

[22] A. M. Prokhorov and Yu. S. Kuzminov. *Physics and chemistry of lithium niobate*. The Adam Hilger series on optics and optoelectronics. IOP publishing, 1990.

[23] M. Yamada, N. Nada, M. Saitoh, and K. Watanabe. 1st-order quasi-phase matched $LiNbO_3$ wave-guide periodically poled by applying an external-field for efficient blue 2nd- harmonic generation. *Applied Physics Letters*, 62(5):435–436, 1993.

[24] I. E. Barry, G. W. Ross, P. G. R. Smith, R. W. Eason, and G. Cook. Microstructuring of lithium niobate using differential etch-rate between inverted and non-inverted ferroelectric domains. *Materials Letters*, 37(4-5):246–254, 1998.

[25] J. A. Chaos, R. W. Dreyfus, A. Perea, R. Serna, J. Gonzalo, and C. N. Afonso. Delayed release of Li atoms from laser ablated lithium niobate. *Applied Physics Letters*, 76(5):649–651, 2000.

[26] Z. C. Wu, W. S. Hu, J. M. Liu, M. Wang, and Z. G. Liu. Effects of substrate temperature on the growth of oriented $LiNbO_3$ thin films by pulsed laser deposition. *Materials Letters*, 34(3-6):332–335, 1998.

[27] A.A. Anderson, C.L. Bonner, D.P. Shepherd, R.W. Eason, C. Grivas, D.S. Gill, and N. Vainos. Low loss (0.5 db/cm) $Nd:Gd_3Ga_5O_{12}$ waveguide layers grown by pulsed laser deposition. *Optics Communications*, 144(4-6):183–186, 1997.

[28] J. A. Chaos, V. Pruneri, J. Gonzalo, and C. N. Afonso. Second-harmonic generation in highly textured $LiNbO_3$ films prepared by pulsed laser deposition. *Journal of Applied Physics*, 88(6):3768–3770, 2000.

[29] S. B. Ogale, R. Nawatheydikshit, S. J. Dikshit, and S. M. Kanetkar. Pulsed laser deposition of stoichiometric $LiNbO_3$ thin-films by using O_2 and Ar gas-mixtures as ambients. *Journal of Applied Physics*, 71(11):5718–5720, 1992.

[30] D. W. Kim, S. M. Oh, T. W. Noh, and S. H. Lee. Epitaxial $LiNbO_3$ thin films grown by the "eclipse method". *Journal of the Korean Physical Society*, 32:S1408–S1410, 1998.

[31] C. H. Huang and L. McCaughan. Er-indiffused $Ti:LiNbO_3$ channel waveguide optical amplifiers pumped at 980 nm. *Electronics Letters*, 32(3):215–216, 1996.

[32] J. K. Jones, J. P. Desandro, M. Hempstead, D. P. Shepherd, A. C. Large, A. C. Tropper, and J. S. Wilkinson. Channel wave-guide laser at 1μm in Yb-indiffused $LiNbO_3$. *Optics Letters*, 20(13):1477–1479, 1995.

[33] S.J. Field, D.C. Hanna, D.P. Shepherd, A.C. Tropper, P.J. Chandler, P.D. Townsend, and L. Zhang. Ion-implanted Nd-MgO-$LiNbO_3$ planar waveguide laser. *Optics Letters*, 16(7):481–483, 1991.

[34] J. E. Alfonso, M. J. Martin, and C. Zaldo. Photoluminescence of Nd-doped $LiNbO_3$ films prepared by pulsed laser deposition. *Applied Physics Letters*, 71(20):2904–2906, 1997.

[35] J. E. Alfonso, M. J. Martin, and C. Zaldo. Nd^{3+} photoluminescence in lithium niobate thin films. *Boletin De La Sociedad Espanola De Ceramica Y Vidrio*, 37(2-3):221–226, 1998.

[36] F. L. Xiong, R. P. H. Chang, M. E. Hagerman, V. L. Kozhevnikov, K. R. Poeppelmeier, H. T. Zhou, G. K. Wong, J. B. Ketterson, and C. W. White. Pulsed excimer-laser deposition of potassium titanyl phosphate films. *Applied Physics Letters*, 64(2):161–163, 1994.

[37] F. L. Xiong, M. Hagerman, H. Zhou, V. Kozhevnikov, G. K. Wong, K. Poeppelmeier, J. B. Ketterson, R. P. H. Chang, and C. W. White. Deposition of nonlinear-optical films of potassium titanyl phosphate ($KTiOPO_4$) by pulsed excimer-laser ablation. *Journal of Vacuum Science & Technology A-Vacuum Surfaces and Films*, 12(4):1446–1450, 1994.

[38] P. M. Lundquist, H. Zhou, D. N. Hahn, J. B. Ketterson, G. K. Wong, M. E. Hagerman, K. R. Poeppelmeier, H. C. Ong, F. Xiong, and R. P. H. Chang. Potassium titanyl phosphate thin-films on fused quartz for optical wave-guide applications. *Applied Physics Letters*, 66(19):2469–2471, 1995.

[39] K.M. Wang, B.R. Shi, N. Cue, Y.Y. Zhu, R.F. Xiao, F. Lu, W. Li, and Y.G. Liu. Waveguide laser film in erbium-doped $KTiOPO_4$ by pulsed laser deposition. *Applied Physics Letters*, 73(8):1020–1022, 1998.

[40] K. M. Wang, B. R. Shi, N. Cue, Y. Y. Zhu, R. F. Xiao, F. Lu, H. Hu, and Y. G. Liu. Waveguide structure of Er-doped $KTiOPO_4$ films on different substrates by pulsed-laser deposition. *Journal of Vacuum Science & Technology A-Vacuum Surfaces and Films*, 19(2):394–397, 2001.

[41] R. F. Xiao, L. C. Ng, L. C. Yu, and G. K. L. Wong. Preparation of crystalline beta-barium borate (Beta-BaB_2O_4) thin-films by pulsed-laser deposition. *Applied Physics Letters*, 67(3):305–307, 1995.

[42] H. B. Liao, R. F. Xiao, P. Yu, and G. K. L. Wong. Growth of beta barium borate (beta-BaB_2O_4) thin films for nonlinear optical applications. *Journal of Crystal Growth*, 174(1-4):434–439, 1997.

[43] M. Ezaki, H. Kumagai, K. Kobayashi, K. Toyoda, and M. Obara. Crystal growth of Nd:YAG laser films on various substrates by pulsed laser deposition. *Japanese Journal of Applied Physics Part 1-Regular Papers Short Notes & Review Papers*, 34(12B):6838–6841, 1995.

[44] M. Ezaki, M. Obara, H. Kumagai, and K. Toyoda. Characterization of Nd:$Y_3Al_5O_{12}$ thin films grown on various substrates by pulsed laser deposition. *Applied Physics Letters*, 69(20):2977–2979, 1996.

[45] H. Kumagai, K. Adachi, M. Ezaki, K. Toyoda, and M. Obara. Epitaxial growth of Nd:YAG thin films by pulsed laser deposition. *Applied Surface Science*, 110:528–532, 1997.

[46] N.A. Vainos, C. Grivas, C. Fotakis, R.W. Eason, A.A. Anderson, D.S. Gill, D.P. Shepherd, M. Jelinek, J. Lancok, and J. Sonsky. Planar laser waveguides of Ti : sapphire, Nd : GGG and Nd : YAG grown by pulsed laser deposition. *Applied Surface Science*, 129:514–519, 1998.

[47] S Fukaya, K Adachi, M Obara, and H Kumagai. The growth of Cr^{4+}:YAG and Cr^{4+}:GGG thin films by pulsed laser deposition. *Optics Communications*, 187:373–377, 2001.

[48] A. Sennaroglu, C. R. Pollock, and H. Nathel. Efficient continuous-wave chromium-doped YAG laser. *Journal of the Optical Society of America B-Optical Physics*, 12(5):930–937, 1995.

[49] J. J. Zayhowski and C. Dill. Diode-pumped passively Q-switched picosecond microchip lasers. *Optics Letters*, 19(18):1427–1429, 1994.

[50] J. X. Wang, W. Z. Zhang, Q. R. Xing, and Q. Y. Wang. Investigation of Cr^{4+}: YAG passive mode-locking in a pulsed Nd : YAG laser. *Optics and Laser Technology*, 30(5):303–305, 1998.

[51] S.J. Field, D.C. Hanna, A.C. Large, D.P. Shepherd, A.C. Tropper, P.J. Chandler, P.D. Townsend, and L. Zhang. An efficient, diode-pumped, ion-implanted Nd-GGG planar waveguide laser. *Optics Communications*, 86(2):161–166, 1991.

[52] R. Gerhardt, J. Kleine-Borger, L. Beilschmidt, M. Frommeyer, H. Dotsch, and B. Gather. Efficient channel-waveguide laser in Nd:GGG at 1.062µm wavelength. *Applied Physics Letters*, 75(9):1210–1212, 1999.

[53] D.S. Gill, R.W. Eason, J. Mendiola, and P.J. Chandler. Growth of crystalline $Gd_3Ga_5O_{12}$ thin-film optical wave-guides by pulsed-laser deposition. *Materials Letters*, 25(1-2):1–4, 1995.

[54] D.S. Gill, A.A. Anderson, R.W. Eason, T.J. Warburton, and D.P. Shepherd. Laser operation of an Nd:$Gd_3 3Ga_5O_{12}$ thin-film optical waveguide fabricated by pulsed laser deposition. *Applied Physics Letters*, 69(1):10–12, 1996.

[55] C.L. Bonner, A.A. Anderson, R.W. Eason, D.P. Shepherd, D.S. Gill, C. Grivas, and N. Vainos. Performance of a low-loss pulsed-laser deposited Nd:$Gd_3Ga_5O_{12}$ waveguide laser at 1.06 and 0.94µm . *Optics Letters*, 22(13):988–990, 1997.

[56] Y Ishida, S Fukaya, T Shimoda, and M Obara. Nd:$G_3G_5G_{12}$ waveguide laser fabricated by pusled laser deposition method with ceramic target. In *CLEO/QELS 2000*, page CNF2, San Fransico, America, 2000. OSA.

[57] S Fukaya, T Hasegawa, N Ishida, and M Obara. Nd, Cr co-doped gadolinium gallium garnet laser waveguide structure formed by pulsed laser deposition. In *CLEO Pacific Rim 1999*, 1999.

[58] S. H. Zhou, K. K. Lee, Y. C. Chen, and S. Q. Li. Monolithic self-Q-switched Cr,Nd-YAG laser. *Optics Letters*, 18(7):511–512, 1993.

[59] S. Q. Li, S. H. Zhou, P. Wang, Y. C. Chen, and K. K. Lee. Self-q-switched diode-end-pumped Cr,Nd-YAG laser with polarized output. *Optics Letters*, 18(3):203–204, 1993.

[60] P. R. Willmott, P. Manoravi, and K. Holliday. Production and characterization of Nd,Cr : GSGG thin films on Si(001) grown by pulsed laser ablation. *Applied Physics A-Materials Science & Processing*, 70(4):425–429, 2000.

[61] P. F. Moulton. Spectroscopic and laser characteristics of Ti-Al_2O_3. *Journal of the Optical Society of America B-Optical Physics*, 3(1):125–133, 1986.

[62] P. M. W. French, J. A. R. Williams, and J. R. Taylor. Femtosecond pulse generation from a titanium-doped sapphire laser using nonlinear external cavity feedback. *Optics Letters*, 14(13):686–688, 1989.

[63] V S Ban and D A Kramer. Thin films of semiconductors and dielectrics produed by laser evaporation. *Journal of Materials Science*, 5:978–982, 1970.

[64] R. W. Dreyfus, F. A. McDonald, and R. J. Vongutfeld. Laser energy deposition at sapphire surfaces studied by pulsed photothermal deformation. *Applied Physics Letters*, 50(21):1491–1493, 1987.

[65] P.E. Dyer, S.R. Jackson, P.H. Key, W.J. Metheringham, and M.J.J. Schmidt. Excimer laser ablation and film deposition of Ti:sapphire. *Applied Surface Science*, 96-8:849–854, 1996.

[66] P.E. Dyer, J. Gonzalo, P.H. Key, D. Sands, and M.J.J. Schmidt. Studies of target materials and wavelength for laser ablation- deposition of Ti:sapphire. *Applied Surface Science*, 110:345–349, 1997.

[67] A.A. Anderson, R.W. Eason, M. Jelinek, C. Grivas, D. Lane, K. Rogers, L.M.B. Hickey, and C. Fotakis. Growth of Ti:sapphire single crystal thin films by pulsed laser deposition. *Thin Solid Films*, 300(1-2):68–71, 1997.

[68] A.A. Anderson, R.W. Eason, L.M.B. Hickey, M. Jelinek, C. Grivas, D.S. Gill, and N.A. Vainos. Ti:sapphire planar waveguide laser grown by pulsed laser deposition. *Optics Letters*, 22(20):1556–1558, 1997.

[69] L. M. B. Hickey and J. S. Wilkinson. Titanium diffused waveguides in sapphire. *Electronics Letters*, 32(24):2238–2239, 1996.

[70] L. M. B. Hickey, E. Martins, J. E. Roman, W. S. Brocklesby, and J. S. Wilkinson. Fluorescence of Ti^{3+} ions thermally diffused into sapphire. *Optics Letters*, 21(8):597–599, 1996.

[71] M. Jelinek, R.W. Eason, J. Lancok, A.A. Anderson, C. Grivas, C. Fotakis, L. Jastrabik, F. Flory, and H. Rigneault. Waveguiding pulsed laser deposited Ti : sapphire layers on quartz. *Thin Solid Films*, 322(1-2):259–262, 1998.

[72] P. Manoravi, P. R. Willmott, J. R. Huber, and T. Greber. Deposition of Ti : sapphire thin films by reactive pulsed laser ablation using liquid metals and oxygen. *Applied Physics A-Materials Science & Processing*, 69:S865–S867, 1999.

[73] P. R. Willmott, P. Manoravi, J. R. Huber, T. Greber, T. A. Murray, and K. Holliday. Production and characterization of Ti : sapphire thin films grown by reactive laser ablation with elemental precursors. *Optics Letters*, 24(22):1581–1583, 1999.

[74] H. Uetsuhara, S. Goto, Y. Nakata, N. Vasa, T. Okada, and M. Maeda. Fabrication of a Ti : sapphire planar waveguide by pulsed laser deposition. *Applied Physics A-Materials Science & Processing*, 69:S719–S722, 1999.

[75] C.N. Afonso, J.M. Ballesteros, J. Gonzalo, G.C. Righini, and S. Pelli. Rare-earth doped glass waveguides prepared by pulsed laser deposition. *Applied Surface Science*, 96-8:760–763, 1996.

[76] R. Serna and C. N. Afonso. In situ growth of optically active erbium doped Al_2O_3 thin films by pulsed laser deposition. *Applied Physics Letters*, 69(11):1541–1543, 1996.

[77] R. Serna, C.N. Afonso, J.M. Ballesteros, and A. Zschocke. Pulsed laser deposition for optical doping of active waveguide films. *Applied Surface Science*, 110:524–527, 1997.

[78] R. Serna, J. M. Ballesteros, M. J. de Castro, J. Solis, and C. N. Afonso. Optically active Er-Yb doped glass films prepared by pulsed laser deposition. *Journal of Applied Physics*, 84(4):2352–2354, 1998.

[79] R. Serna, M. J. de Castro, J. A. Chaos, C. N. Afonso, and I. Vickridge. The role of Er^{3+} - Er^{3+} separation on the luminescence of Er- doped Al_2O_3 films prepared by pulsed laser deposition. *Applied Physics Letters*, 75(26):4073–4075, 1999.

[80] K.E. Youden, T. Grevatt, R.W. Eason, H.N. Rutt, R.S. Deol, and G. Wylangowski. Pulsed-laser deposition of Ga-La-S chalcogenide glass thin-film optical wave-guides. *Applied Physics Letters*, 63(12):1601–1603, 1993.

[81] D. S. Gill, R. W. Eason, C. Zaldo, H. N. Rutt, and N. A. Vainos. Characterization of Ga-La-S chalcogenide glass thin-film optical wave-guides, fabricated by pulsed-laser deposition. *Journal of Non-Crystalline Solids*, 191(3):321–326, 1995.

[82] S. Mailis, A.A. Anderson, S.J. Barrington, W.S. Brocklesby, R. Greef, H.N. Rutt, and R.W. Eason. Photosensitivity of lead germanate glass waveguides grown by pulsed laser deposition. *Optics Letters*, 23(22):1751–1753, 1998.

[83] S. Mailis, C. Riziotis, J. Wang, E. Taylor, A.A. Anderson, S.J. Barrington, H.N. Rutt, R.W. Eason, N.A. Vainos, and C. Grivas. Growth and characterization of pulsed laser deposited lead germanate glass optical waveguides. *Optical Materials*, 12(1):27–33, 1999.

[84] S. Mailis, L. Reekie, S. Pissadakis, S. J. Barrington, R. W. Eason, N. A. Vainos, and C. Grivas. Large photoinduced refractive index changes in pulsed-laser- deposited lead germanate glass waveguides with controllable refractive index sign change. *Applied Physics A-Materials Science & Processing*, 69:S671–S674, 1999.

[85] K. G. Cho, D. Kumar, D. G. Lee, S. L. Jones, P. H. Holloway, and R. K. Singh. Improved luminescence properties of pulsed laser deposited Eu:Y_2O_3 thin films on diamond coated silicon substrates. *Applied Physics Letters*, 71(23):3335–3337, 1997.

[86] K. G. Cho, D. Kumar, P. H. Holloway, and R. K. Singh. Luminescence behavior of pulsed laser deposited eu : Y_2O_3 thin film phosphors on sapphire substrates. *Applied Physics Letters*, 73(21):3058–3060, 1998.

[87] M. B. Korzenski, P. Lecoeur, B. Mercey, P. Camy, and J. L. Doualan. Low propagation losses of an Er : Y_2O_3 planar waveguide grown by alternate-target pulsed laser deposition. *Applied Physics Letters*, 78(9):1210–1212, 2001.

[88] A. Huignard, A. Aron, P. Aschehoug, B. Viana, J. Thery, A. Laurent, and J. Perriere. Growth by laser ablation of Y_2O_3 and tm : Y_2O_3 thin films for optical applications. *Journal of Materials Chemistry*, 10(2):549–554, 2000.

[89] R. Chety, E. Millon, A. Boudrioua, J. C. Loulergue, A. Dahoun, and J. Perriere. Growth of $Ca_4GdO(BO_3)_3$ thin films by pulsed-laser deposition for nonlinear optical applications. *Journal of Materials Chemistry*, 11(2):657–659, 2001.

[90] G. Aka, A. KahnHarari, D. Vivien, J. M. Benitez, F. Salin, and J. Godard. A new non-linear and neodymium laser self-frequency doubling crystal with congruent melting: $Ca_4GdO(BO_3)_3$ (GdCOB). *European Journal of Solid State and Inorganic Chemistry*, 33(8):727–736, 1996.

[91] Z. Zhuo, Y. Zhou, E. Y. B. Pun, S. J. Zhang, Z. X. Cheng, and H. C. Chen. Analysis of optical waveguide formed in x-cut Yb : GdCOB crystal by He^+ implantation. *Optics Communications*, 181(4-6):313–316, 2000.

[92] P.A. Atanasov, R.I. Tomov, J. Perriere, R.W. Eason, N. Vainos, A. Klini, A. Zherikhin, and E. Millon. Growth of Nd : potassium gadolinium tungstate thin-film waveguides by pulsed laser deposition. *Applied Physics Letters*, 76(18):2490–2492, 2000.

[93] F. Qian, R.K. Singh, S.K. Dutta, and P.P. Pronko. Laser deposition of diamond-like carbon-films at high intensities. *Applied Physics Letters*, 67(21):3120–3122, 1995.

[94] Z. Zhang, P. A. VanRompay, J. A. Nees, R. Clarke, X. Pan, and P. P. Pronko. Nitride film deposition by femtosecond and nanosecond laser ablation in low-pressure nitrogen discharge gas. *Applied Surface Science*, 154:165–171, 2000.

[95] M. Okoshi, K. Higashikawa, and M. Hanabusa. Pulsed laser deposition of ZnO thin films using a femtosecond laser. *Applied Surface Science*, 154:424–427, 2000.

[96] S. Acquaviva, A. Perrone, A. Zocco, A. Klini, and C. Fotakis. Deposition of carbon nitride films by reactive sub-picosecond pulsed laser ablation. *Thin Solid Films*, 373(1-2):266–272, 2000.

[97] A. V. Rode, B. Luther-Davies, and E. G. Gamaly. Ultrafast ablation with high-pulse-rate lasers. part II: Experiments on laser deposition

of amorphous carbon films. *Journal of Applied Physics*, 85(8):4222–4230, 1999.

[98] E. G. Gamaly, A. V. Rode, and B. Luther-Davies. Ultrafast ablation with high-pulse-rate lasers. part I: Theoretical considerations. *Journal of Applied Physics*, 85(8):4213–4221, 1999.

[99] K. F. MacDonald, V. A. Fedotov, R. W. Eason, N. I. Zheludev, A. V. Rode, B. Luther-Davies, and V. I. Emel'yanov. Light-induced metallization in laser-deposited gallium films. *Journal of the Optical Society of America B-Optical Physics*, 18(3):331–334, 2001.

[100] A. V. Rode, M. Samoc, B. Luther-Davies, E. G. Gamaly, K. F. MacDonald, and N. I. Zheludev. Dynamics of light induced reflectivity switching in gallium films depositied on silica by pulsed laser depostion. *Optics Letters*, 26(7):441–443, 2001.

[101] I. Zergioti, S. Mailis, N.A. Vainos, C.P. Grigoropoulos, and C. Fotakis. Direct microdeposition of diffractive structures using femtosecond excimer laser. *Laser Physics*, 8(1):313–315, 1998.

[102] I. Zergioti, S. Mailis, N.A. Vainos, P. Papakonstantinou, C. Kalpouzos, C.P. Grigoropoulos, and C. Fotakis. Microdeposition of metal and oxide structures using ultrashort laser pulses. *Applied Physics A-Materials Science & Processing*, 66(5):579–582, 1998.

[103] S.J. Barrington, T. Bhutta, D.P. Shepherd, and R.W. Eason. The effect of particulate density on performance of Nd : $Gd_3 3Ga_5O_{12}$ waveguide lasers grown by pulsed laser deposition. *Optics Communications*, 185(1-3):145–152, 2000.

[104] M. Pollnau, R. P. Salathe, T. Bhutta, D. P. Shepherd, and R. W. Eason. Continuous-wave broadband emitter based on a transition-metal-ion-doped waveguide. *Optics Letters*, 26(5):283–285, 2001.

Chapter 4

Experimental and analytical techniques

4.1 Introduction

This chapter details most of the experimental and analytical techniques that have been used during the course of this thesis. Some techniques were more appropriate to discuss alongside the relevant work have been omitted from this chapter and are presented in later chapters.

4.2 Compositional analysis

In PLD it is desirable to fabricate a film that has the same stoichiometry as that of the bulk target and possesses a preferred crystal orientation. A broad range of analysis techniques are available to test for these conditions. It is, however, not always necessary to reproduce the exact stoichiometry as long as the film still performs the task for which it was grown. For this reason characterisation of Nd:GGG was restricted mainly to X-ray diffractometry and spectroscopic measurements to confirm it had grown as per previous experiments (on which more detailed composi-

tional analysis had been performed). Similarly, the growth conditions of lead germanate were altered to optimise its photosensitivity (measurement of which is described in section 5.4.2) as opposed to its composition.

4.2.1 Energy dispersive X-ray spectroscopy

Energy Dispersive X-Ray Spectroscopy (EDX) is usually incorporated into a Scanning Electron Microscope (SEM). The high energy electrons from the scanning probe of the SEM are used to excite the atoms in the material under observation. The excited state atoms will decay to the ground state producing X-rays that are characteristic of that particular atom. Deconvolution of the resultant X-ray data is complicated, especially for complex compositions but can give the approximate percentage composition of the different elements within the sample.

Due to many factors however, including re-absorbtion of the emitted X-rays, and sampling of substrate for thin ($\sim$1μm) films, EDX is a notoriously poor source of quantitative information. Absorption of the X-rays generated from light elements ($Z < 11$) by the detector windows is a further complication when working with oxide films. EDX should only be used if merely semi-quantitative analysis is desired as detailed in 5.3.2.

4.2.2 X-ray diffraction

X-ray diffraction (XRD) is possibly the most useful diagnostic tool for characterising PLD films. It is fast, convenient, cheap, non destructive and reveals much information about the film.

Figure 4.1 shows the layout of typical XRD apparatus.

Electrons are accelerated into a copper target to produced intense characteristic X-ray lines (see table 4.1). A nickel filter is commonly used to remove the CuK_β lines.

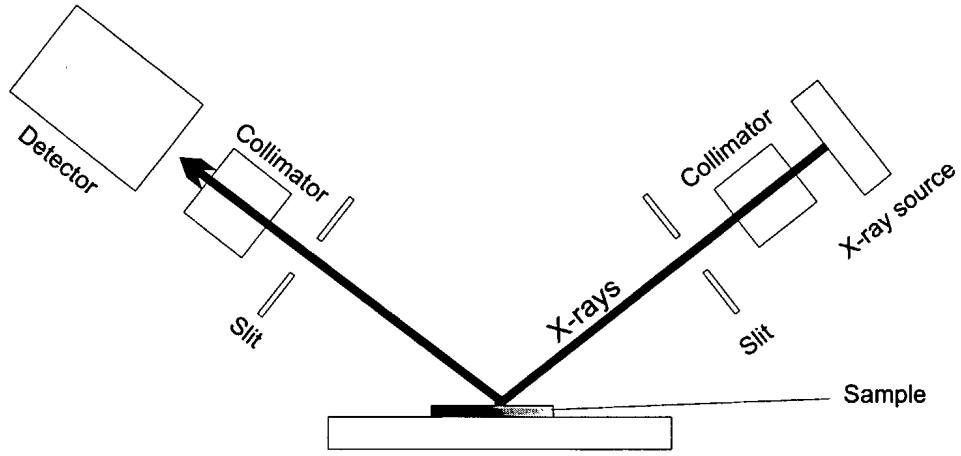

Figure 4.1: Simple X-ray diffractometer apparatus

Line	λ(Å)	E(keV)	Relative intensity
$CuK_{\alpha 2}$	1.544398	8.02779	50
$CuK_{\alpha 1}$	1.540562	8.04778	100
$CuK_{\beta 1,3}$	1.392218	8.90529	20

Table 4.1: Wavelength, energy and relative intensity for the 3 largest CuK X-ray lines.

The X-rays are collimated and directed towards the crystal target. The crystal and detector are rotated such that the source and detector maintain equal and opposite angles to the normal of the sample plane. X-ray diffraction is observed from the crystalline planes when the Bragg condition is met. The diffracted beam intensity is recorded at the detector as a function of angle.

Since a film may exist as a solid single crystal as opposed to a polycrystalline or powdered sample, it is possible that diffracted X-rays from the sample will not be aligned to the detector. To compensate for this the sample is rotated once during the course of measuring a particular angle. It is important that an integer number of complete rotations be performed during a measurement or aliasing effects may be seen.

By comparing the resultant scan with the powder diffraction databases that are available it is possible to discern the phase and orientation of the crystal. By measuring the full width at half maximum (FWHM) of the diffraction peaks a measure of crystal quality can also be obtained. For instance a broad peak measured in Nd:GGG can imply two possibilities: A slight discrepancy between the molar ratio of the bulk sample with that of the PLD grown film (usually a Ga deficiency) or a high particle density (see figure 8.6 in chapter 8). Optical microscopy can eliminate or confirm the latter.

4.2.3 Absorption spectroscopy

Absorption spectroscopy in bulk crystals is fast and simple and by comparison with known databases can give you insight into the composition of the sample. In waveguides, however, it is more complicated. Ideally waveguide absorption would be measured through the waveguide but this is not trivial due to difficulties in launching white light into the waveguide. Here we have opted for the easier process of launching through the face of the waveguide and background correcting for the presence of

the substrate. Etalon effects due to the thin film and the short interaction lengths give rise to further complications, so these results must be interpreted with care.

4.3 Surface morphology analysis

As discussed in chapter 8 the surface morphology of the film is of great importance to the quality of the final device. For the work presented in this thesis it was studied with the following techniques.

4.3.1 Atomic force microscopy

An atomic force microscope (AFM) allows the surface topography to be easily studied at a resolution that was only previously accessible by electron microscopes. Figure 4.2 below shows the basic setup for an AFM.

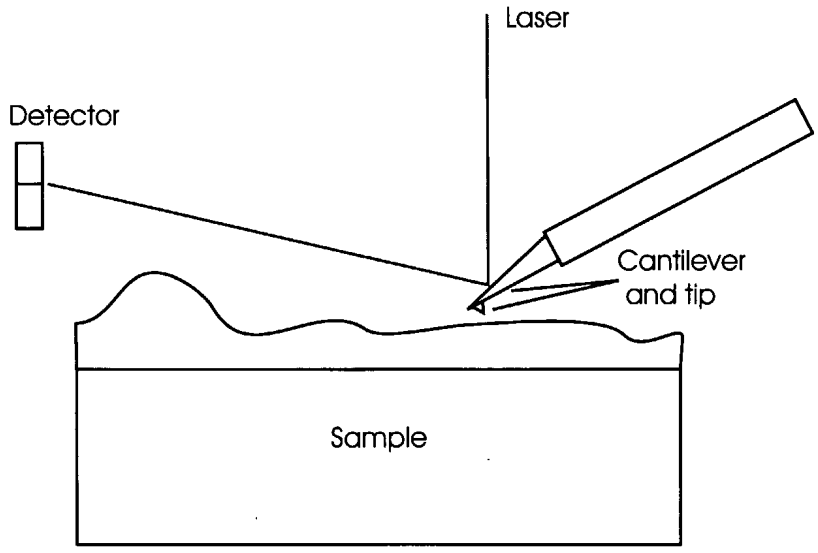

Figure 4.2: Simple Atomic Force Microscope Set-up.

The cantilever is a flexible reflective structure usually etched out of silicon nitride. It contains a tip which is dragged across the surface of the sample either by moving the sample base or the tip with piezoelectric actuators. The changing topology of the surface causes the tip to rise and fall, which in turn flexes the cantilever. This alters the angle the laser reflects off the cantilever, and thus its position on the detector. A quadrant detector ensures very small changes in position can be detected. The vertical resolution of the AFM is on the order of $\sim$ nm. The spatial resolution in the plane of the sample is limited by, and is of the same order as, the width of the tip. Tip widths can be as low as 10nm at their point.

The limiting factor of the AFM is the maximum distance over which it can scan. As the tip is moved by piezoelectric stacks the maximum field of view in one scan is typically 40µm $\times$ 40µm . Location of small features not visible by the eye can therefore be time consuming and difficult. This also renders AFM impractical for counting particulates.

4.3.2 Surface profiler

To ascertain the uniformity of the film thickness an interferometric surface profiler was utilised (Zygo NewView 5000 3-D Surface Profiler). This device (as shown in Figure 4.3) is essentially a calibrated interferometer. Coherent light is incident on the sample surface and reflected back to a CCD where it is combined with a reference beam to build an interference pattern. Computer analysis of the resultant interference pattern generates an accurate 3D image of the sample surface.

For the image shown in chapter 6 a Michelson objective was used, which is a microscope objective with a built-in reference arm.

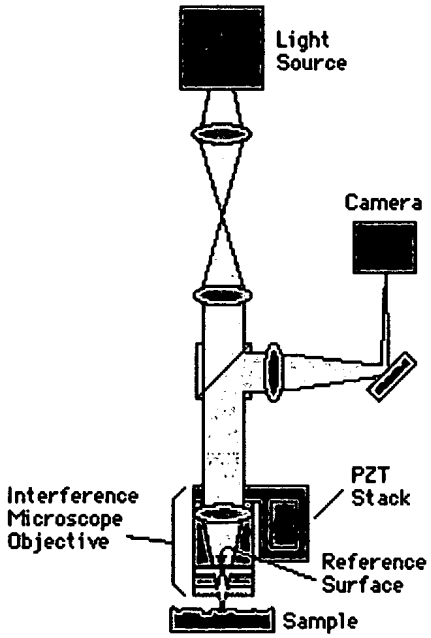

Figure 4.3: Schematic of a surface profiler.

4.3.3 Optical microscopy

For studying the particle density of the waveguides used in chapters 8 and 9 an optical microscope was used as this could easily resolve the particulates generated in PLD. The camera was connected to a PULNIX 2010 CCD camera which could take photos of resolution 770 $\times$ 580 pixels.

For each image taken of the film a corresponding control image is taken to compensate for particulates observed that are not on the sample surface (i.e they are actually dust on elements in the microscope. These elements cannot be cleaned due to their position or frailty). The control image is simply a completely unfocussed image of the object.

These images are imported into an image analysis package where the control image is inverted and added to the sample image to eliminate those particulates not generated from the sample. The resultant image is then inverted again and a rolling background subtraction is performed. This essentially performs a fourier analysis of the image and removes the low frequency components (the slowly changing background) whilst ignoring

the higher frequency components (the particulates). The background is now zeroed and the image is thresholded, i.e leaving a monochrome (black and white) image with the background black and the particulates white. This image is now suitable for particle analysis where the size and number density of particulates can be mapped.

4.4 Waveguide techniques

In this section some of the techniques used for waveguide analysis are described.

4.4.1 Waveguide preparation

The waveguides used in this study are typically 10mm wide, 2mm long, between 2μm and 8μm thick and are grown on a 1mm thick substrate. The small dimensions require great care when polishing to ensure both ends are parallel to each other in both the horizontal and vertical plane.

The waveguides are arranged in a stack that can contain up to 10 guides. These are glued together using silver paint and are fixed to a polishing jig with wax. One side of the stack is polished optically flat. The stack is then carefully rotated by heating up the wax so the stack is free to move but with the guides still held in place with respect to each other by the silver paint. The second side is then lapped until the surface is roughly flat and a reflection can be seen. The jig can then be removed and the stack can be probed with a He:Ne Laser to check for parallelism of the front and back surfaces by observing the divergence of the two reflected beams. Adjustments can then be made and the stack is re-lapped and polished to an optical flatness.

4.4.2 Launch configuration

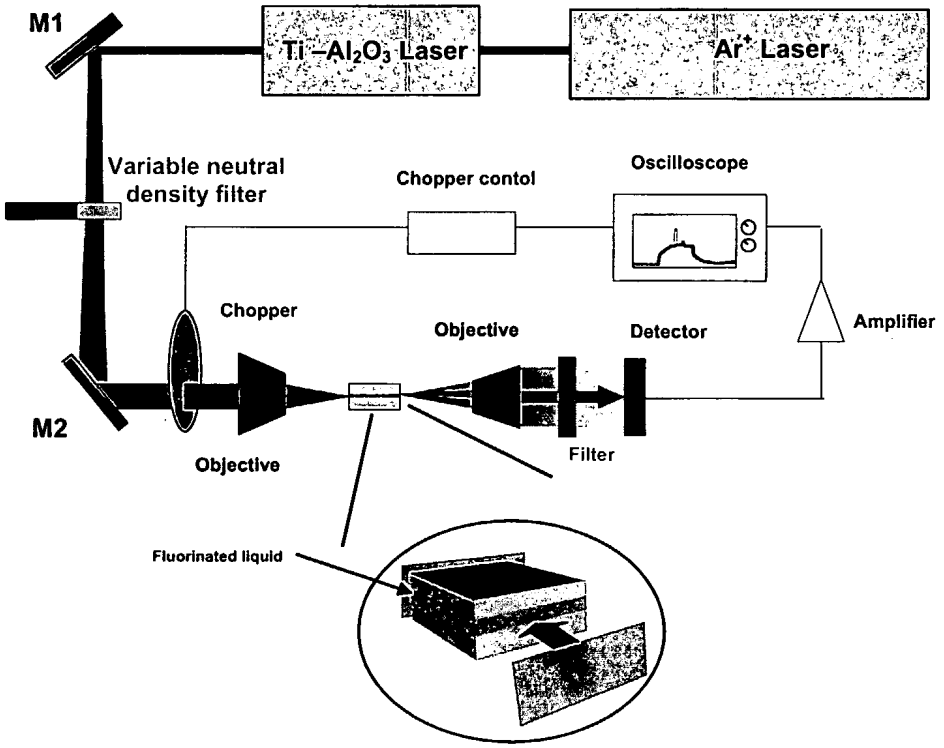

Figure 4.4: Pumping configuration.

The pumping configuration can be seen in figure 4.4. The Nd:GGG waveguides were pumped using an Ar^+ pumped Ti:sapphire laser tuned to 808nm. The beam from the Ti:sapphire was first passed through an optical chopper which enabled the lasing action of the waveguides to be more easily distinguished from fluorescence. If just the pump light is detected (i.e the pump beam is launched into the undoped substrate) a simple square wave is observed (with $\sim$1 µs decay time). When the beam is launched into the doped waveguide a fluorescence decay is now observed on the trailing edge of the square wave (see section 4.4.7) as seen in figure 4.5. When lasing action occurs in the guide this is clearly seen as a spike in the fluorescence superimposed on the curve in figure 4.5.

The waveguide is mounted on a stage allowing 2 directional and 2 angular degrees of freedom. The waveguide end face is positioned in the pump

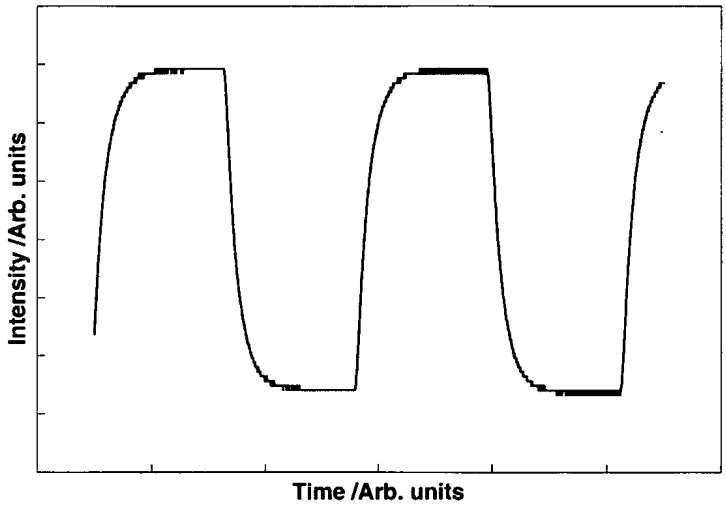

Figure 4.5: Observation of fluorescence decay

beam and back reflections from the waveguide end are used to align the pump beam normal to the end face. Two mirrors coated for high reflectivity at the lasing wavelength and high transmission at the pump wavelength are then positioned on the waveguides and are held in place by a small drop of Fluorinert liquid.

Light is coupled into the waveguide using microscope objectives, the focal length of which is optimised for the size of the waveguide. The input coupler is mounted first, whereupon fringes can be observed exiting the waveguide (Lloyd's mirror effect [1]). By use of a 3 axis stage (x, y, z) the objective is positioned at the point where the fringes have greatest width. This corresponds to the point of greatest launch efficiency. The output coupler can now be positioned so the detection of the fluorescence or any laser signal is possible.

4.4.3 Threshold measurement

Maximising the fluorescence signal by careful adjustment of the input coupler and waveguide mount stages will initiate lasing within the guide. This assumes the pump power lasing threshold of the particular waveg-

uide is below the incident pump power, initially set at the maximum output power of the Ti:sapphire laser (~700mW). Once lasing is achieved, the waveguide position is then further optimised to produce the strongest output signal. A variable neutral density filter is then used to reduce the pump beam power to the point at which lasing is only just possible. The input power is then measured and recorded as the threshold power for lasing. This process is repeated at all points along the waveguide face.

4.4.4 Loss measurements

Losses in the lead germanate films grown in chapter 5 were ascertained by the two methods described in this section.

4.4.4.1 Sliding prism technique

The sliding prism technique for determination of loss within a waveguide [2] utilises prism coupling [3] to launch light into the guide. Figure 4.6 shows the basic set-up for this technique.

Compression of a prism onto the waveguide surface reduces the air gap between the prism and surface to such a distance that the evanescent fields protruding from the prism and guide overlap. Under the right conditions an input beam launched at the correct angle into the input prism can couple directly into the active layer of the waveguide. The requirements for this condition are that the prism be of a higher refractive index than the guide (typically rutile prisms are used for which n_e = 2.87 and n_o = 2.58) and that the propagation constant of the guided wave is equal to the propagation constant along the prism/air interface. Since the propagation constant in the waveguide defines the mode of the guided wave this requirement means, in practice, that different input angles couple into different waveguide modes.

An identical prism attached to the other end of the waveguide will act as

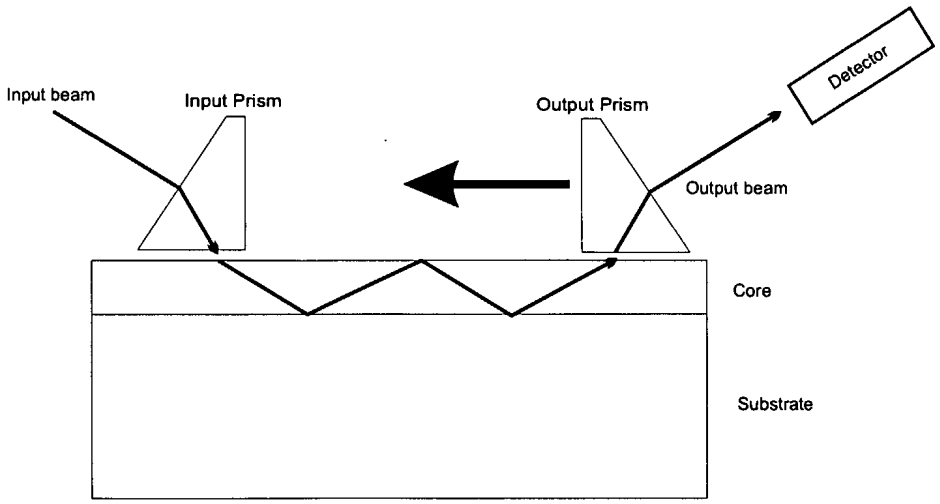

Figure 4.6: Apparatus for loss measurement with the sliding prism technique

an output coupler. Detection of a signal from the output coupler prism should give a value equal to the input power minus the waveguide loss and the input/output coupling losses. By sliding the output coupler prism towards the input coupler, several loss measurements can be made along the waveguide, allowing the elimination of the unknown coupling losses. A value of the waveguide scattering loss can then be obtained. This assumes, though, that the output coupling loss is constant at each measurement, this is not always the case. The output coupler prism tends to damage the waveguide surface, therefore this prism must be moved *towards* the input coupler prism so the damage does not effect the loss measurement. Except with exceptionally hard films, the prism sliding loss measurement technique a destructive process.

4.4.4.2 Streak imaging

Streak imaging is a more recent method of determining the optical loss in a waveguide [4]. Light is coupled into the guide using a rutile prism, as in

the sliding prism technique. A CCD camera is then used to capture an image of the resultant streak of light that is visible due to scattering from the waveguide. The intensity loss measured in the streak as a function of distance travelled within the guide is then used to determine the loss within the guide. This method is less destructive than the previous technique and quicker to perform. Getting quantitative information from a CCD camera, however, is difficult due to their non linear response and often requires rigorous calibration.

4.4.5 Laser mode measurements

Measurement of the spatial profile of the laser output is necessary to establish the number of modes that are lasing and for calculations that require the output beam waist.

This is achieved by focusing the output signal so that the beam waist is incident upon a Cohu 4800 CCD array in which the pixel spacing has previously been calibrated. Using the CCD and beam view analyser software (Big Sky Software and Coherent) it is possible to monitor the output beam profile in real time. It is also possible to get an accurate measurement of the size of the beam waist allowing the output mode size to be calculated by working backwards using Gaussian optics.

The input mode size w_0 can be determined from the input coupler focal length f,

$$w_0 = \left(\frac{\lambda f}{w\pi}\right) \tag{4.1}$$

where w is is the input beam waist and λ is the pump wavelength.

4.4.6 Fluorescence and lasing spectra measurements

Fluorescence measurements from waveguides are useful to confirm the incorporation of the lasing ions within the film and possible information about their valence state. A measurement of the fluorescence intensity versus wavelength be compared with both previous bulk and waveguide results (assuming they are available) to confirm the ion's incorporation into the lattice structure. Fluorescence measurements can also be taken along the length of the waveguide to gauge the homogeneity of the lasing ion distribution within the waveguide.

The output signal from the waveguide is first filtered to remove pump light. The fluorescence and lasing spectra are measured with an EG&G Princeton Applied Research model 1235 digital triple grating spectrograph. This device uses three gratings (150,600,1200 lines/mm) to convert spectral information into a spatial profile which is collected by a CCD array. The spectrograph has been previously calibrated with helium, argon and neon discharge lamps. Furthermore, it is computer controlled and works in real time, which is a useful feature for establishing whether the waveguide is lasing or not. The lasing spectrum has a much narrower linewidth than the fluorescence spectrum therefore the spectrograph can be used to confirm lasing action.

4.4.7 Upper state lifetime measurement

Measurement of the upper laser state lifetime is another method of comparing newly fabricated waveguides to previously grown samples and to bulk materials. As described in section 7.6 the fluorescence lifetime can confirm which laser transition is operating. The experimental setup detailed in figure 4.4 already allows for lifetime measurements to be taken. The optical chopper is rotated sufficiently fast so the on/off transition time is negligible compared to the fluorescence lifetime. Likewise the photode-

tector, amplifier and oscilloscope have a sufficiently fast response time not to affect the measurement. By using a digital oscilloscope the fluorescence decay can be captured after the chopper has blocked the pump source. The data is then transferred to a computer where an exponential decay curve can be fitted to ascertain the decay constant.

4.5 References

[1] E. Hecht. Chapter 9 - interference. In *Optics*, pages 345–347. Addison Wesley Publishing Corp. Inc., 2nd ed edition, 1974.

[2] H. P. Weber, F. A. Dunn, and W. N. Leibolt. *Applied Optics*, 12:755, 1973.

[3] R Ulrich and R Torge. Measurement of thin film parameters with a prism coupler. *Applied Optics*, 12(12):2901–2908, 1973.

[4] Y. Okamura, S. Yoshinaka, and S. Yamamoto. Measuring mode propagation losses of integrated optical- waveguides - a simple method. *Applied Optics*, 22(23):3892–3894, 1983.

Chapter 5

Photosensitive lead germanate layers

5.1 Introduction

Photosensitive glasses represent a fruitful area for potential applications in optical communications and photonics. The most commonly studied case of light induced refractive index change is that of germanium doped silica. Photosensitive germano-silica fibres and planar waveguides are currently used for fabrication of many devices used in the telecommunications industry. However, the small refractive index changes that can be obtained in untreated (non hydrogenated) germano-silica glasses may limit the performance of devices such as direct UV written optical circuits. The demand for larger refractive index changes is ever present and hence the search for new glass materials having the desired optical and chemical properties is increasing.

Lead germanate glasses are good candidates for highly photosensitive materials mainly because of their large absorption in the UV spectral region. The maximum phonon energy of the glass composition studied in this work is 810 cm^{-1}, which is a low phonon energy compared to many other

glasses. Lead germanate glass is therefore an important low phonon energy laser host, that possesses a range of desirable optical properties. Efficient 1.9μm lasing action has been demonstrated for these glasses with Tm^{+} doping [1] and the intrinsic infrared transmission can extend up to 5.5μm [2]. An active length of only 3 cm is required, and hence lead germanate planar integrated optical devices are particularly suitable for applications in LIDAR and medicine. The refractive index of lead germanate glasses is high, with a bulk value of ($n_D = 1.812 \pm 0.005$), this is also attractive for non-linear optical applications involving $\chi^{(3)}$ processes.

This chapter reports on the growth of lead germanate optical waveguides by PLD and studies the photosensitivity exhibited by the material. The work reported in this chapter is the result of an ongoing collaboration between the University of Southampton and FORTH in Greece.

5.2 Growth of lead germanate

5.2.1 Target composition

The target glass composition in mole% is $55GeO_2$ - 20PbO- 10BaO- 10ZnO - $5K_2O$, with some targets having a partial substitution of Al^{3+} for Zn^{2+}. The bulk glasses were prepared from anhydrous oxide powders for Ge, Al, Zn, Pb, and anhydrous carbonate powders for Ba and K. All chemicals were of common analytical grade except for GeO_2, which was of electronic grade (99.999% purity, Aldrich Chemicals). Glass batches in quantities of 150-200g of powder were mixed for at least half an hour, in a clean glass container, mounted on a rotating lathe. Batches were then melted in a platinum crucible, placed in an electrically heated furnace containing an air atmosphere, at temperatures of between 1000 °C and 1250 °C depending on the glass. The melts were kept well stirred with a silica rod to achieve homogeneous mixing and later refined to remove bubbles. The refined

Parameter	KrF depositions	ArF depositions
Laser pulse energy	160mJ	190mJ
Spot size on target	2.5 mm × 8.5 mm	2 mm × 6 mm
Laser energy density	0.75 Jcm^{-2}	1.6 Jcm^{-2}
Target-Substrate distance	8 cm	8 cm
Pulse repetition rate	20 Hz	8 Hz
Substrate Temperature	Room temperature	Room temperature
Background Pressure	3.5×10^{-5} mbar	3.5×10^{-5} mbar
Oxygen ambient pressure	5.0×10^{-3} - 1.0×10^{-1} mbar	1.5×10^{-2} - 5.0×10^{-2} mbar
Oxygen flow rate	Not recorded	0.6 - 3.1 sccm
Number of pulses	24 000	21 600-63 000
Film thickness produced	1.8 - 2.7 μm	1.2 - 12 μm

Table 5.1: Parameters for deposition

glass-melts were removed from the furnace at 1150 °C and cast into a pre-warmed stainless steel mould, before being annealed in a muffle furnace at ~500 °C .

5.2.2 Deposition parameters

Films were fabricated using the above mentioned lead germanate glass targets in a background oxygen gas atmosphere. The chamber was pumped down to a base pressure of $\sim 10^{-5}$ mbar, and background oxygen was then admitted. The range of background (molecular) oxygen pressures investigated was varied between 5.0×10^{-3} mbar and 1.0×10^{-1} mbar. The excimer laser used for ablation was a Lambda Physik LPX 200, operating with either KrF or ArF gas mixtures giving ablation wavelengths of 248nm and 193nm respectively. All other deposition parameters of interest are listed in table 5.1.

As set out in section 6.2 both the target and substrate were asynchronously rotated in order to achieve a degree of radial uniformity. Film thicknesses were measured using profilometers (Tallystep, Alphastep), across a step region introduced at the edge of each film. Although the deposition times,

and all other conditions, were nominally identical for each growth run (apart from varying oxygen pressures for example), the resultant film thicknesses obtained varied between 1.8μm and 2.7μm . For equal deposition times, thicker films were produced at lower ambient oxygen pressures, this is to be expected due to the reduced mean free path of the plasma at higher background pressure.

Cleaned microscope slides and fused silica discs were used as substrates. At critical values of oxygen pressure, films were grown that showed a brown-clear-yellow colour trend on a single substrate. Although growth on heated substrates is routinely performed for crystalline film growth, no temperature other than room temperature was used here. For multi-component targets (such as the glass here) stoichiometric variations between target and film can be exacerbated when deposited at elevated temperatures. Since the film photosensitivity is believed to be due largely to the inherent strain the film acquires during growth, heated substrates will only reduce strain in the film and, in turn, decrease photosensitivity.

5.3 Properties of lead germanate

5.3.1 Material appearance

The films obtained show distinct colour variations, depending on the ambient oxygen pressure used during the growth. For low oxygen pressures ($\sim 10^{-3}$ mbar) the films produced were brown in colour. At higher pressures ($\sim 10^{-2}$ mbar) uncoloured films were produced, while for the highest pressures ($\sim 10^{-1}$ mbar) pale yellow to deep yellow films were grown. Apart from those grown at the very highest oxygen pressure (which were opaque and flakey in character) all of the films showed good adhesion to the substrates. A range of as-deposited films are shown in figure 5.1.

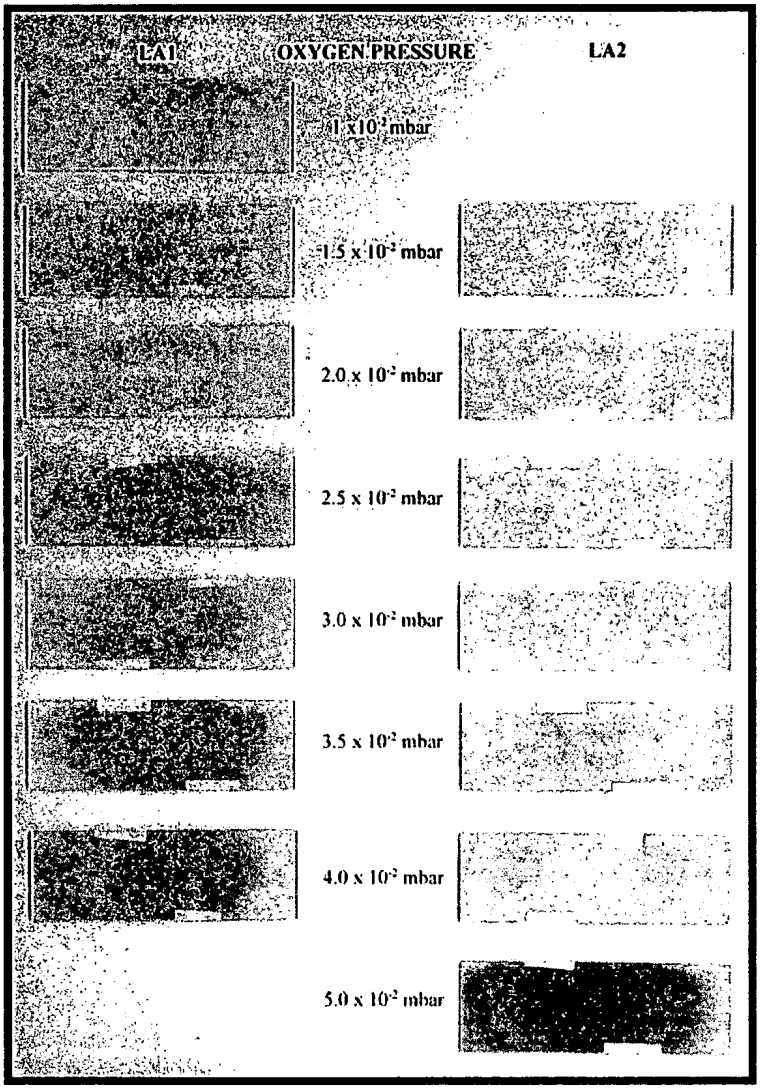

Figure 5.1: Lead germanate film appearance under different oxygen pressures. All films here were grown with 248nm laser radiation. Labels LA1 and LA2 refer to slightly different target compositions.

The films show a systematic difference in material appearance, as seen with atomic force microscopy (AFM) surface topographic scans, dependant on the excimer laser wavelength used for growth. Using 248 nm excimer deposition, films composed of macroscopic sized particles (~µm scale) were grown. The films possessed a high level of internal scattering and therefore losses were difficult to measure. 193 nm excimer laser deposition however, produced transparent, smooth films, with dramatically improved optical properties. A slightly discontinuous element is still present in the films grown at 193nmm but it is far less apparent than those grown at 248nm. This wavelength dependant topology variation has also been observed previously but to a more marked degree, during earlier (unreported) experiments at FORTH on the growth of phosphate glass films.

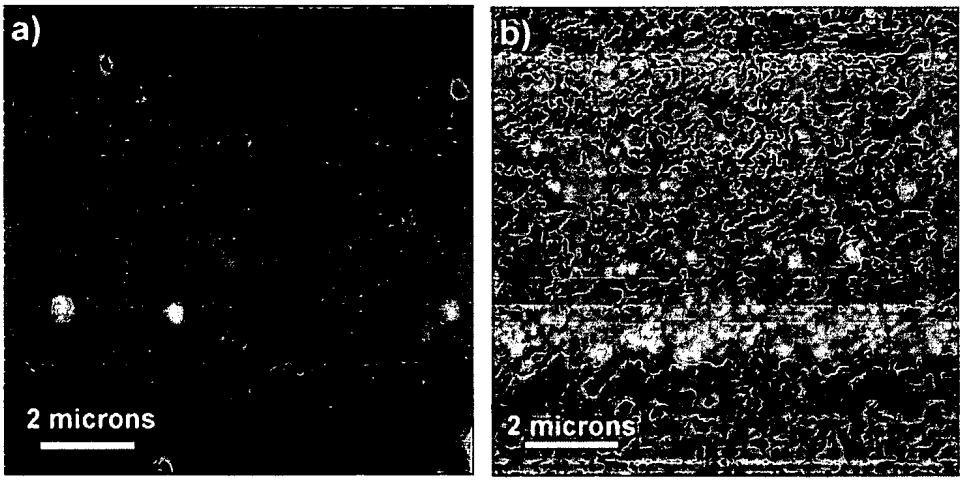

Figure 5.2: (a) AFM scan of the film surface for a 193 nm excimer laser PLD grown film. Note the apparent smooth surface, with < micron sized individual particulates present. (b) AFM scan of the film surface for a 248 nm excimer laser PLD grown film. The scan here shows that the surface is composed of densely packed sub-micron sized glass particles.

Figure 5.2 shows AFM scans for 10µm × 10µm areas of films grown using

193 nm and 248 nm excimer laser deposition. It is clear that while figure 5.2(a) shows a fairly uniform, continuous surface, with only a few isolated particulates, figure 5.2(b) exhibits a much more discontinuous surface, composed almost entirely of an assembly of particles. A count of particulates was performed for the films grown using 193 nm excimer deposition only. An area of 100μm by 100μm was selected and using image processing as detailed in section 4.3.3 a histogram of particulate size distribution was compiled. The results reveal that the mean size of particulate lies between 0.2 and 0.4μm , with very few particulates of size greater than 1μm present. Typical values of particulate densities were relatively high at around 6-7 $\times 10^6$ particulates cm^{-2}.

5.3.2 Characterisation of film properties

Figure 5.3 shows spectrophotometer traces of a set of films grown using 248 nm excimer laser deposition, within an oxygen pressure range of 1.5 $\times 10^{-2}$ mbar to 4 $\times 10^{-2}$ mbar. These films varied in colour from clear, to pale yellow. The short wavelength absorption edge is seen to shift to progressively higher wavelengths as the oxygen pressure increases. The oscillatory behaviour seen is due to etalon effects within the thin glass layer. Figure 5.4 shows the value of the absorption coefficient, derived from the traces in figure 5.3, and evaluated at a wavelength of 400 nm, as a function of oxygen pressure. This value of wavelength was chosen as it falls conveniently between the absorption edge and region of high transparency. The data has been corrected for the varying film thickness of the samples (as mention above), this was deduced via interference fringe analysis.

Figures 5.5 and 5.6 show similar results for films grown with 193nm excimer laser deposition. While the trend is similar, the transmission losses of the 193 nm grown films are systematically lower than those grown using 248 nm excimer deposition.

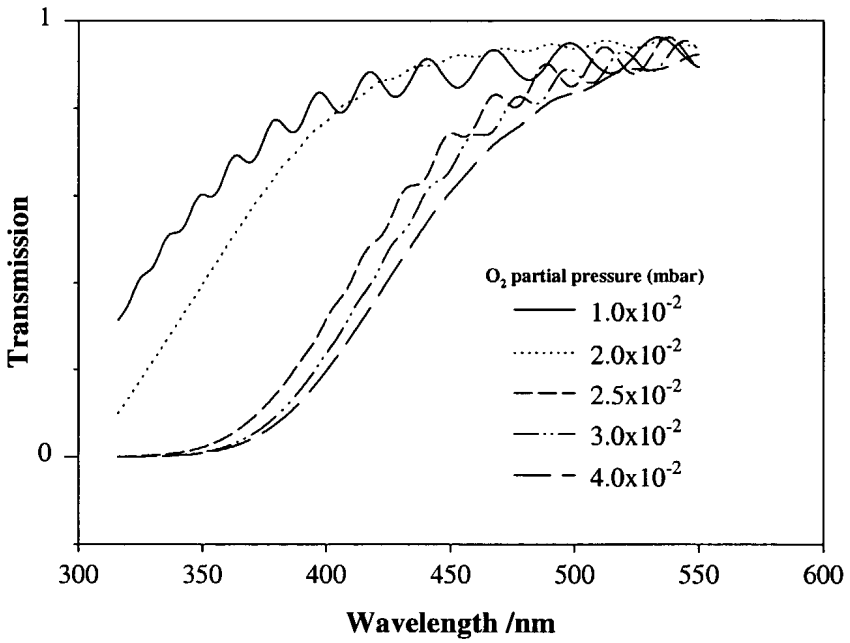

Figure 5.3: Spectrophotometer traces of films grown using 248 nm excimer laser deposition.

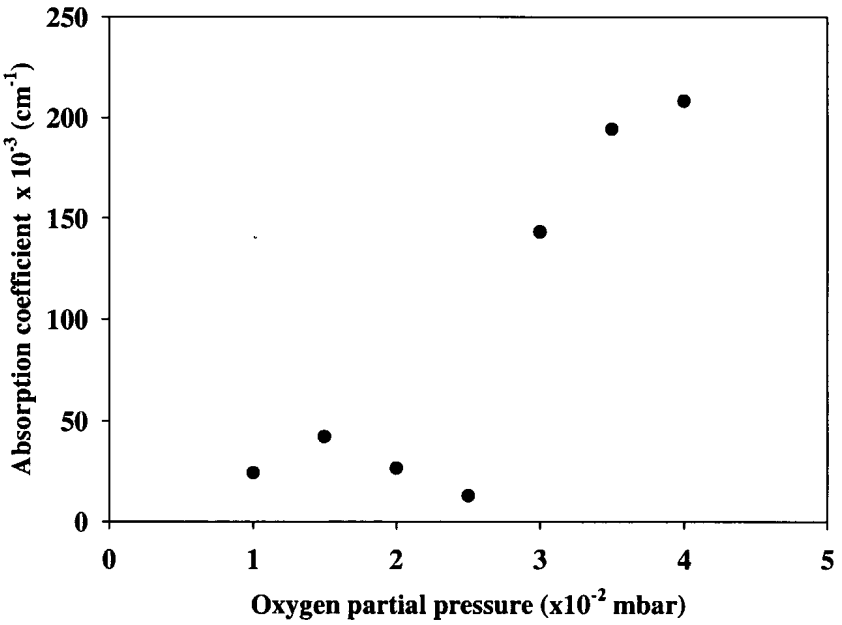

Figure 5.4: Absorption coefficient, at λ = 400 nm, against oxygen partial pressure during film growth with a 248 nm excimer laser.

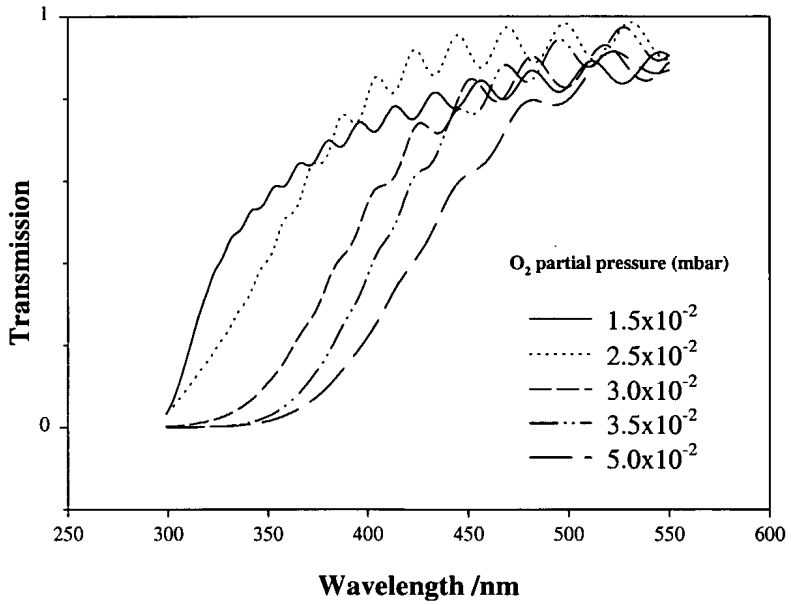

Figure 5.5: Spectrophotometer traces of films grown using 193 nm excimer laser.

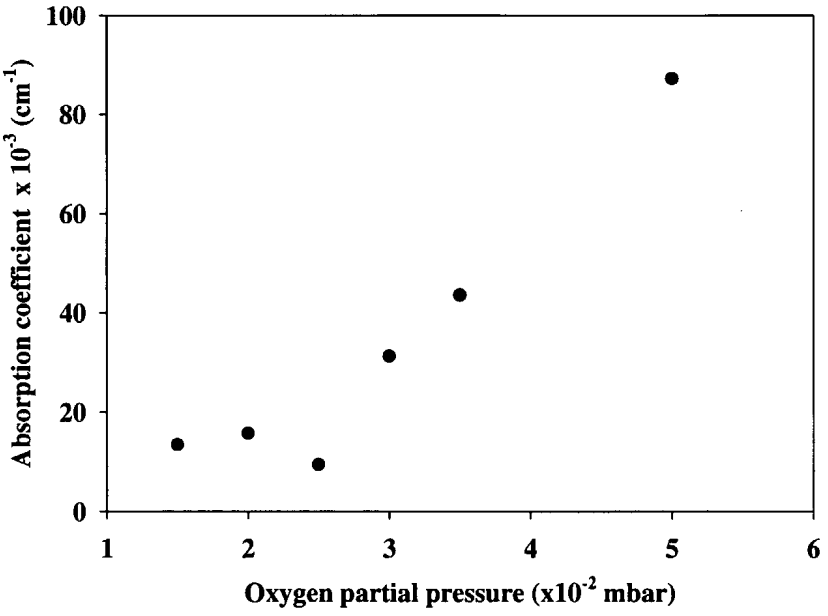

Figure 5.6: Absorption coefficient, at λ = 400 nm, against oxygen partial pressure during film growth with a 193 nm excimer laser.

Waveguide loss measurements were performed on the films produced. All guides were multimode as the index difference between film and substrate is large (~0.3), and the guides are ~2μm thick. Losses were measured by both the sliding prism [3] and imaged streak technique [4] (see section 4.4.4. With the second method, a rutile right-angle prism was used to couple He-Ne laser light into the waveguide. The streak of light was imaged by a lens onto the surface of a detector. Measurements of the scattered power were made at various distances along the waveguide, as shown in figure 5.7. The fit is a least squares best fit curve. Inferred losses for this film, which was grown at an oxygen partial pressure of 3.5 $\times 10^{-2}$ mbar, are 4.5 dBcm^{-1}. Figure 5.8 shows the final loss results for 5 such films, grown using 193 nm excimer laser deposition under different partial pressures of oxygen. The losses measured vary between 4 dBcm^{-1} and 7 dBcm^{-1} . These are rather high values, possibly due to the high particulate density, the slightly discontinuous nature of the film and inhomogeneous film thickness. Annealing was carried out on some of the films, but this had the adverse affect of reducing, or even eliminating, the photosensitivity in the deposited layer.

The above losses were measured on films grown *before* off-centre rotation was introduced as described in section 6.2. Films were also grown from ~1wt% Nd doped glass, using 248 nm excimer laser deposition. For these films, the substrate rotation axis was offset by ~ 1.5 cm in the lateral direction, with respect to the target rotation axis. Losses were measured at between 2.1 dBcm^{-1} and 3.4 dBcm^{-1} using the sliding prism technique.

The observable differences in colour between the films is a result of several factors. Quantitative energy dispersive x-ray analysis (EDX) measurements have been performed using a JEOL JSM-6400 scanning electron microscope with a PGT IMIX EDS system, on two samples grown at the extrema of the oxygen pressure range investigated. Interpretation of the results is somewhat complicated due to the different thickness of the two films examined, and also due to the presence of the substrate (borosili-

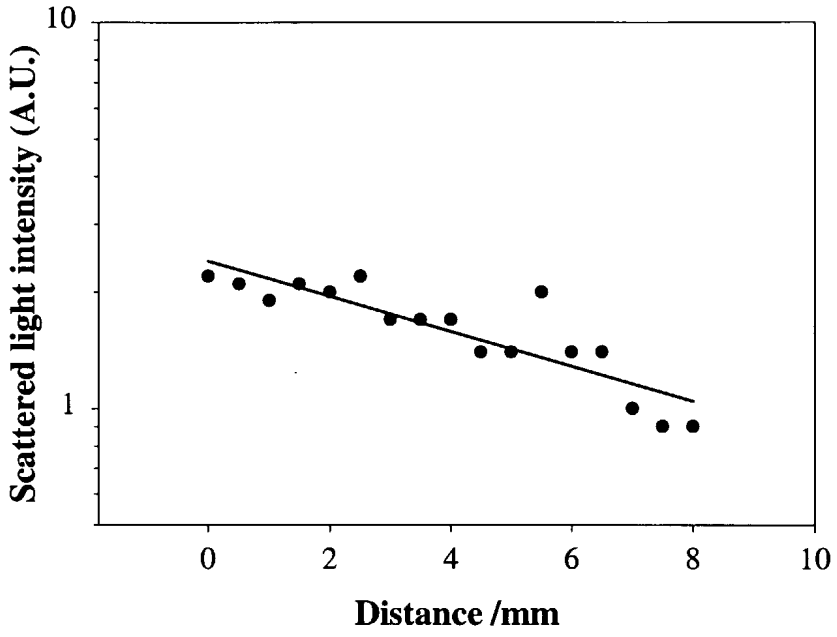

Figure 5.7: Waveguide loss measurement results obtained using the imaged streak technique.

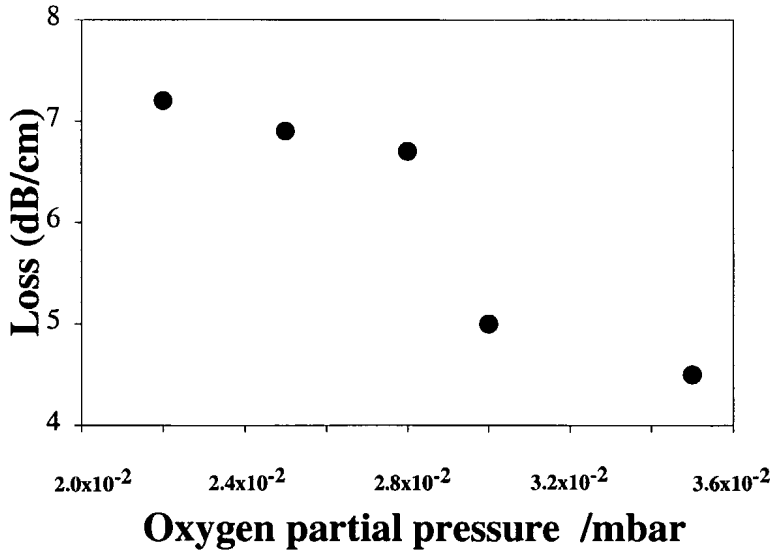

Figure 5.8: Waveguide loss results for films grown using 193 excimer laser deposition, as a function of the oxygen partial pressure during growth. Higher pressure leads to lower losses within the pressure region investigated.

cate glass), which also contains oxygen. What is apparent however, is that there is a systematic difference between the percentage of oxygen in the two films examined. Care needs to be exercised here however, as the accuracy of light element analysis is notoriously poor using EDX. Using data that has been normalised to remove the oxygen background signal from the substrate, we find that there is almost 50% more oxygen in the film grown at a partial pressure of 3.5×10^{-2} mbar, than the one grown at 1×10^{-2} mbar. By comparison, the EDX data for germanium and lead contents show only a difference of $\leq 10\%$ between the two films. The dramatic change in oxygen content implied by EDX is supported by the change in colour observed in the films grown at different oxygen pressures. The colour of the films can vary from dark brown to pale yellow, which suggests a change in oxidation state of the the lead contained within the film, which in turn suggests a large change in oxygen content.

5.4 Photosensitivity of lead germanate

5.4.1 The cause of photosensitivity

Ultraviolet light, particularly at the defect absorption bands (240nm), can have a pronounced affect on the local refractive index of germanium doped silica glass. The same general behaviour is also observed in these lead germanate glass films, where the oxygen content, varied during the PLD growth process, has a pronounced effect on the material photosensitivity.

It has long been believed that the photosensitivity in germanate glasses is critically dependent on the bond structure with respect to the germanium-oxygen co-ordination behaviour. This is usually refered to as the 'colour centre' model [5–7]. The exact mechanism underlying the colour centre model is the subject of intense debate and involves complex photochemistry which is not within the scope of this thesis. Much of the compu-

tational work based on this model yields theoretical values of refractive index change that can be an order of magnitude lower than that which has been observed in practice. More recent work indicates that the refractive index change may be due to structural transformations within the guide [8–10]. Of particular interest is the model of refractive index change by stress relaxation proposed by Sceats *et al* [10]. The refractive index change measured in our devices is one the highest reported for germanium based glass systems and we believe this is largely due to the deposition process itself. In depositions where the substrates are kept at room temperature the developing film does not have sufficient surface mobility to migrate into states of lower potential energy. This can result in a large build up of stress in the as-deposited film which could explain the large refractive index changes. It should be noted however, that characteristic colour centre absorption bands are observed in these films and that both positive and negative refractive index changes can be obtained. This implies there is more than one mechanism present in generating the refractive index change.

5.4.2 Measurement of photosensitivity

The method used for the quantitative measurement of the photoinduced refractive index changes Δn was the measurement of the diffraction efficiency for diffraction gratings recorded in the material as further discussed below. It is straightforward to calculate the value of Δn achieved for films of known thickness, using the standard diffraction grating expression [11]:

$$\eta = tanh^2 \left(\frac{\Delta n \pi d}{\lambda cos\theta} \right)$$

Where η is diffraction efficiency, d is the film thickness, and λ is the wavelength of the incident light. If, however, the absorption depth of the film at the writing wavelength is appreciably smaller than the actual film thickness, then an effective thickness, d_{eff}, must be used, as it is only this re-

duced thickness that contributes to the observed diffraction effects. The method of establishing d_{eff} is described later.

The recording of diffraction gratings was achieved either by using an interferometric arrangement or a π-phase mask, depending on the spatial-temporal coherence characteristics of the sources used for recording. The use of a π-phase mask enables recording using sources with poor spatial-temporal coherence such as excimer lasers.

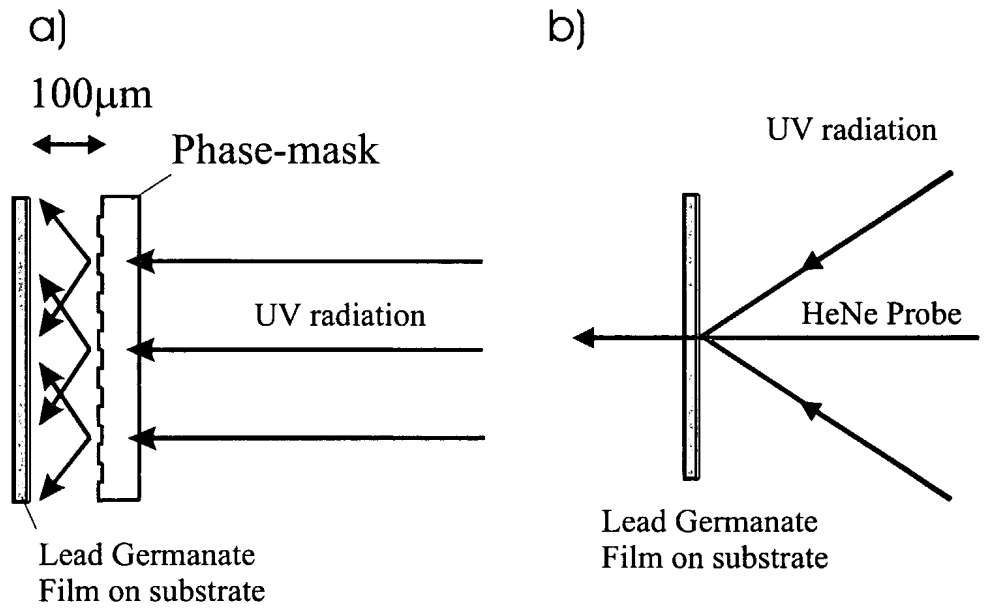

Figure 5.9: Experimental arrangement for a) π-phase mask recording and b) interferometric recording.

A schematic of the two recording methods is shown in figure 5.9. Figure 5.9a shows a schematic of the π-phase mask method. The sample is brought into close proximity with the phase mask (~100μm) using appropriate spacers in order to take advantage of the near field Fresnel diffraction intensity pattern. Figure 5.9b shows the outline of the interferometric recording arrangement including a HeNe probe beam transmitted through the exposed area and diffracted from the recorded grating. Monitoring the diffracted part of the HeNe beam using an optical power metre gives both the diffraction efficiency value and the recording-decay dynamics.

The diffraction efficiency measurements in the case of the phase mask recording were performed after the exposure and removal of the phase mask, by using a HeNe probe beam and measurement of the diffracted power.

To establish the value of d_{eff}, films were grown with progressively decreasing thicknesses, covering the range ~350nm to ~0.3 nm, by limiting the number of laser pulses used for deposition. Figure 5.10 shows spectrophotometer traces for several such films grown on fused silica substrates to enable recording of UV transmission spectra. The number of laser pulses used for these films was 10, 10^2, 10^3 and 10^4 respectively. Alphastep surface profile measurements indicated a film thickness of ~350 nm for 10,000 laser pulses, (equivalent to 0.035 nm per pulse). A log plot of film transmission versus thickness yields a 1/e absorption depth of ~75nm at a wavelength of 244 nm, equivalent to an absorption constant (α) of 13.3μm $^{-1}$. We thus set d_{eff} = 75 nm. Also shown in figure 5.10 is the characteristic absorption band centred at ~ 240nm which is accessed via 244 nm exposure.

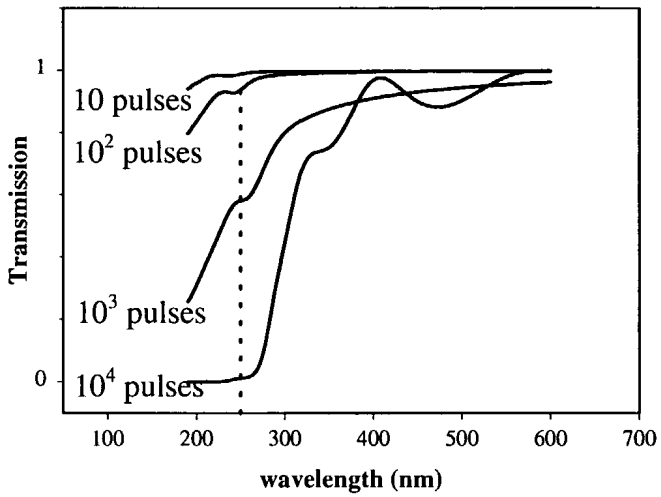

Figure 5.10: Absorption spectra of lead germanate films of various thicknesses grown on fused silica substrates. The vertical dotted line indicates the absorption band around 240 nm.

5.5 Experimental results

5.5.1 244nm c.w. radiation

The lead germanate films were initially exposed to a 244nm c.w. frequency doubled argon ion laser (Coherent inc. FRED laser). For writing laser powers of 60mW, at power densities of 0.5 W cm^{-2}, the diffraction efficiency saturated within 120 seconds. A standard writing time of double this value (i.e 4 mins) was therefore adopted for all subsequent films examined. Figure 5.11 shows the calculated values of induced index change, Δn, as a function of the oxygen pressure used during film growth, over the range 1×10^{-2} mbar to 6×10^{-2} mbar. Oxygen pressures of less than 1×10^{-2} mbar produced films which were dark in colour compared to the clear/pale yellow at higher pressures. At pressures approaching 1×10^{-1} mbar, the films were cloudy, or opaque, and had poor transmission at 633nm.

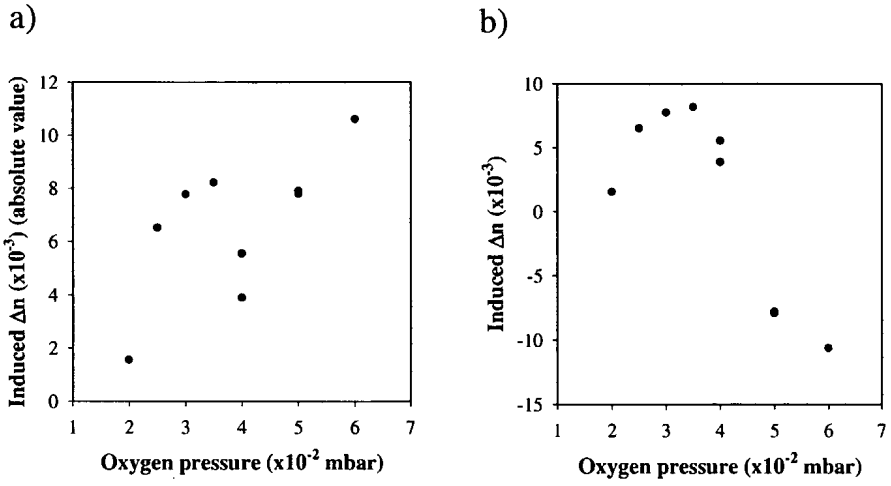

Figure 5.11: a) Plot of the absolute values of the refractive index changes as a function of the oxygen pressure during growth. b) Replot of the calculated values taking account of the sign.

Figure 5.11(a) shows a plot of the Δn values, obtained by the diffraction efficiency formula, where d_{eff} is a function of the oxygen pressure during the growth. It can be seen that there is a sharp minimum of Δn values for an oxygen pressure of 4×10^{-2} mbar. These results can be interpreted in terms of positive and negative refractive index changes. Diffraction efficiency measurements are not sensitive to the sign of the refractive index change but only to its magnitude. As discussed below, we believe that the minimum observed in the plot represents the point of change between two competing processes that leads to refractive index changes with different signs. This type of behaviour is not uncommon, and has been seen before in photosensitivity measurements as a function of UV fluence [12], rather than the variable oxygen content recorded here.

Ellipsometer measurements have been performed on films grown at oxygen pressures of 3×10^{-2} and 6×10^{-2} mbar. 5 mm square areas of the film were exposed to an expanded 244 nm laser beam, for periods up to 1 hour, to ensure a saturated exposure. The ellipsometer results for the film grown at 6×10^{-2} mbar indicate the presence of a lowered refractive index, accompanied by a volume expansion. The best fit values obtained for this lowered refractive index are $\sim$1.80. Atomic force microscope (AFM) scans of the regions exposed through the phase mask show clear evidence of surface relief gratings induced via material expansion in regions of high light intensity. These can be seen in figure 5.12. This is in agreement with reports of material expansion in negative photoinduced refractive index changes in germanium doped silica optical fibres [5]. Conversely, ellipsometer data for the film grown at a pressure of 3×10^{-2} mbar, indicates a positive refractive index increase. No relief gratings have been observed in AFM scans of exposed films grown at this pressure.

Using such ellipsometer data, we can replot the Δn versus oxygen pressure curves, as shown in figure 5.11(b). This result is also supported by other studies discussed in section 5.5.2. Using excimer laser pulses at 193nm to write gratings in these films, where the diffraction efficiency,

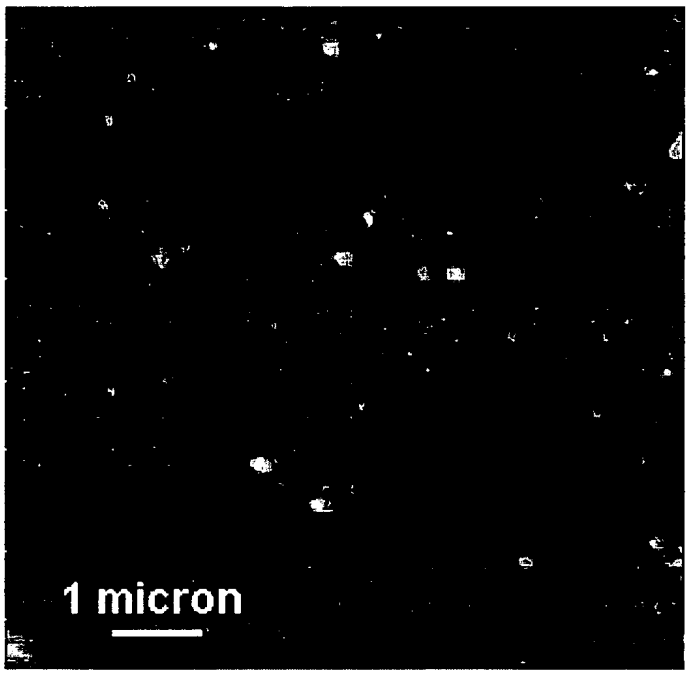

Figure 5.12: Relief gratings observed in exposed films grown at higher oxygen pressures. Expanded regions are believed to possess negative Δn.

monitored both during and after exposure, shows the characteristics of competition between two different (increasing and decreasing) refractive index modifying processes.

UV illumination of these waveguides will produce a Δn change that is a function of both depth (via the absorption constant, α) and the saturation characteristics of the photosensitivity mechanism. Whereas an exponential variation of Δn with depth into the guide is intuitively more satisfactory, in the absence of detailed knowledge of saturation mechanisms, we have assumed an average value of Δn change over d_{eff}.

For the film grown at a pressure of 6×10^{-2} mbar therefore, the measured diffraction efficiency, using d_{eff} =75 nm, yields a large Δn of -9 $\times$ 10^{-3}. When Fresnel reflections are taken into account, this yields a high value of -1.06 $\times$ 10^{-2}. So far no attempts have been made to either hydrogen load these films, or conduct any post-annealing studies.

5.5.2 248nm pulsed radiation

5.5.2.1 Nanosecond pulsed radiation

A comparison between c.w. and pulsed grating recording can now be undertaken by recording gratings on similar films (to those used in the previous section) with a pulsed KrF (248 nm) excimer laser delivering pulses of 20 nsec or 0.5 psec duration. The exposure of the films was kept well below the multi pulse ablation threshold, which was determined beforehand for each wavelength and pulse duration. The recording was mainly performed by using appropriate phase masks due to the poor coherence characteristics of the above mentioned lasers. For all pulsed grating recording the films were exposed to pulsed radiation until saturation occurred. Typical total (i.e accumulative) exposure values were of the order of 0.3 J/cm^2-0.4 J/cm^2 and peak powers from 0.4 MW for the 20 nsec source to 12 MW for the 0.5 psec source.

Since the relaxation of the gratings occurred over the time scale of minutes, the time evolution of the gratings could be monitored after removing the phase mask at a constant time delay (15 sec) after the last recording pulse.

The relationship between the oxygen pressure (during growth) and the refractive index change induced by the 20 nsec excimer laser exposure appears to follow the same trend as in the c.w. case. A dip in Δn at around 3×10^{-2} - 4×10^{-2} mbar and an increase by almost an order of magnitude at higher oxygen pressure suggests that the same mechanism for recording is operating for both cases. However, the diffraction efficiency of the gratings becomes saturated at levels lower than the ones recorded with the c.w. 244nm FRED laser. A possible explanation for this could be the simultaneous excitation of positive and negative refractive index changes with significant steady state residues as a result of the six orders of magnitude higher intensity of the pulsed recording. The two, opposite sign, refractive index changes partially cancel each other out and eventually

decrease the overall refractive index change. Evidence for simultaneous excitation of two competing refractive index change mechanisms was also shown by monitoring the diffraction efficiency development after recording. The relaxation of the recorded gratings leads to an overall increase of the diffraction efficiency which could be a signature of two refractive index change mechanisms with opposite sign which decay with different time constants [13], as shown in figure 5.13.

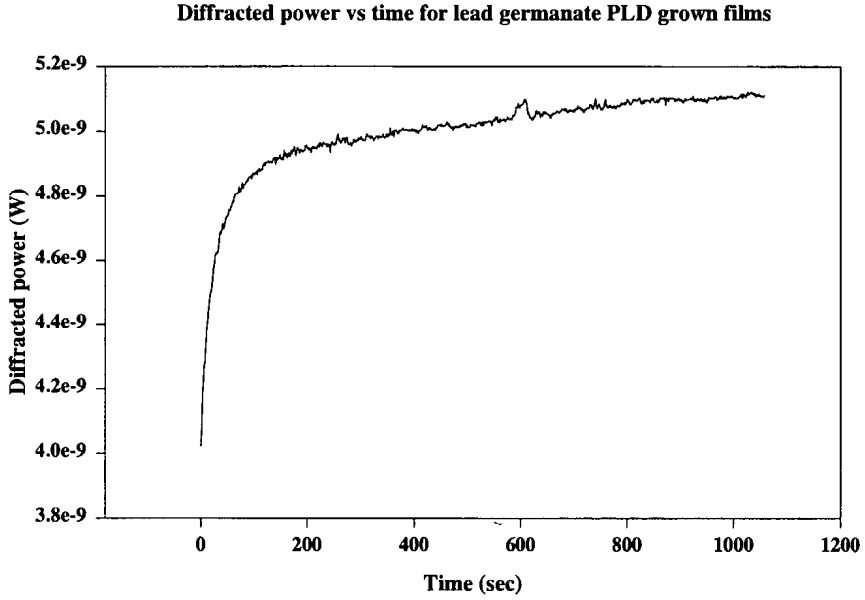

Figure 5.13: Increase in diffraction efficiency of grating immediately after exposure to UV radiation.

5.5.2.2 Sub-picosecond pulsed radiation

In order to study the effect of the writing beam intensity on the photosensitivity of lead germanate films, gratings were also recorded with a 500 femtosecond pulse duration excimer laser using a phase mask arrangement. The saturation level of the induced refractive index change was lowered in this case. The photosensitivity also showed a marked insensitivity to the growth conditions, a fact that further supports the intensity dependent hypothesis. Plots of the photoinduced refractive index change

as a function of the oxygen partial pressure during growth are depicted in figure 5.14a for 20 nsec KrF recording and figure 5.14b for 0.5 psec KrF recording.

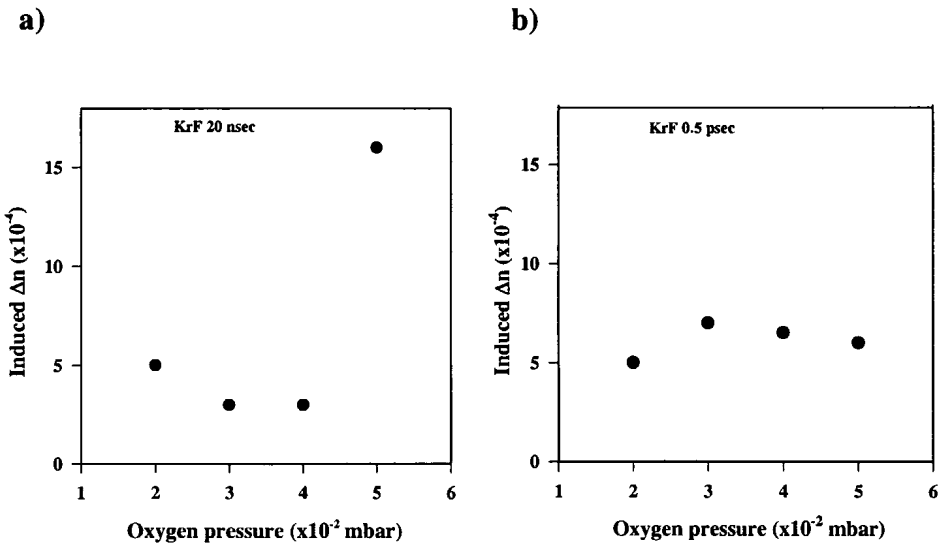

Figure 5.14: Plot of the absolute value of the photoinduced refractive index change versus oxygen partial pressure by a) 20 nsec KrF excimer laser and b) 0.5 psec KrF excimer laser.

5.5.3 193nm pulsed radiation

The photosensitivity of the films was also examined at 193 nm using an ArF excimer laser delivering pulses of 20 nsec duration. Typical accumulative exposure values were, as before, of the order of 0.3 J/cm^2 - 0.4 J/cm^2 and peak powers from 0.4 MW, also being under the laser ablation threshold. A study was made using both phase mask and interferometric arrangement. The 193nm ArF wavelength gives access to the second absorption band of the Ge-O defect which peaks at 195 nm [5]. The samples showed an increase in the refractive index change with increasing oxygen partial pressure although the overall saturated refractive index change did not exceed 10^{-4}. The inefficiency of the 193 nm recording is again attributed to the simultaneous recording of two competing, opposite sign,

Laser	Method	Exposure J cm^{-2}	$\|\Delta n\|$
HeCd: c.w. @ 325nm	Interferometer	500	10^{-4}
FRED: c.w. @ 244nm	Phasemask	110	10^{-3}-10^{-2}
KrF: pulsed(20nsec) @ 248nm	Phasemask	0.3	10^{-3}
KrF: pulsed(0.5psec) @ 248nm	Phasemask	0.3	10^{-3}-10^{-4}
ArF: pulsed(20nsec) @ 193nm	Interferometer & Phasemask	0.4	10^{-4}

Table 5.2: Summary of the grating recording methods, lasers used, exposures and measured refractive index changes.

refractive index changes.

5.5.4 325nm c.w. radiation

Efficient recording has been observed for 325 nm (HeCd laser) illumination of lead germanate samples using the interferometric set-up. With the power output available (5 mW) at 325 nm the grating strength saturates after ~800 sec. After exposure and decay of all transient components of the grating, the measured steady state value of diffraction efficiency corresponds to a final permanent refractive index change. Typical measured values were of the order of 10^{-4} .

5.6 Summary

The refractive index change results are summarised in table 5.2, indicating the method used, the UV sources, and the calculated Δn.

The table shows 244nm radiation allows the highest degree of refractive index change in the lead germanate films. However c.w. radiation effectively limits the use of the interferometric set-up as the vibrations (primarily due to water cooling of the laser) induced during the recording phase do not allow for a high contrast grating to be written. The short coher-

ence length of the 244nm Argon ion laser (~3cm) also places constraints on interferometric grating writing. Phase mask or short pulsed writing techniques are more insensitive to such vibrations.

Interferometric recording set-ups are often preferable as they allow a large range of grating sizes to be written. A phase masks, however, can only write one grating size with a small amount of tuning possible by varying the incident writing beam angle.

5.7 References

[1] J. R. Lincoln, W. S. Brocklesby, C. J. Mackechnie, J. Wang, R. S. Deol, D. C. Hanna, and D. N. Payne. New class of fiber laser based on lead-germanate glass. *Electronics Letters*, 28(11):1021–1022, 1992.

[2] W. H. Dumbaugh. Infrared transmitting germanate glasses. *Proceedings of the Society of Photo-Optical Instrumentation Engineers*, 297:80–85, 1981.

[3] H. P. Weber, F. A. Dunn, and W. N. Leibolt. *Applied Optics*, 12:755, 1973.

[4] Y. Okamura, S. Yoshinaka, and S. Yamamoto. Measuring mode propagation losses of integrated optical- waveguides - a simple method. *Applied Optics*, 22(23):3892–3894, 1983.

[5] R. J. Campbell and R. Kashyap. The properties and applications of photosensitive germanosilicate fiber. *International Journal of Optoelectronics*, 9(1):33–57, 1994.

[6] A. V. Amossov and A. O. Rybaltovsky. Oxygen-deficient centers in silica glasses - a review of their properties and structure. *Journal of Non-Crystalline Solids*, 179:75–83, 1994.

[7] A. V. Amossov and A. O. Rybaltovsky. Radiation color-center formation in silica glasses - a review of photo-chemical and thermo-chemical aspects of the problem. *Journal of Non-Crystalline Solids*, 179:226–234, 1994.

[8] J. Canning and M. Aslund. Correlation of ultraviolet-induced stress changes and negative index growth in type IIa germanosilicate waveguide gratings. *Optics Letters*, 24(7):463–465, 1999.

[9] A. I. Gusarov and D. B. Doyle. Contribution of photoinduced densification to refractive-index modulation in Bragg gratings written in Ge-doped silica fibers. *Optics Letters*, 25(12):872–874, 2000.

[10] M. G. Sceats and J. Canning. In *Summer School on Photosensitivity in Optical Waveguides and Glasses*, Vitznau, Switzerland, 1998.

[11] E. Kratzig and O. F. Schirmer. Photorefractive centers in electro-optic crystals. In *Topics in Applied Physics*, volume 61, pages 131–166. Springer Verlag, 1988.

[12] M.V. Bazylenko, D. Moss, and J. Canning. Complex photosensitivity observed in germanosilica planar waveguides. *Optics Letters*, 23(9):697–699, 1998.

[13] S. Mailis, L. Boutsikaris, and N. A. Vainos. Multiplexed static and dynamic photorefraction in Bi12SiO20 crystals at 780nm. *Journal of the Optical Society of America B-Optical Physics*, 11(10):1996–1999, 1994.

Chapter 6

Mechanical improvements to PLD

6.1 Introduction

PLD has always been an attractive method of fabricating waveguides. The ability to quickly and easily grow stoichiometric, epitaxial films of a large variety of laser media makes it an almost ideal fabrication process. PLD has been avoided as a *preferred* method, however, due to two main problems of uneven film thickness and high particulate densities. Section 6.2 of this chapter deals with the former problems whilst chapter 8 discusses the particulate problem in more depth.

Homogeneously heating a substrate in any vacuum deposition system is also problematic. A useful and practical solution to homogenous substrate heating is presented in section 6.3.

6.2 Improving film thickness profile

Figure 6.1 shows the angular distribution of neutral and ionised Ti atoms within the plasma plume ejected from the target [1]. If the target and substrate are stationary during a deposition, this would lead to a simi-

lar thickness profile of the resultant film. This is a problem inherent in PLD that limits its use in large area depositions. Advances have already been made in this area using translating substrate stages [2], x-y scanned half-cylindrical targets [3], modification of the ablation laser beam [4] or machine preparation of the target [5].

In this section we present the two simple solutions utilised to improve the thickness profile of the two films grown for study in this thesis; Nd:GGG and lead germanate. The work detailed in these sections builds upon the work already developed by Gill [6]. Small modifications to target geometries are not often reported on their own merit [7], which makes it difficult to ascertain what has and has not been previously reported in this field. The work in this section is not necessarily included as 'new work' but just for completeness of a description of the PLD apparatus.

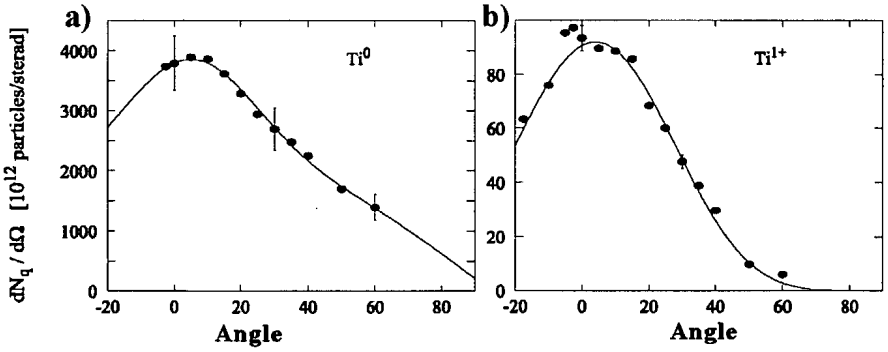

Figure 6.1: Angular distribution of a) neutral and b) ionic Ti atoms taken from [1].

The lead germanate and Nd:GGG targets are shown in figure 6.2. The difference in target geometries requires two different solutions to obtain even thickness profiles. These are detailed separately in the two subsequent sections.

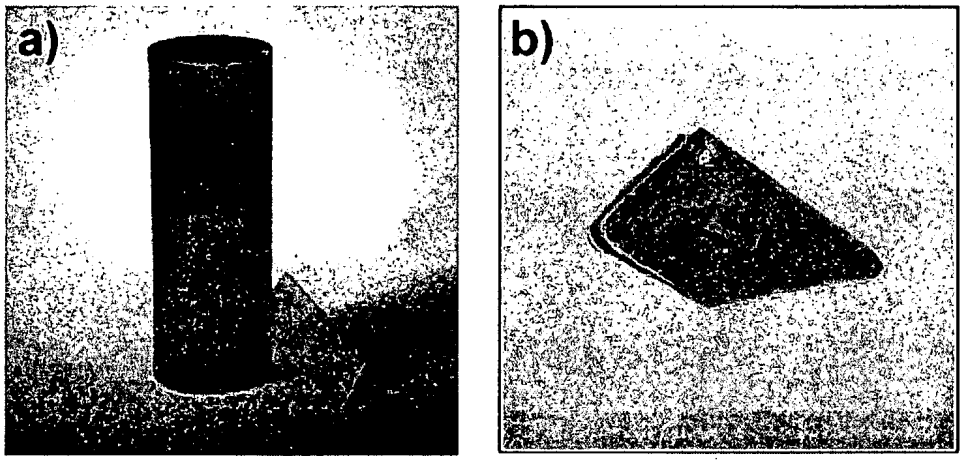

Figure 6.2: a) The cylindrical Nd:GGG target with substrate. and b) The flat lead Germanate target.

6.2.1 Nd:GGG film thickness improvement

Due to ready availability of laser rod off-cuts, PLD single crystal targets are often cylindrical as shown in figure 6.2a. The ablation laser is incident on the side of the cylinder. As the plume is largely ejected perpendicular to the surface of the target, the curved surface of the target makes the plume elongated. This is shown in figure 6.3.

To reduce the occurrence of exfoliation the target is rotated alternately backwards and forwards to uniformly ablate the target [8, 9] (discussed further in section 8.1). By slightly offsetting the position of the target on the rotation stage the laser will impact at different vertical positions on the target, causing the plume to track up and down as the surface normal at the ablation site also changes direction. This is shown in figure 6.4. A uniform thickness profile is now produced in the direction perpendicular to the target's long axis.

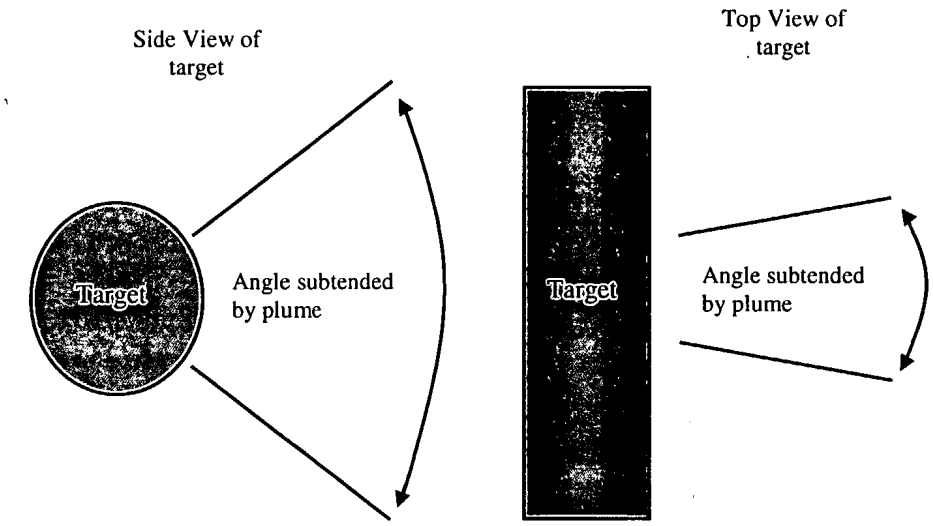

Figure 6.3: Showing the plume subtending a larger angle in the vertical plane due to the geometry of the Nd:GGG target.

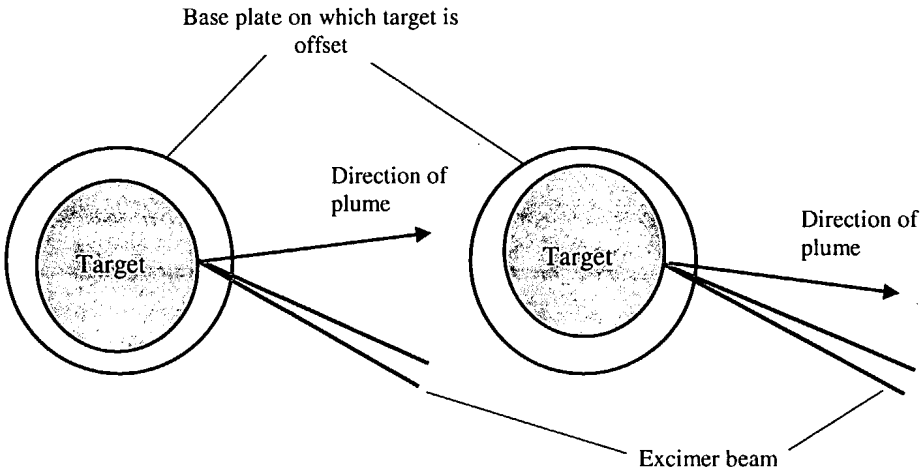

Figure 6.4: Showing how the offset target causes the plume to track up and down.

Figure 6.5 shows the thickness profile along this direction measured with an ALPHASTEP for film depositions with central (a) and offset (b) target rotation.

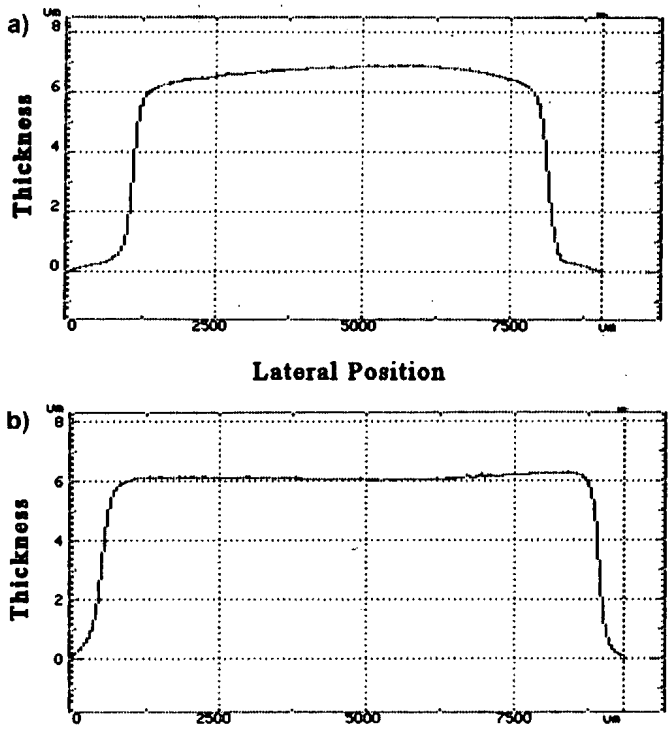

Figure 6.5: Alphastep trace across substrate with a) no off-set target rotation b) Off-set target rotation showing a flatter film profile.

Figure 6.6 shows the 2D and 3D surface profile of the improved film. This is taken with a ZYGO interferometric surface profiler using a 2.5mm Michelson objective.

The absorption length, and hence the actual cavity length, of the Nd:GGG waveguide lasers fabricated in this work is short (~2mm). The thickness profile along this direction, therefore, is not critical. The waveguide is cut from the substrate with the lasing direction perpendicular to the uniform section so that the finished waveguide has a good overall thickness profile.

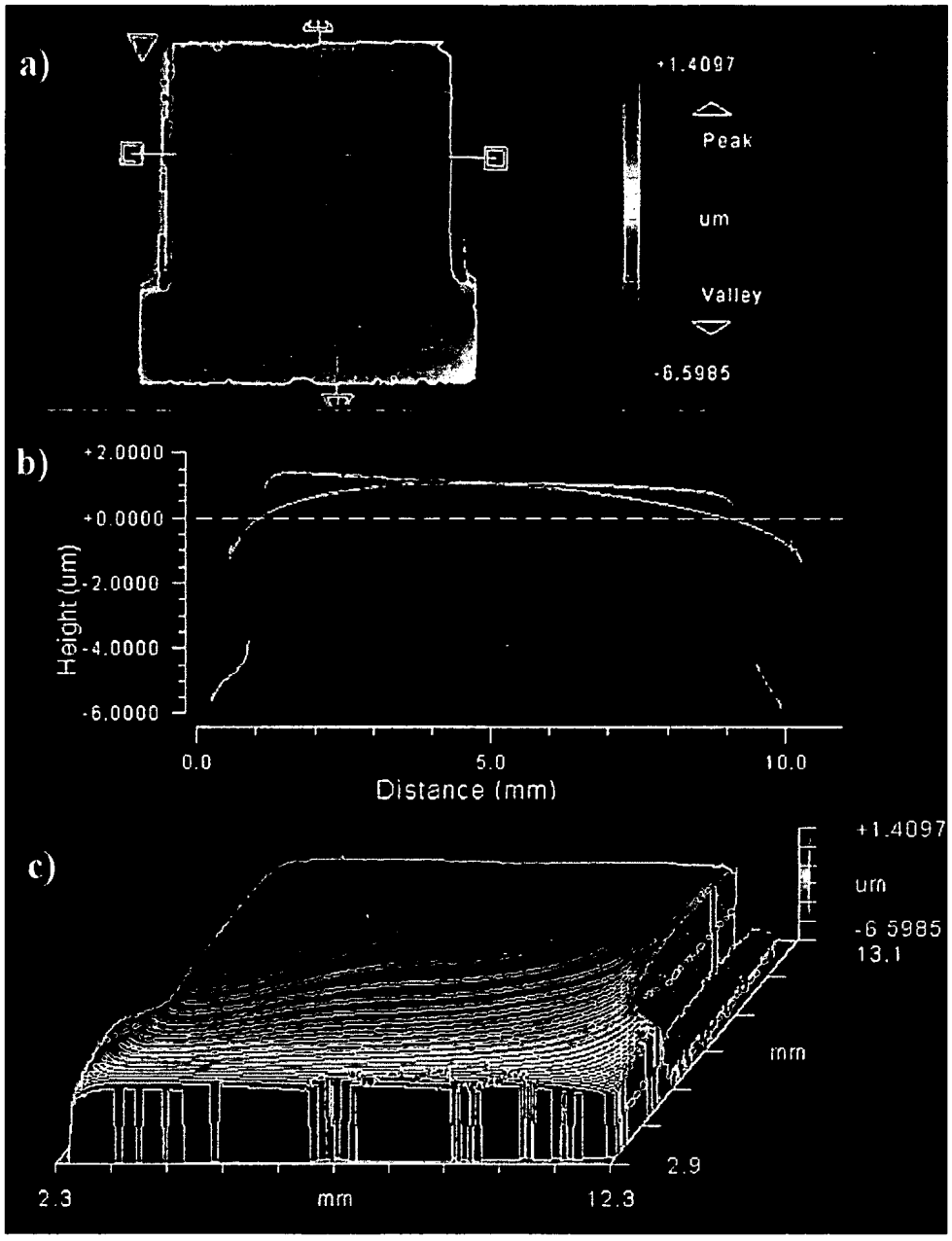

Figure 6.6: a) 2D surface profile of substrate and film b) 1D profile of thickness along line marked in top figure c) Generated 3D image of surface profile.

6.2.2 Lead germanate film thickness improvement

In the case of lead germanate growth, The flatter lead germanate targets are held in a small vice-like holder and are rotated around the axis running through the largest side of the target. The lead germanate films are grown on an unheated substrate which allows the substrate to be rotated easily (heated substrates can be rotated during deposition but this is difficult to achieve whilst maintaining temperature uniformity). Substrate rotation is desirable as the inhomogeneous angular mass distribution of the plasma plume can be averaged out to achieve an even growth of film across the substrate. By offsetting the centre of rotation of the substrate with respect to the plasma plume, the film thickness can be averaged out over a significant area (~cm) [7]. The offset distance is critical though as too much offset will result in 'doughnut' shaped growth whilst too little will result in the familiar humped growth.

6.3 Homogeneous substrate heating

In order to produce crystalline or epitaxial films an appropriately orientated substrate is required which usually needs to be uniformly heated during the deposition process. Literature values for optimum substrate temperature most often fall within the temperature range 600 °C to 800 °C although in some substrate-film combinations, the substrate may need to be heated in excess of 1200 °C [10]. The orientation and phase of the developing film can be highly dependent on the temperature of the substrate during deposition. Uneven temperature distribution across the substrate can lead to undesirable polycrystalline films or a mixture of amorphous and crystalline growth. Additionally, rapid heating in substrates with poor thermal conductivity can cause severe thermal stress if not heated homogeneously, often leading to substrate fracture. It is essential therefore to achieve an even temperature profile of the substrate.

6.3.1 Methods of substrate heating

Resistive wire heating elements, high power filament bulbs [11] and other resistive heating methods have been used with some success to achieve high temperature, homogeneous heating . These methods, however, are extremely inefficient and result in unavoidable heating of the whole deposition chamber, causing severe out-gassing from the chamber walls and any additional vacuum components. Efficient and uniform thermal contact between the heating element and the substrate is also necessary, though is not always practical at high temperatures even if a conductive paste (e.g. indium-gallium alloy) is used. Resistive heating also causes a lengthy turn-around time between depositions as the chamber usually has cool down before installation of a new substrate is possible. This is a severe drawback when one considers that the typical deposition times required for the growth of a 4μm film can be as short as 10mins.

6.3.2 CO_2 laser substrate heating

Laser substrate heating in PLD was originally reported by Dyer *et al* [12] and has already been used with considerable success [10, 13–15]. Such laser heating minimises most of the problems associated with conductive heating and can heat a substrate with minimal heat loss to the chamber. Using Stefan Boltzmann's law the power P (Watts) required to heat a substrate of surface area A (m^2) to a temperature T (Kelvin) is given by:

$$P = A\epsilon\sigma(T^4 - T_R^4) \tag{6.1}$$

Here ϵ is the emissivity of the substrate, σ is the Stefan Boltzmann constant (5.67×10^{-8} $Wm^{-2}K^{-4}$) and T_R is the temperature of the surroundings. The surface area is taken to be twice the area of the substrate faces, i.e. edge effects are ignored.

Using an emissivity of 1 (i.e a black body), an area $A = 2 \times 1$ cm^2 and T_R = 300K, we find that 57 watts are required to heat a substrate to 1500 K (The temperature required for deposition of Ti:sapphire). The substrate is clearly not a black body however and indeed the emissivity is strongly dependent on temperature and wavelength. For a body radiating at 1500 K the wavelength of peak radiance is at ~2μm . The emissivity at 2μm will therefore be assumed to be a reasonable approximation of the overall emissivity. The emissivity of a material is also equal to the absorption at that wavelength. Since 2μm radiation falls within the transparency range of Ti:sapphire its absorption and hence its emissivity will be low. The result of this effect is that a 40W CO_2 laser can easily heat a substrate measuring 10mm×10mm×1mm to the 1500 K required for sapphire growth (in fact a 100W laser is capable of melting sapphire, the melting point of which is 2300 K). For comparison, resistive heating filaments typically require orders of magnitude more power to heat the substrate to the same temperature due to heat loss to the chamber.

To achieve an even heating profile across the substrate, beam homogenisers have been employed [10, 13, 16] but these are often difficult to set-up and maintain in alignment. Additionally, homogenisers do not offer flexibility in size or position of the substrate and, if used within the vacuum chamber, can quickly become coated with target material. This coating can increase the absorbtion of the CO_2 radiation by the homogeniser and thus create a corresponding loss in power delivered to the substrate.

6.3.3 CO_2 raster scanned laser substrate heating

Described in this section is a method of homogeneous heating using a c.w. CO_2 laser and two scanning galvanometric mirrors (General Scanning Inc., Watertown, MA). We also describe a simple temperature monitoring system employed to determine the substrate temperature distribution. The apparatus is detailed in Figure 6.7.

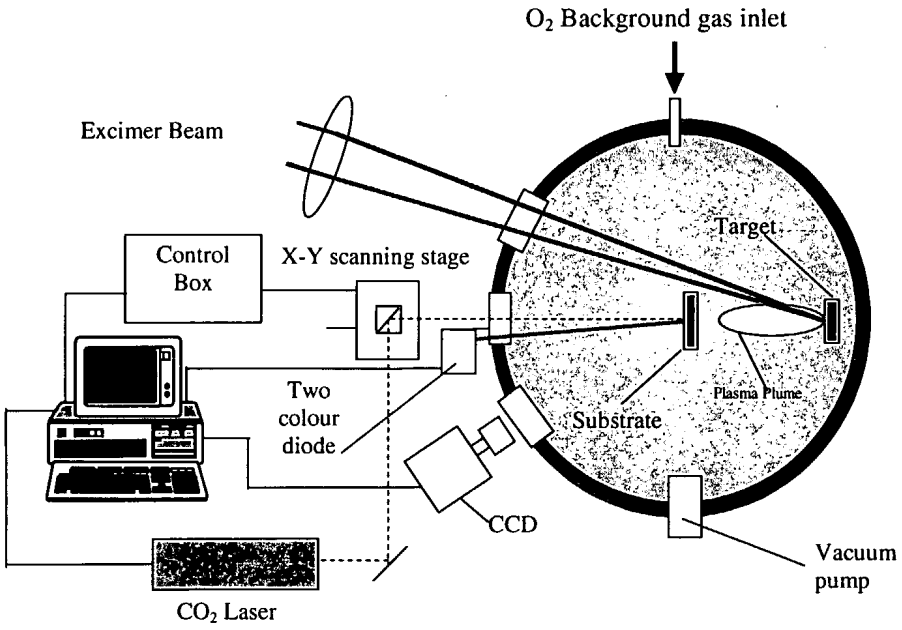

Figure 6.7: Computer controlled, raster scanned, laser heating apparatus.

The mirrors are computer controlled to deflect the CO_2 laser along an appropriate 2-D array of points on the substrate. A laser diode pointer coincident with the CO_2 beam path is used to render the pattern tracked by the CO_2 beam visible to a CCD, for ease of alignment. Figure 6.8 shows a CCD image of the laser pattern on the back of the substrate: a 6×4 array of points.

By varying the dwell time of the laser on each point and the position and number of the points across the substrate, heating uniformity across the substrate can be achieved to a much higher degree than for non-scanned single beam techniques. Absolute uniformity is limited by the number of points that can be scanned across the substrate in a time fast enough to avoid temperature fluctuations due to the transient nature of the heat source on any one particular point.

To estimate the rate of change of temperature of a cooling substrate the Stefan Boltzmann equation is used in differential form as taken from Dyer *et al* [12]

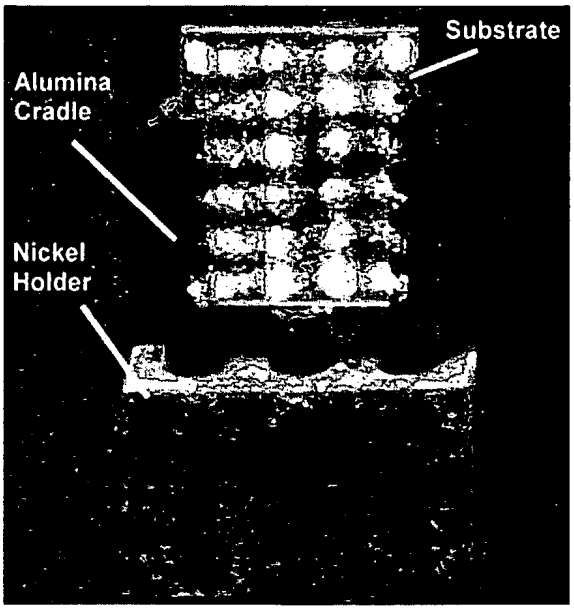

Figure 6.8: Raster scan pattern across the substrate using alignment diode laser to render path visible. Alumina cradle and nickel holder are also marked.

$$\frac{\mathrm{d}T}{\mathrm{d}t} = \frac{A\epsilon\sigma}{h}(T^4 - T_R^4) \tag{6.2}$$

All variables and units are as in equation 6.1, t is time (seconds) and h is the heat capacity of the substrate (J K^{-1}). YAG will used as an example with a density of 4.5gcm^{-3} and a specific heat of 590 J $Kg^{-1}K^{-1}$. This gives a heat capacity of 0.266 J K^{-1} for a sample of dimensions 10mm×10mm×1mm. Using T as 900 K, T_R at 300 K and assuming a linear rate of change over the timescale of interest (~10 milliseconds for one full scan cycle) it is found that a temperature change of 30K s^{-1} occurs in a black body (ϵ = 1) and 3K s^{-1} for a grey body of ϵ = 0.1 . Therefore it is hoped that there will be a temperature change of less than 1°C for the scan cycle times available.

Also shown in Figure 6.8 is the alumina cradle (and the nickel base) that is used to hold the substrate. This design ensures a good compromise between minimum heat loss by conduction, to the surroundings, and ease of substrate replacement

6.3.4 Temperature monitoring

Temperature measurement using a thermocouple is impractical as this will inevitably introduce heat sinking from the substrate and thus promote a temperature inhomogeneity. Temperature is instead measured using a two-colour (silicon and germanium) photodiode (Hamamatsu part K1713-03). Within this single package a silicon photodiode is mounted in front of a germanium photodiode. The germanium photodiode effectively detects the radiation that the silicon detector transmits. The silicon photodiode detects from ~0.32μm to ~1μm and the germanium photodiode from ~1μm to ~1.55 μm . This requires very little space and alignment and also requires no external beam splitters to be used. The temperature of the substrate can be calculated from the ratio of the intensity observed by the two photodiodes within their respective spectral regions. A practical solution for doing this is to assume the emissivity of the substrate is similar for the two observing photodiode wavebands (i.e. assume a grey body) and that the spectral response curve of the two photodiodes can be approximated to a central effective wavelength. The equations for temperature determination can then be simplified to [17]:

$$T \approx \frac{B}{(lnQ) - A} + C$$

Where Q is the ratio of the two photodiode outputs. A, B and C are constants to be determined by calibrating ratio sets $(Q_1, Q_2, \ldots Q_n)$ against known temperatures $(T_1, T_2, \ldots T_n)$ and evaluated through a least squares method. Since this method should be independent of the emissivity, the calibration only needs to be done for one material. It should be noted however that metals are not grey bodies so some deviation from this curve may be seen should a metal substrate be used. Coating the back of the substrate in black soot can solve problems arising with non-grey bodies or substrates semi-transparent to CO_2 laser radiation (10.6μm). The temperature data from the photodiode can be sent via the computer back to the laser power control to stabilise the temperature and automate a constant,

gradual heating process, thereby reducing the chances of substrate fracture. Figure 6.9 shows a graph of the temperature calculated from the two-colour photodiode with a thermocouple reading for comparison against incident power. In this case the thermocouple was firmly heat-sunk to the front surface of a YAG substrate (heating is from the back) in a way designed to minimise temperature inhomogeneity. This process, however renders the substrate unsuitable for deposition purposes.

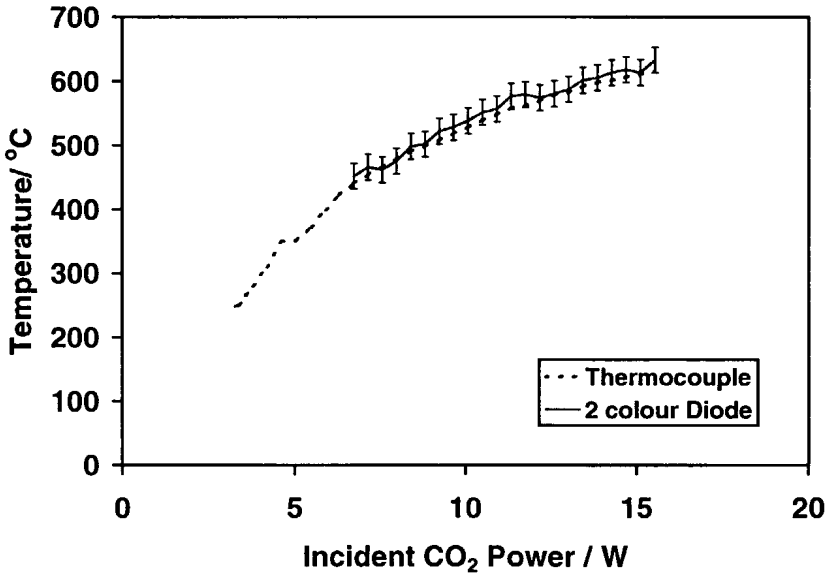

Figure 6.9: Temperature measured with the calibrated two-colour diode and thermocouple against incident CO_2 laser power.

To monitor the relative temperature distribution across the substrate we have used a commercial silicon CCD camera (Pulnix 2010) and $\times 10$ macro zoom lens. At the temperatures routinely used in PLD this is sensitive enough to detect sufficient radiation from the substrate to give a picture of the relative temperature profile with a maximum resolution of 640 by 480 pixels. The information from the CCD can also be fed back to the scanner via the computer to alter the temperature profile. By extending the dwell time of the laser on a particular array point, which is perhaps cooler than its neighbours, the relative temperature distribution can be

controlled to maximise homogeneity. This is particularly useful to offset the increased heating often observed in the centre of the substrate. With the scanning equipment set up it becomes trivial to adjust via the computer to allow for different sizes or positions of substrates without any difficult re-alignment problems. Currently our system allows movement, expansion and contraction of the raster scan during heating and while in vacuum. This permits final adjustment and optimisations if necessary.

6.3.5 Results

Figure 6.10 shows a typical temperature profile, obtained from a CCD camera, of a heated $Y_3Al_5O_{12}$ (YAG) substrate. No feedback control was enabled, making the dwell time of the laser at each point on the surface equal.

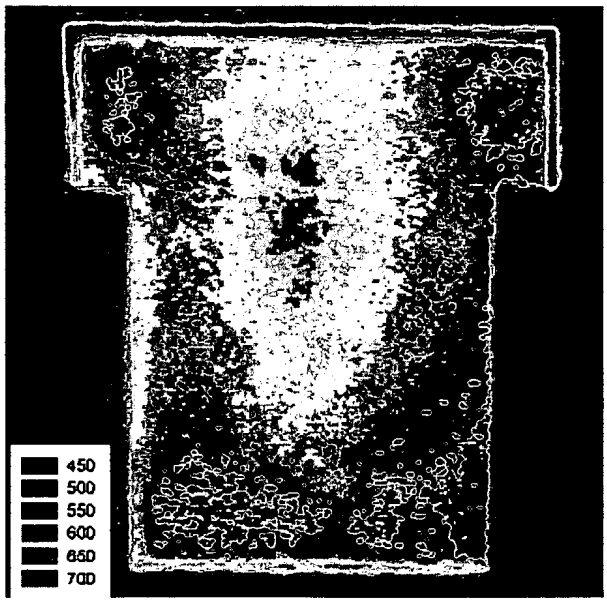

Figure 6.10: Thermal image of the heated substrate without feedback system, showing elevated heating in the central area. The inset chart indicates how the colour relates to temperature in °C .

The increased intensity seen at the edge of the substrate is not due to elevated temperatures as indicated. The high intensity seen is due to the

light from within the substrate that is only able to escape at the edges due to total internal reflection at the face. The CCD camera views the substrate at a slight angle, which makes the top edge appear brightest.

Ignoring such edge effects, the figure shows temperature variations mostly between 590°C and 690°C over the substrate, which has an area of $\sim 1 cm^2$.

Figure 6.11 shows the temperature distribution across the same substrate but with the feedback loop enabled. The beneficial effect this has on temperature homogenisation can be clearly seen. In this figure temperature variations across the same substrate of mostly between 600°C and 650°C are shown.

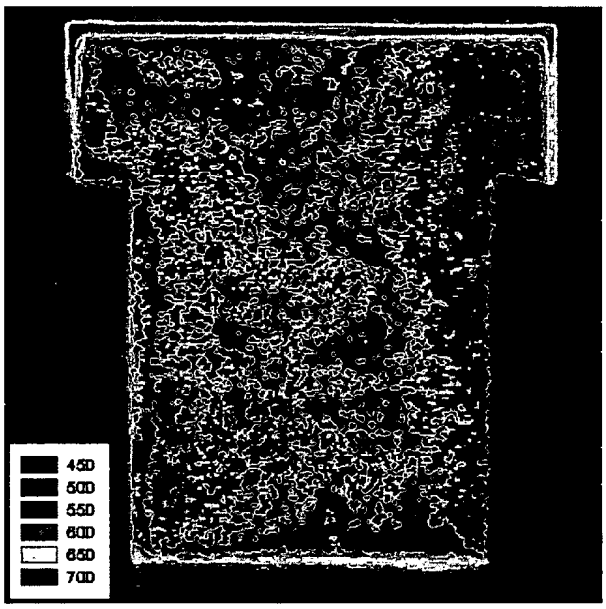

Figure 6.11: Thermal image of the heated substrate with feedback system enabled, showing a more homogeneous temperature distribution across the substrate. The inset chart indicates how the colour relates to temperature in °C .

6.3.6 Conclusions

We have found that for our requirements an array of 6 × 4 raster points produces a heating effect that is adequately uniform across the substrate. We can think of no reason why this technology cannot be scaled up to much larger dimensions or to higher precision. Larger dimensions would imply either an increase in the array size of the raster scan or an increase in the beam size, which can be easily implemented by placing an appropriate lens before the scanning unit. Higher uniformity in temperature homogeneity would imply having a larger array size, which is limited by the speed the scanning mirrors can complete one cycle of the raster scan. Ideally the mirrors should not take longer to complete one cycle than it takes for any particular point in the scan to noticeably change temperature due to the temporary absence of the incident radiation.

Further work will investigate more intelligent methods of raster scanning in order to minimise cycle time. Heating of rotating or moving substrates, employed to improve thickness uniformity would also be possible. Additionally, controlled temperature gradients can be applied to the substrate (provided the substrate is able to withstand such thermal stress) resulting in different doping concentrations of certain elements whose inclusion in the film is temperature dependent. This has been reported before for titanium doping in sapphire [10, 18].

6.4 References

[1] A. Thum-Jager and K. Rohr. Angular emission distributions of neutrals and ions in laser ablated particle beams. *Journal of Physics D-Applied Physics*, 32(21):2827–2831, 1999.

[2] C. Doughty, A.T. Findikoglu, and T. Venkatesan. Steady-state pulsed-laser deposition target scanning for improved plume stability and reduced particle density. *Applied Physics Letters*, 66(10):1276–1278, 1995.

[3] R. Dietsch, T. Holz, H. Mai, M. Panzner, and S. Vollmar. Pulsed-laser deposition (PLD) - an advanced state for technical applications. *Optical and Quantum Electronics*, 27(12):1385–1396, 1995.

[4] F.E. Fernandez. Enhancement of thickness uniformity of thin-films grown by pulsed-laser deposition. *Journal of Vacuum Science & Technology A-Vacuum Surfaces and Films*, 13(2):421–427, 1995.

[5] I. Weaver and C.L.S. Lewis. A case study with a novel geometry for pulsed laser deposition. *Journal of Physics D-Applied Physics*, 33(3):175–179, 2000.

[6] D. S. Gill. *Fabrication and characterisation of thin film optical waveguides by pulsed laser deposition.* PhD thesis, University of Southampton, 1996.

[7] Z. J. Xin, R. J. Peaty, H. N. Rutt, and R. W. Eason. Epitaxial growth of high-quality ZnS films on sapphire and silicon by pulsed laser deposition. *Semiconductor Science and Technology*, 14(8):695–698, 1999.

[8] N. Arnold and D. Bauerle. Uniform target ablation in pulsed-laser deposition. *Applied Physics A-Materials Science & Processing*, 68(3):363–367, 1999.

[9] H.L. Spindler, R.M. Gilgenbach, and J.S. Lash. Effects of laser-ablation target damage on particulate production investigated by laser scattering with deposited thin film and target analysis. *Applied Physics Letters*, 68(23):3245–3247, 1996.

[10] A.A. Anderson, R.W. Eason, M. Jelinek, C. Grivas, D. Lane, K. Rogers, L.M.B. Hickey, and C. Fotakis. Growth of Ti:sapphire single crystal thin films by pulsed laser deposition. *Thin Solid Films*, 300(1-2):68–71, 1997.

[11] R. Campion, R.G. Ormson, C.A. Bashford, and P.J. King. Design and performance of a reliable and low-cost substrate heater for superconducting thin-film deposition. *Vacuum*, 46(2):195–197, 1995.

[12] P.E. Dyer, A. Issa, P.H. Key, and P. Monk. A cw CO_2-laser substrate heater for superconducting thin-film deposition. *Superconductor Science & Technology*, 3(9):472–475, 1990.

[13] A.A. Anderson, C.L. Bonner, D.P. Shepherd, R.W. Eason, C. Grivas, D.S. Gill, and N. Vainos. Low loss (0.5 db/cm) Nd:$Gd_3Ga_5O_{12}$ waveguide layers grown by pulsed laser deposition. *Optics Communications*, 144(4-6):183–186, 1997.

[14] P.A. Atanasov, R.I. Tomov, and V.S. Serbezov. Plasma-assisted in-situ laser deposition of $Y1Ba_2Cu_3O_7$-X superconducting thin-films with laser-heating and annealing. *Vacuum*, 45(12):1215–1219, 1994.

[15] S. Ohashi, M. Lippmaa, N. Nakagawa, H. Nagasawa, H. Koinuma, and M. Kawasaki. Compact laser molecular beam epitaxy system using laser heating of substrate for oxide film growth. *Review of Scientific Instruments*, 70(1):178–183, 1999.

[16] F. J. Villarreal, H. J. Baker, R. H. Abram, D. R. Jones, and D. R. Hall. Beam reformatting of one- and two-dimensional arrays of CO_2 waveguide lasers. *IEEE Journal of Quantum Electronics*, 35(3):267–272, 1999.

[17] G. Ruffino. Inceasing precision in two colour pyrometry. In *Inst. Phys. Conf.Ser No.26*, page 264, 1975.

[18] L. M. B. Hickey and J. S. Wilkinson. Titanium diffused waveguides in sapphire. *Electronics Letters*, 32(24):2238–2239, 1996.

Chapter 7

Optical Waveguide Theory

7.1 Introduction

This chapter describes the theory of planar waveguides. The first part presents a model of the spatial mode profile of a guided wave in a generalised planar waveguide device. This model follows the general work of Yariv [1] and Lee [2,3] and the more specialised derivation of Bonner [4]. The model developed is then applied to the waveguides fabricated during the course of this thesis. The second part of this chapter presents the basic laser theory of bulk and waveguide lasers and in particular it looks at the relationship between device thickness and the pump power threshold required for lasing.

7.2 Ray-optical picture

Firstly we will consider a simple 3 layer symmetric waveguide to introduce common terminology. Figure 7.1 shows a geometrical interpretation of light confined within a waveguide structure.

The core is the active layer, the region in which light is usually confined

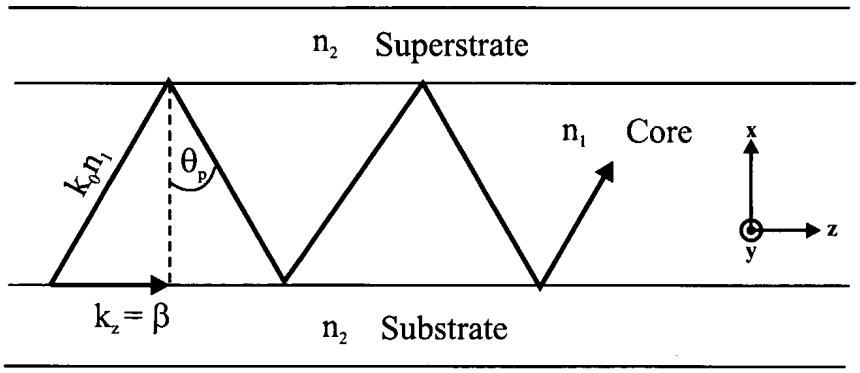

Figure 7.1: Confined light propagating in a symmetric 3 layer waveguide.

unless cladding pumping geometries are used. The substrate and superstrate are the media surrounding the core and which could be air in either case. The condition for confinement or guidance is that light incident upon the two boundaries is totally internally reflected. This requires that $n_2 < n_1$ (where n_1 and n_2 are the refractive indices of the core and substrate/superstrate respectively) and that the angle of incidence θ_p is greater than the critical angle θ_c given by Snells law

$$\sin\theta_c = \left(\frac{n_2}{n_1}\right) \tag{7.1}$$

Rather than use the propagation angle, it is more convenient to think of the z-component of the propagating wavefront (k_z) propagating in an effective refractive index. The propagation constant β is defined as:

$$\beta = k_0 n_1 sin\theta_p \tag{7.2}$$

Where k_0 is defined as $2\pi/\lambda_0$ (λ_0 is the wavelength of light in vacuum)

The quantity $n_1 \sin\theta_p$ is known as the effective refractive index n_{eff} so we

can write

$$\beta = k_0 n_{eff} \tag{7.3}$$

7.3 The wave equation

Light propagating in the waveguide will obey Maxwells equations for electromagnetic waves. The generalised form of these equations is written as:

$$\nabla \times \mathbf{E}(\mathbf{r}, t) = -\frac{\partial \mathbf{B}(\mathbf{r}, t)}{\partial t} \tag{7.4}$$

$$\nabla \times \mathbf{H}(\mathbf{r}, t) = \frac{\partial \mathbf{D}(\mathbf{r}, t)}{\partial t} + \mathbf{J}(\mathbf{r}, t) \tag{7.5}$$

$$\nabla \cdot \mathbf{D}(\mathbf{r}, t) = \rho(\mathbf{r}, t) \tag{7.6}$$

$$\nabla \cdot \mathbf{B}(\mathbf{r}, t) = 0 \tag{7.7}$$

where $\mathbf{E}$ is the electric field, $\mathbf{H}$ is the magnetic field, $\mathbf{D}$ is the electric displacement vector, $\mathbf{B}$ is the magnetic flux density, ρ is the charge density, $\mathbf{J}$ is the current density, t is time and $\mathbf{r}$ is the position vector.

For dielectric materials we can set $\mathbf{J} = 0$ and $\rho = 0$ (no current flow) and use the relations.

$$\mathbf{B} = \mu_0 \mu_r \mathbf{H} = \mu \mathbf{H} \tag{7.8}$$

$$\mathbf{D} = \epsilon_0 \epsilon_r \mathbf{E} = \epsilon \mathbf{E} \tag{7.9}$$

where ϵ_0 and ϵ_r are the permittivity of free space and the relative permittivity of the medium respectively and μ_0 and μ_r are the permeability of free space and the relative permeability of the medium respectively

Now 7.4...7.7 can be written as.

$$\nabla \times \mathbf{E}(\mathbf{r}, t) = -\mu \frac{\partial \mathbf{H}(\mathbf{r}, t)}{\partial t} \tag{7.10}$$

$$\nabla \times \mathbf{H}(\mathbf{r}, t) = \epsilon \frac{\partial \mathbf{E}(\mathbf{r}, t)}{\partial t} \tag{7.11}$$

$$\nabla \cdot \mathbf{E}(\mathbf{r}, t) = 0 \tag{7.12}$$

$$\nabla \cdot \mathbf{H}(\mathbf{r}, t) = 0 \tag{7.13}$$

By using the identity $\nabla \times (\nabla \times \mathbf{A}) = \nabla(\nabla \cdot \mathbf{A}) - \nabla^2 \mathbf{A}$ for any vector and taking the curl of 7.10 we can produce the wave equation for a lossless dielectric medium.

$$\nabla \times \mathbf{E}(\mathbf{r}, t) = -\mu\epsilon \frac{\partial^2 \mathbf{E}(\mathbf{r}, t)}{\partial t^2} \tag{7.14}$$

For a wave propagating in the z-direction, this has a travelling wave solution of the form:

$$\mathbf{E}(\mathbf{r}, t) = \mathbf{E}(x, y) e^{i(\omega t - \beta z)} \tag{7.15}$$

In practice, the output modes observed from the planar guides fabricated during the course of work presented in this thesis all possess transverse electric (TE) polarisation (i.e the polarisation of the E-field is parallel to the y-axis). We will, therefore, only consider the TE solution of the wave equation.

Due to the planar nature of the waveguide $\partial E/\partial y = 0$ so we can write

$$\mathbf{E}(\mathbf{r}, t) = \mathbf{E_y}(x)e^{i(\omega t - \beta z)} \tag{7.16}$$

7.4 Five layer asymmetric planar waveguide

Now we can introduce the generalised 5 layer asymmetric planar waveguide structure as shown in figure 7.2

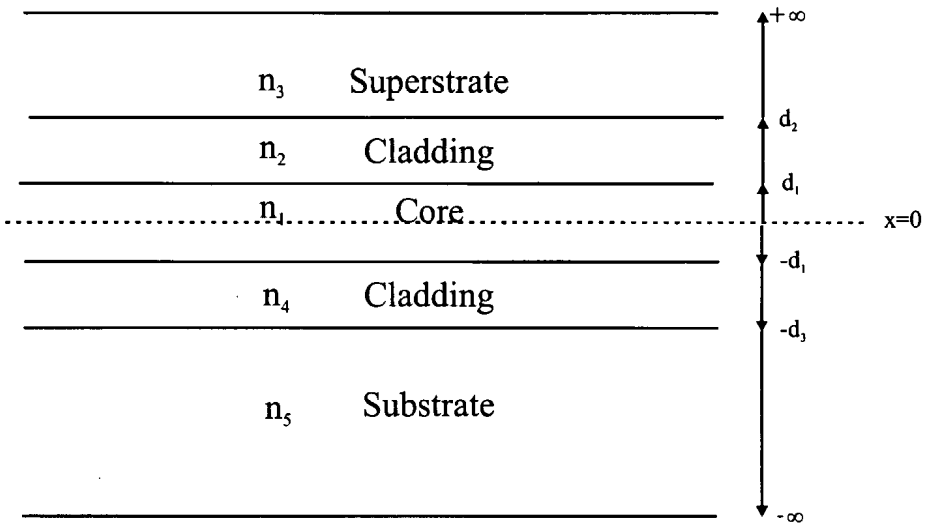

Figure 7.2: 5 layer asymmetric waveguide

Solutions are assumed for the five regions within the waveguide :

$$E(\mathbf{r}, t) = \begin{cases} E_1 e^{-\alpha_1 x} e^{i(\omega t - \beta z)} & x \geq d_2 \\ (E_2 e^{-\alpha_2 x} + E_2' e^{\alpha_2 x}) e^{i(\omega t - \beta z)} & d_1 \leq x \leq d_2 \\ cos(kx + \psi) e^{i(\omega t - \beta z)} & for \quad d_1 \geq x \geq -d_1 \\ (E_4 e^{\alpha_4 x} + E_4' e^{-\alpha_4 x}) e^{i(\omega t - \beta z)} & -d_1 \leq x \leq -d_2 \\ E_5 e^{\alpha_5 x} e^{i(\omega t - \beta z)} & x \leq -d_2 \end{cases} \tag{7.17}$$

E_1, E_2, E_2', E_4, E_4', E_5 are all coefficients of the electric field amplitude, ψ is a phase offset and α_1, α_2, α_4, α_5, and k are wave numbers,

These solutions correspond to an oscillating wave in the core, oscillating ($\alpha_{2,4}$ imaginary) or exponentially decaying waves ($\alpha_{2,4}$ real) in the cladding and exponential decay in the substrate and superstrate.

By substitution of the solutions in equation 7.17 into the wave equation the following dispersion relations are found.

$$\alpha_1 = \sqrt{\beta^2 - \omega^2 \mu_1 \epsilon_1} \tag{7.18}$$

$$\alpha_2 = \sqrt{\beta^2 - \omega^2 \mu_2 \epsilon_2} \tag{7.19}$$

$$k = \sqrt{\omega^2 \mu_3 \epsilon_3 - \beta^2} \tag{7.20}$$

$$\alpha_4 = \sqrt{\beta^2 - \omega^2 \mu_4 \epsilon_4} \tag{7.21}$$

$$\alpha_5 = \sqrt{\beta^2 - \omega^2 \mu_5 \epsilon_5} \tag{7.22}$$

These equations can be rearranged in terms of the effective refractive index,

$$k = k_0 \sqrt{n_3^2 - n_{eff}^2} \tag{7.23}$$

$$\alpha_m = k_0 \sqrt{n_{eff}^2 - n_m^2} \tag{7.24}$$

where m is the layer number.

Boundary conditions require E_y and $\partial E_y / \partial x$ to be continuous at all boundaries.

Equating the solutions at boundaries d_1 and d_2 gives 4 equations which can be combined to solve for E_1, E_2, E_2'

This yields:

$$E_1 = \frac{2\left(\frac{\alpha_2}{\alpha_2+\alpha_1}\right)\cos(kd_1+\psi)e^{\alpha_2(d_1-d_2)}e^{\alpha_1 d_2}}{1+\left(\frac{\alpha_2-\alpha_1}{\alpha_2+\alpha_1}\right)e^{2\alpha_2(d_1-d_2)}} \tag{7.25}$$

$$E_2 = \frac{\cos(kd_1+\psi)e^{\alpha_2 d_1}}{1+\left(\frac{\alpha_2-\alpha_1}{\alpha_2+\alpha_1}\right)e^{2\alpha_2(d_1-d_2)}} \tag{7.26}$$

$$E_2' = \frac{\cos(kd_1+\psi)e^{-\alpha_2 d_1}}{1+\left(\frac{\alpha_2+\alpha_1}{\alpha_2-\alpha_1}\right)e^{2\alpha_2(d_2-d_1)}} \tag{7.27}$$

by the symmetry of the guide structure we can deduce the form of E_y and solve for E_4, E_4', E_5.

$$E_4 = \frac{\cos(-kd_1+\psi)e^{\alpha_4 d_1}}{1+\left(\frac{\alpha_4-\alpha_5}{\alpha_4+\alpha_5}\right)e^{2\alpha_4(d_1-d_3)}} \tag{7.28}$$

$$E_4' = \frac{\cos(-kd_1+\psi)e^{-\alpha_4 d_1}}{1+\left(\frac{\alpha_4+\alpha_5}{\alpha_4-\alpha_5}\right)e^{2\alpha_4(d_3-d_1)}} \tag{7.29}$$

$$E_5 = \frac{2\left(\frac{\alpha_4}{\alpha_4+\alpha_5}\right)\cos(-kd_1+\psi)e^{\alpha_4(d_1-d_3)}e^{\alpha_5 d_3}}{1+\left(\frac{\alpha_4-\alpha_5}{\alpha_4+\alpha_5}\right)e^{2\alpha_4(d_1-d_3)}} \tag{7.30}$$

Substitution of equations 7.25, 7.26 and 7.27, back into those derived by equating boundary conditions at $x = d_1$ gives,

$$\tan(kd_1+\psi) = \frac{\alpha_2}{k}\cdot\frac{\alpha_1+\alpha_2\tanh(\alpha_2 t_{cl1})}{\alpha_2+\alpha_1\tanh(\alpha_2 t_{cl1})} \tag{7.31}$$

where t_{cl1} is the thickness of the cladding layer adjoining the core and the superstrate, (i.e $d_2 - d_1$).

Similarly at $x = -d_1$,

$$\tan(kd_1 - \psi) = \frac{\alpha_4}{k} \cdot \frac{\alpha_5 + \alpha_4 \tanh(\alpha_4 t_{cl2})}{\alpha_4 + \alpha_5 \tanh(\alpha_4 t_{cl2})} \tag{7.32}$$

where t_{cl2} is the thickness of the cladding layer adjoining the core and the substrate. (i.e $d_3 - d_1$).

Equations 7.31 and 7.32 can be combined to eliminate ψ. Also introduced is the relationship $tan(\theta) = tan(\theta \pm p)$ to account for allowable modes.

$$p\pi = kt_{core} - \tan^{-1}\left(\frac{\alpha_4}{k} \cdot \frac{\alpha_5 + \alpha_4 \tanh(\alpha_4 t_{cl2})}{\alpha_4 + \alpha_5 \tanh(\alpha_4 t_{cl2})}\right) -$$

$$- \tan^{-1}\left(\frac{\alpha_2}{k} \cdot \frac{\alpha_1 + \alpha_2 \tanh(\alpha_2 t_{cl1})}{\alpha_2 + \alpha_1 \tanh(\alpha_2 t_{cl1})}\right) \tag{7.33}$$

where t_{core} is the thickness of the active layer (i.e $2 \times d_1$).

This equation is known as the mode guidance condition equation. Substitution of equations 7.23 and 7.24 into equation 7.33 results in a transcendental equation in terms of n_{eff}. Using numerical techniques this can be solved for each n_{eff} of a particular mode p. All wave numbers k and α_m can then be deduced and the intensity profile of each mode plotted.

7.5 Three and four layer planar waveguides

A generalised model has now been formulated which can be modified to predict the spatial mode profile of the actual waveguides grown during the course of this thesis.

The four layer asymmetric waveguides grown in chapter 9 consist of a 1mm substrate of YAG on which is grown 4µm of Nd:GGG followed by 2µm of YAG (with an air superstrate).

For this case we can set $n_4 = n_5 = n_2$ and $T_{cl2} = 0$.

This reduces the guidance equation to:

$$p\pi = kt_{core} - \tan^{-1}\left(\frac{\alpha_2}{k}\right) - \tan^{-1}\left(\frac{\alpha_2}{k} \cdot \frac{\alpha_1 + \alpha_2 \tanh(\alpha_2 t_{cl1})}{\alpha_2 + \alpha_1 \tanh(\alpha_2 t_{cl1})}\right) \tag{7.34}$$

For single mode propagation within the core where T_{cl1} is large ($\gtrsim 1$ µm for this case)the evanescent field in the cladding does not see the superstrate (or air for the 4 layer case) and so the mode profile observed is that of a 3 layer symmetric waveguide as depicted in figure 7.3.

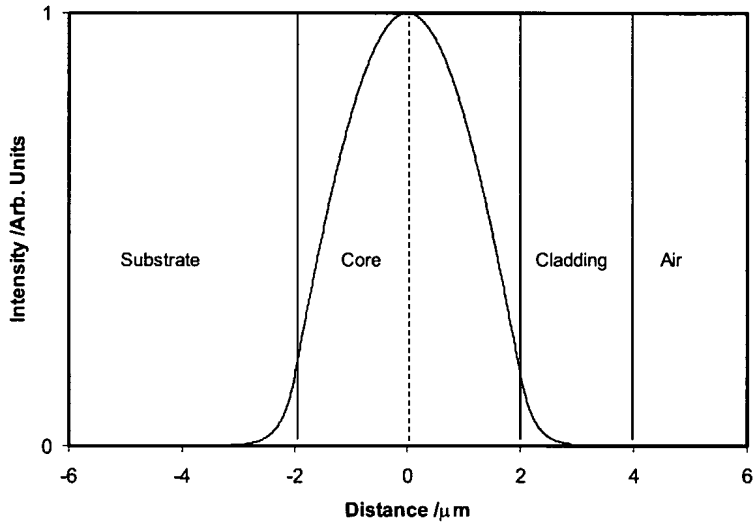

Figure 7.3: 4 layer asymmetric waveguide with thick cladding layer in which the evanescent field does not penetrate to the surface.

In this case the guidance condition can be reduce further to:

$$\tan\left(\frac{kt_{core}}{2}\right) = \frac{\alpha_2}{k} \tag{7.35}$$

For comparison figure 7.4 shows a mode profile for a waveguide with a 100nm cladding layer in which the asymmetry of mode profile and the phase offset can be observed.

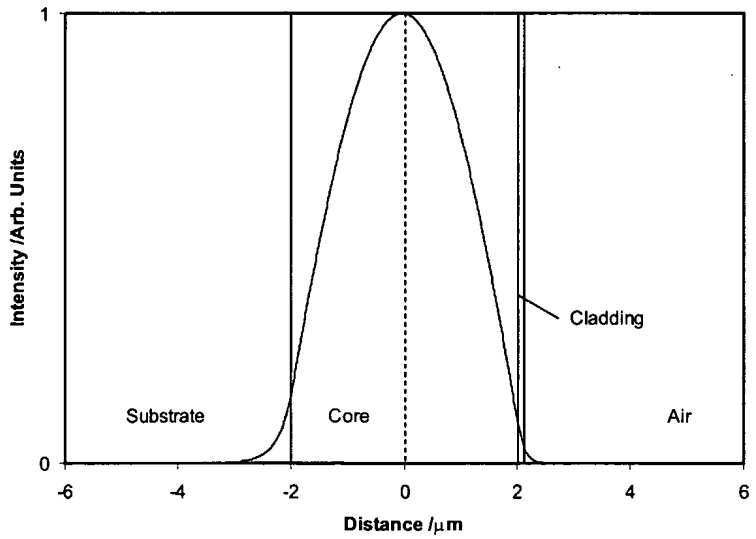

Figure 7.4: 4 layer asymmetric waveguide with thin cladding layer in which the evanescent field penetrates to the surface.

In the limiting case of $T_{cl1} \rightarrow 0$ the waveguide is reduced to the more common three layer asymmetric waveguide. Figure 7.5 depicts the mode profile expected for a 4μm GGG waveguide grown on a YAG substrate as grown in chapter 8.

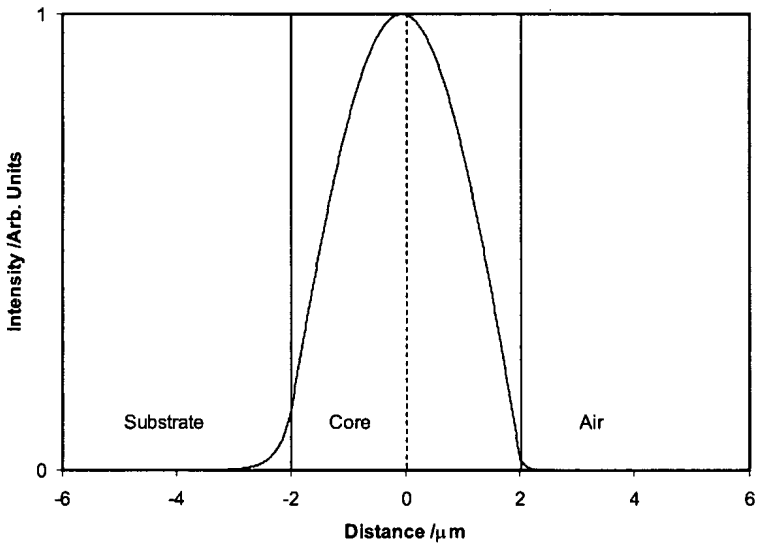

Figure 7.5: 3 layer asymmetric waveguide.

The guidance condition for this geometry is:

$$p\pi = kt_{core} - \tan^{-1}\left(\frac{\alpha_1}{k}\right) - \tan^{-1}\left(\frac{\alpha_4}{k}\right) \tag{7.36}$$

7.6 Laser theory

The theory surrounding laser oscillation has been well reviewed in both bulk [5–7] and waveguide form [8, 9]. This section aims to demonstrate analytically the advantages of a waveguide geometry over its bulk counterpart. The Nd^{3+} ion will be used as an example in this section as this is the laser system used in chapter 8 and 9 of this thesis.

7.6.1 Four-level lasers

Laser action of the Nd^{3+} ion is a 4 four-level laser system as depicted in figure 7.6.

Laser action is initiated by excitation of the ground state electrons to the excited upper pump level.[1] This is followed by rapid decay via non-radiative (multi-phonon) transitions to an upper $^4F_{3/2}$ laser level. The upper state life time for the Nd^{3+} ion in the metastable $^4F_{3/2}$ level is ~260 µs (in GGG at 1 at. %) [10] which allows a population inversion between the $^4F_{3/2}$ level and the $^4I_{11/2}$ lower laser level (for 1.06µm radiation). Electrons in this state can undergo stimulated emission to the $^4I_{11/2}$ level and subsequent rapid decay by non-radiative processes to the ground state. When population inversion is achieved, gain can be observed for the $^4F_{3/2}$ - $^4I_{11/2}$ transition on which lasing action can result in an appropriate geometry laser cavity.

[1] Technically the levels referred to here are correctly termed *manifolds* as they consist of a number of stark-split sub-levels. As this discussion does not go into the details of stark splitting, however, the term *level* will be used throughout for simplicity.

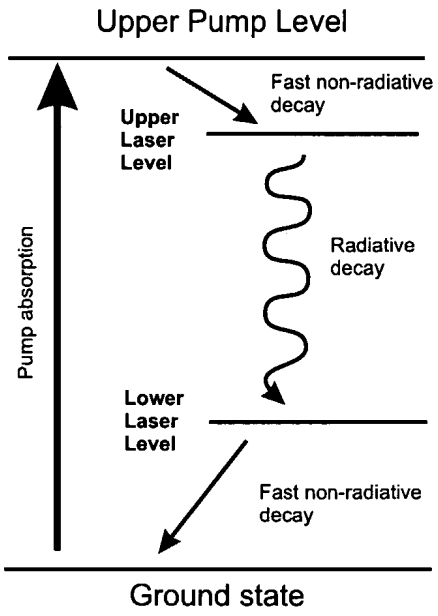

Figure 7.6: Schematic diagram of the four level laser system.

The threshold pump power required for lasing in bulk media is given by [9]:

$$P_{th} = \left(\frac{\pi h \nu_p L}{4\sigma_e \eta_p \tau_{fl}(1 - e^{-\alpha_p l})}\right) \sqrt{\left(\overline{W}_p^2 + \overline{W}_l^2\right)} \tag{7.37}$$

Where h = Planck's constant, ν_p is the pump laser frequency, σ_e is the stimulated emission cross section, α_p is the absorption coefficient at the pump wavelength η_p is the pump quantum efficiency, l is the cavity length and τ_{fl} is the fluorescence lifetime. $\overline{W}_l$ and $\overline{W}_p$ are the average spot sizes for the laser and pump beam respectively. L is the fractional round trip loss for the signal beam which includes output coupling terms from the cavity mirrors (i.e if all power is dissipated in exactly one round trip then the loss is unity. Complete power dissipation before one round trip is complete gives rise to values of loss higher than unity). If high reflectivity mirrors are used at both cavity ends then this term will be almost solely due to scattering within the cavity as absorption is negligible for the signal wave-

length. This model assumes Gaussian beam profiles with no astigmatism. All units are SI.

It can be seen that minimisation of the average pump and signal beam waists will lower the threshold power required. Tighter focusing of the pump and signal beam enables smaller beam waists but at the cost of higher divergence in the cavity. The minimum average beam waist size is given by:

$$\overline{W}_{p,l}^2 = \frac{l\lambda_{p,l}}{\sqrt{3}\pi n} \tag{7.38}$$

Where $\lambda_{p,l}$ is the wavelength at the the pump or signal wavelengths respectively, l is the cavity length and n is the refractive index of the lasing medium.

Substituting of equation 7.38in equation 7.37 gives the optimum threshold as:

$$P_{th} = \frac{l\pi h\nu_p L}{4\sqrt{3}\pi n\sigma_e \eta_p \tau_{fl}(1 - e^{-\alpha_p l})}(\lambda_p + \lambda_l) \tag{7.39}$$

7.6.2 Lasing in waveguide structures

In a typical waveguide cavity the pump power threshold for lasing in a four level system is given by [6].

$$P_{th} = \left(\frac{\pi h\nu_p L}{4\sigma_e \eta \alpha_p \tau_{fl}}\right)\left[\int_0^l \frac{\exp(-\alpha_p z)}{\left(W_{lx}^2 + W_{px}^2\right)^{1/2}\left(W_{ly}^2 + W_{py}^2\right)^{1/2}}\,\mathrm{d}z\right]^{-1} \tag{7.40}$$

Where W_l and W_p are the spot sizes for the laser and pump beam respectively in the guided (x) and unguided (y) direction.

By assuming average spot sizes, $\overline{W}$, and no spatial hole burning this equation can be evaluated to:

$$P_{th} = \left(\frac{\pi h \nu_p L}{4\sigma_e \eta_p \tau_{fl}(1 - e^{-\alpha_p l})}\right) \sqrt{\left(\overline{W}_{lx}^2 + \overline{W}_{px}^2\right)} \sqrt{\left(\overline{W}_{ly}^2 + \overline{W}_{py}^2\right)} \quad (7.41)$$

This can now be compared to the bulk equivalent. The ratio of the bulk threshold to the waveguide threshold is obtained by dividing equation 7.41 by 7.37:

$$\frac{P_{th}^{waveguide}}{P_{th}^{bulk}} = \left(\frac{\sqrt{3} n \pi}{l\,(\lambda_p + \lambda_l)}\right) \sqrt{\left(\overline{W}_{lx}^2 + \overline{W}_{px}^2\right)} \sqrt{\left(\overline{W}_{ly}^2 + \overline{W}_{py}^2\right)} \cdot \frac{L_{waveguide}}{L_{bulk}} \quad (7.42)$$

For a planar waveguide we will assume optimum focussing (equation 7.38) in the unguided direction, which gives:

$$\frac{P_{th}^{waveguide}}{P_{th}^{bulk}} = \left(\frac{\sqrt{3} n \pi}{l\,(\lambda_p + \lambda_l)}\right)^{1/2} \sqrt{\left(\overline{W}_{lx}^2 + \overline{W}_{px}^2\right)} \cdot \frac{L_{waveguide}}{L_{bulk}} \quad (7.43)$$

From this equation it can be seen that the advantage of waveguides is the confinement of the pump and signal beam which leads to small values of $\overline{W}_{lx}^2$ and $\overline{W}_{px}^2$. It might also be implied from equation 7.43 that devices requiring long cavity lengths would also benefit from guided geometries. This is due to the fact that the average spot size in the guided direction is not length dependent as it is in the unguided regime. This must be balanced, however, with the inevitable increase in cavity loss $L_{waveguide}$ compared to that of L_{bulk}.

We can substitute into equation 7.43 typical values for the devices grown in chapter 8, i.e l = 2mm, λ_p = 808nm, λ_l = 1060nm and n=1.96. By making the rough approximation of similar average pump and signal beam waists and the *very* rough approximation of equal losses in bulk and waveguide the result obtained shows that the threshold of the waveguide device will be less than the bulk when the average beam waist radii are below 13µm . As a rule of thumb the average beam waist diameter will be about a third

of the size of the device thickness (This can be seen on the model of a three layer waveguide in figure 7.5 where the $1/e^2$ diameter is $\sim$1.4μm for a 4 μm device). This implies that lower thresholds might be seen in waveguides of $<$ 80μm thickness. Real waveguides devices, however, have significantly higher losses than bulk due to scattering from the device surface. Scattering losses can be minimised by capping but are unlikely to be as low as those in bulk materials. If we take general case of bulk materials possessing $\sim$1 order of magnitude lower loss than waveguide devices then these devices would need to be $\lesssim$ 8μm thick before significant improvement would be seen.

To complicate matters further results in chapter 8 suggest that losses seen in an uncapped device may also be a function of device thickness, that is, as the thickness decreases, the losses are seen to increase. This makes optimisation of the waveguide thickness device a complicated task.

7.7 Conclusions

A model describing the spatial mode profile of a guided wave in a planar waveguide device has been presented. The model is for a general asymmetric five layer waveguide which allows for modelling of devices grown during the course of this work and for devices proposed for future growth. A basic look at laser theory has also been presented with a more detailed look at the equations governing lasing threshold. A rough theoretical comparison between bulk and waveguide devices show that waveguides should produce smaller lasing thresholds than bulk as beam confinement is increased, although loss mechanisms within the guide complicate the issue.

7.8 References

[1] A Yariv. Chapter 22 - Guided wave optics - propagation in optical fibres. In *Quantum electronics*, pages 600–650. John Wiley & Sons, 1989.

[2] D H Lee. Chapter 4 - The slab dielectric waveguide. In *Electromagnetic principles of integrated optics*, pages 77–112. Chapman and Hall, 1986.

[3] D H Lee. Chapter 5 - Practical waveguiding geometries. In *Electromagnetic principles of integrated optics*, pages 113–145. Chapman and Hall, 1986.

[4] C. L. Bonner. *Multi-watt, diode pumped planar waveguide lasers*. PhD thesis, University of southampton, 2000.

[5] W.P. Risk. Modeling of longitudinally pumped solid-state lasers exhibiting reabsorption losses. *Journal of the Optical Society of America B-Optical Physics*, 5(7):1412–1423, 1988.

[6] W.A. Clarkson and D.C. Hanna. Effects of transverse-mode profile on slope efficiency and relaxation oscillations in a longitudinally-pumped laser. *Journal of Modern Optics*, 36(4):483–498, 1989.

[7] T.Y. Fan and R.L. Byer. Diode laser-pumped solid-state lasers. *IEEE Journal of Quantum Electronics*, 24(6):895–912, 1988.

[8] K Kubodera and K Otsuka. Single transverse-mode $LiNdP_4O_{12}$ slab waveguide laser. *Journal of Applied Physics*, 50(2):653, 1978.

[9] M.J.F. Digonnet and C.J. Gaeta. Theoretical-analysis of optical fiber laser-amplifiers and oscillators. *Applied Optics*, 24(3):333–342, 1985.

[10] J. Geusic, H. M. Marcos, and L. G. Van Uitert. *Applied Physics Letters*, 4:182–184, 1964.

Chapter 8

Particulates in PLD

8.1 Introduction

Large numbers of particulates can occur on the film surface during growth by PLD . These particulates originate from the target and are believed to occur, in the growth of dielectric films, through two main processes [1].

The first process is due to incomplete vaporisation of the target area by the ablation laser. The area directly surrounding the vaporised material melts and is subsequently expelled by the recoil pressure of the plasma plume shock wave. As a result liquid droplets of target material form into particulates on the growing film. Increasing the density of the target material has been found to minimise this process of particulate production. Single crystal targets are therefore the optimum material for film fabrication as opposed to alternatives such as compressed ceramic targets [2]. Alternatively, the use of a femtosecond ablation source has also been considered as a potential way of avoiding particulates produced by this process [3] (see section 3.4.1).

The second process, termed exfoliation, is due to poor surface quality of the target. As the ablation laser pulses continually hit the same region of the target, thin structures of μm dimensions can develop on the target.

These cone-like structures point towards the direction of the laser radiation, due to a shadowing effect [4]. The cones can eventually break off and form particulates on the film surface. Rotating the target and constantly changing the direction of rotation and also re-polishing the target after use can reduce, but not eliminate, this effect.

There have been many reports on the parameters that effect the number of particulate in PLD. There have also been many innovative attempts to remove particulates from the plasma plume including: dual cross plumes [5], fast spinning targets [6], mechanical shutters [7] and cross magnetic fields [8] however these have often involved complicated set-ups or sensitive triggering equipment and may be considered to be generally impractical.

Other systems that involve backscattering deposition or substrate shadowing can eliminate almost all particulates but at the expense of extremely low deposition rates [9–11].

However, there has been no measured correlation to date, relating the number of particulates seen on the films and the losses generated when used as a waveguide. In this chapter we report on the implementation of a method of particulate removal. We also report on a systematic comparison between the lasing threshold observed in PLD waveguides of differing thickness and varying particulate densities.

8.2 Growth of comparable films

Using conditions similar to those reported by Anderson *et al* [2], we have grown pulsed laser deposited films from a 1 at % Nd doped, single crystal, GGG target on a (100) YAG substrate. A brief outline of the important growth parameters are as follows: the vacuum chamber is first evacuated and back filled with oxygen to a pressure of $\sim 5 \times 10^{-2}$ mbar. A (100) YAG substrate is heated to a temperature of ~750°C using a scanning CO_2 laser.

The substrate is positioned 3.5cm from the target. The target is rotated and ablated with a 248nm KrF excimer laser at a 20Hz repetition rate and at a fluence of 50 mJ cm^{-2}. A deposition time between ~5 to 20 minutes is required depending on the desired thickness of the film film.

8.2.1 Gas jet assisted variation of particulate density

Films were grown at thicknesses of the order of 2μm , 4μm and 8μm . A piezoelectric gas valve was used to modify the particulate density in the film during growth as used by Murakami and Schenck [12, 13]. This is shown in Figure 8.1.

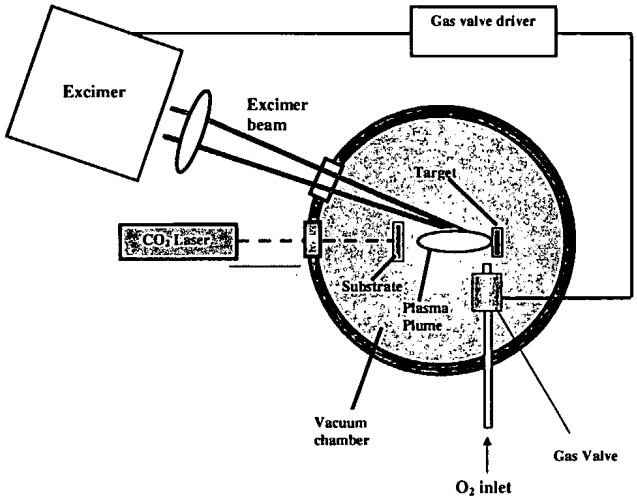

Figure 8.1: Experimental set-up showing piezoelectric gas valve mounted in chamber.

Opening of the gas valve (backed with O_2) ejects a beam of molecular oxygen in a direction perpendicular to the expanding plasma plume. The particulates contained within the plasma plume have a significantly lower velocity (~1 × 10^4 cm s^{-1}) than the fast neutral and ionic species (~1 × 10^6 cm s^{-1}) assumed to contribute to good stoichiometric film growth [12]. The firing of the ablation laser is triggered from the valve such that the beam of molecular oxygen is both temporally and spatially coincident

with the particulates in the ablation plume. The particulates are deflected, by collision with the oxygen molecules, away from the substrate.

A fast rise time (in pressure) of the oxygen pulse and, consequently, the gas valve opening time is critical for the molecular beam to interact with only the slower, detrimental, particulates and not interfere with the faster neutral and ionic species. Gas pulse rise times of the order of ~200μs are required, and for this reason we chose a piezoelectric gas valve. A Maxtek MV-112 gas valve was used but modified such that the gas had less distance to travel within the valve before its ejection into the chamber, this helps the gas pulse maintain a fast rise time. Modifications to the valve can be seen in figure 8.2. Solenoid gas valves can achieve rise times as fast as piezoelectric valves, but at far greater expense. A further advantage to piezoelectric valves is that, the driving circuits are trivial to build compared to those required for solenoid devices.

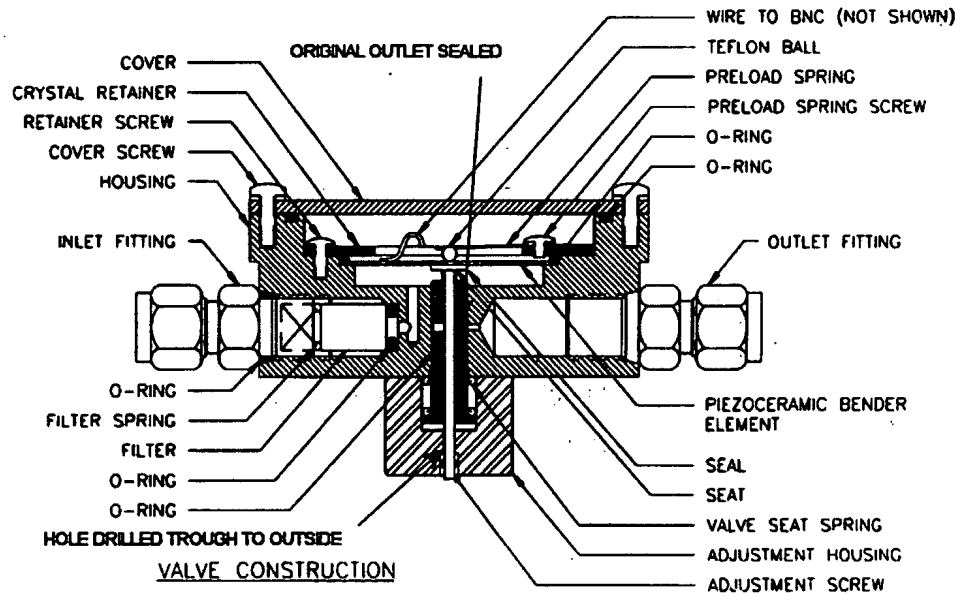

Figure 8.2: Original schematic of the valve altered to show the modifications in blue.

The gas valve nozzle was placed 2 mm below the ablation area. The close proximity of the nozzle to the ablation area maximises the probability of

collision as the density of both the oxygen pulse and the plasma plume are at a maximum. Typical delays between gas valve and laser pulse triggering were around 1ms. The backing pressure of oxygen on the valve was ~2 bar. The piezoelectric valve was also used as the oxygen source for reactive PLD by keeping the valve open for ~3ms to achieve an oxygen pressure in the chamber of $\sim 5 \times 10^{-2}$ mbar during ablation.

8.2.2 Properties of the films

The XRD data shown in Figure 8.3 confirm the crystallinity of the films and shows growth in the (400) Nd:GGG direction parallel to the (400) YAG plane.

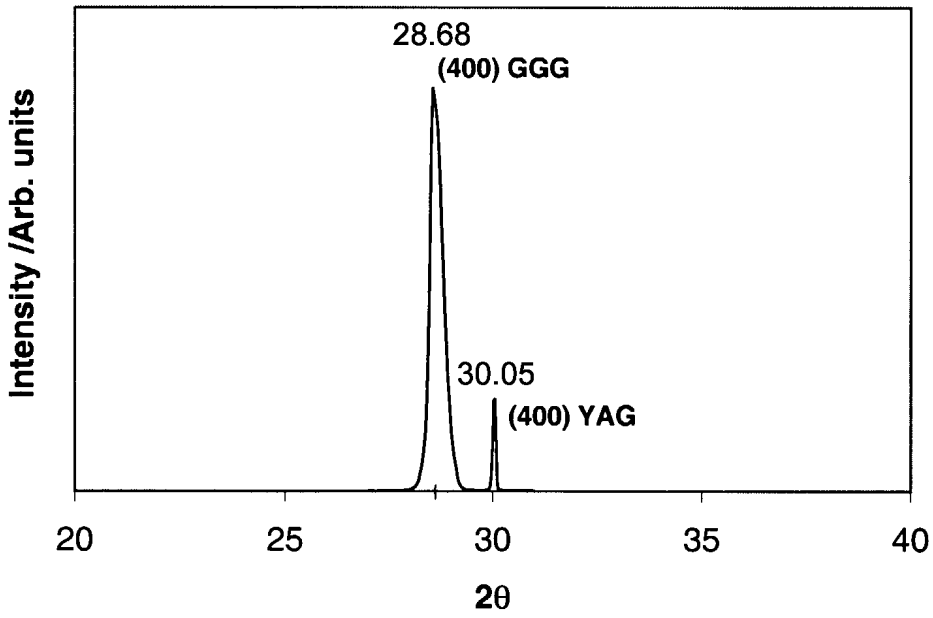

Figure 8.3: X-ray diffraction data for the Nd:GGG films. The YAG (400) line is weak due to the thickness of the sample. No other peaks are observed.

Figure 8.4 shows the surface of a film with a high particulate density that was grown without the gas-jet. Figure 8.5 shows a film of lower particulate density that was grown with the aid of gas jet.

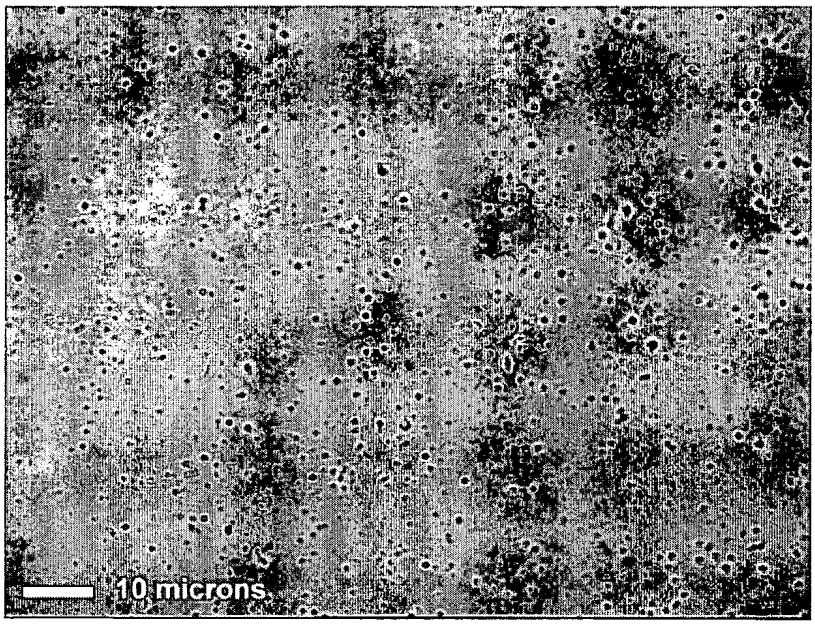

Figure 8.4: Optical microscopy image of film surface under normal growth conditions.

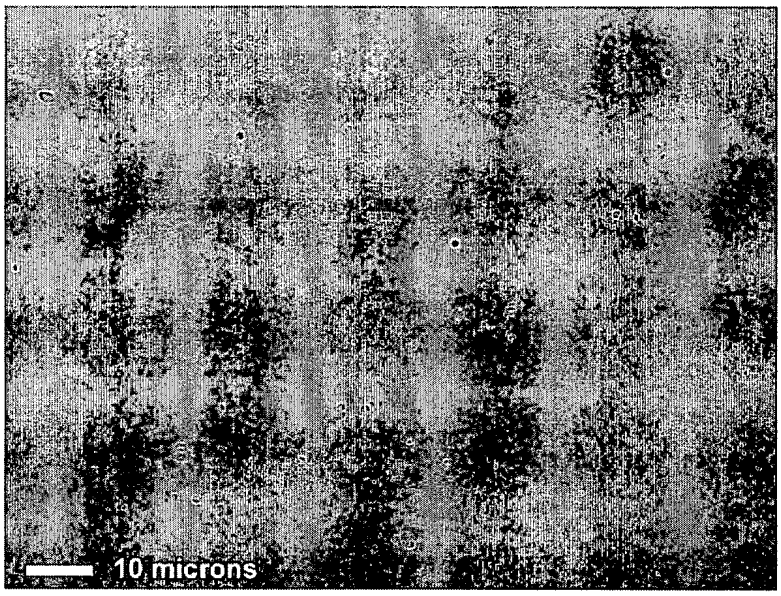

Figure 8.5: Optical microscopy image of film surface with gas-jet directed into plume during growth.

We have grown films with particulate densities that vary between 10^4 and 10^7 particulates/cm^2. This large difference in particulate densities may not be entirely due to the gas jet and can be attributed in part to the increased degradation of the target and increased exfoliation. XRD spectra show a slight broadening of the (400) GGG peak with increased particulate density, implying a slight degradation in crystallinity. Figure 8.6 shows the increase in the FWHM (in degrees) of the (400) GGG peak in a number of 4μm thick waveguides with increased particulate density.

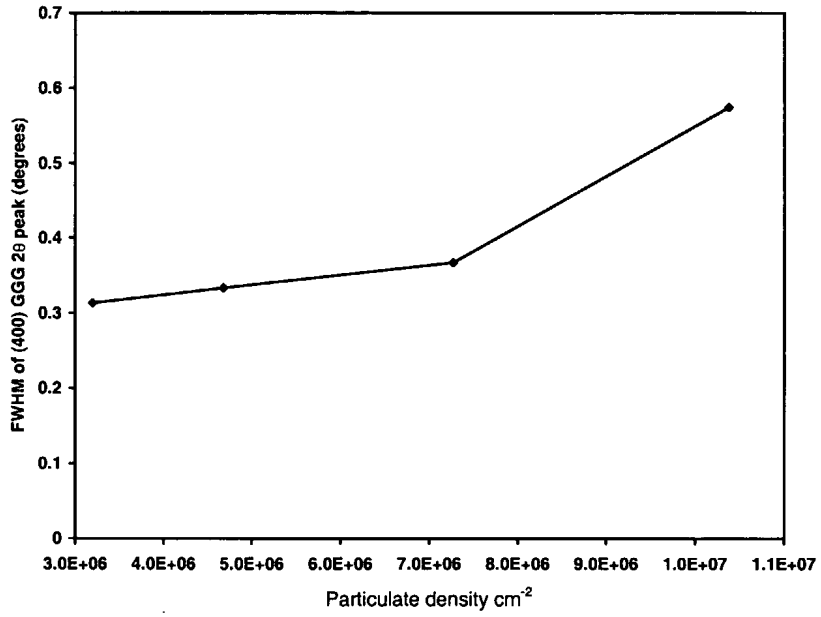

Figure 8.6: Increase of FWHM of the (400) GGG peak with particulate density.

Figure 8.7 shows typical particle size distributions for films containing the high and low particulate densities. All films show an approximately normal distribution of particle sizes.

The films were cut back to 2mm in length, corresponding approximately to a 1/e absorption length for the pumping wavelength of 808nm, and polished to optical flatness on both ends. Horizontal and vertical parallelism was maintained between the end faces by a laser collimator.

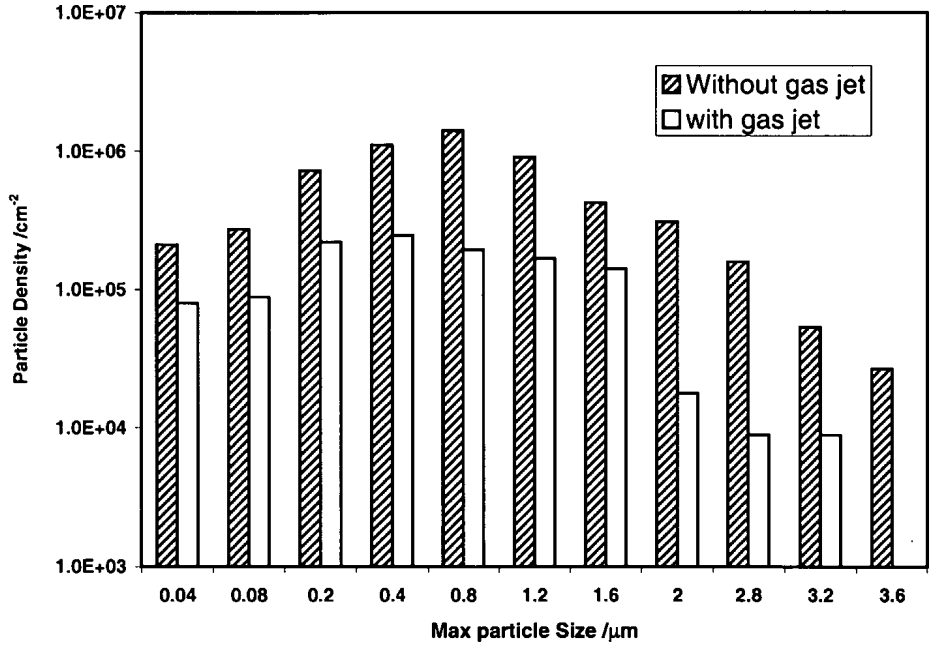

Figure 8.7: Typical particle size distributions for films with high and low particulate distributions.

8.3 Threshold results for waveguide lasing

To confirm spectroscopic properties, the waveguides were pumped using an Ar^+pumped Ti:sapphire laser capable of delivering 600mW at 808nm, matching the strongest absorption band of Nd:GGG [14]. Light was coupled into the active layer using $\times 25$ objectives for the 2μm and 4μm guides and $\times 16$ for the 8μm guide. Figure 8.8 shows the fluorescence spectrum of the Nd doped waveguide.

This agrees with previous results [2], showing peak fluorescence around 1060nm. Fluorescence lifetime was measured to be 260μs , in close agreement with previous results [2] and the bulk crystal value results [15–17].

Two plane dielectric mirrors were carefully attached to the end faces using Fluorinert FC-70 fluorinated liquid. Both mirrors were high reflectivity (>99.5%) mirrors at the signal wavelength. A typical lasing spectrum of the fabricated waveguide lasers is shown in Figure 8.9, and consists of a

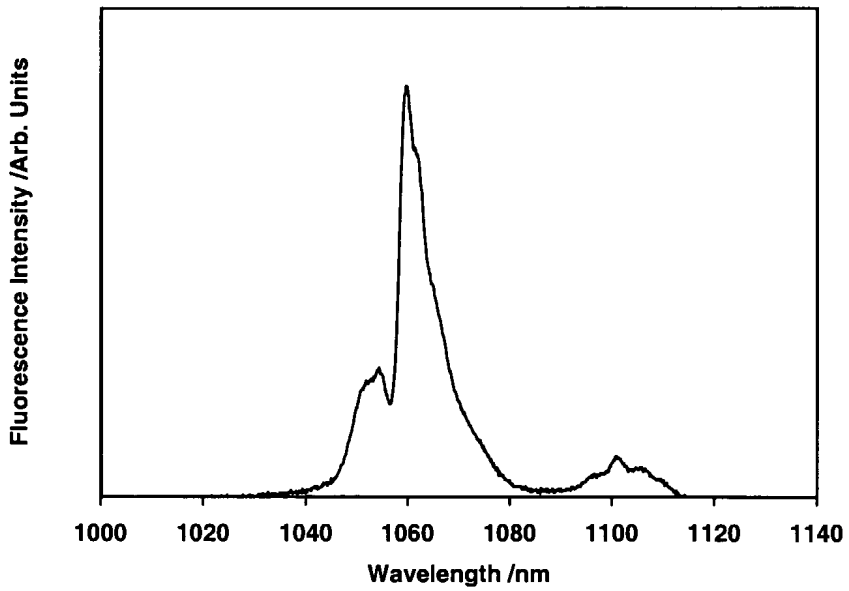

Figure 8.8: Typical fluorescence spectrum of a waveguide.

broad emission over ~3nm. Multiple peaks (splitting) can be seen due to etalon effects within the dielectric mirrors. The spatial output profile at the lasing wavelength was single mode for all waveguides, regardless of how many spatial modes could, in theory, be supported within the waveguide.

The lasing threshold was measured for films of varying thickness and particulate density. Figure 8.10 shows the threshold recorded for the three different thickness films.

It can be seen that the high particulate density has a detrimental effect on the lasing threshold of the film. The effect is largely due to the particulates acting as scattering sites for light within the guide, which consequently increases the loss in a waveguide. From equation 8.1 it can seen that lasing threshold is expected to increase linearly with loss [18] (and see section 7.6.2).

$$P_{th} = \left(\frac{\pi h \nu_p L}{4\sigma_e \eta_p \tau_{fl}(1 - e^{-\alpha_p l})}\right) \sqrt{\left(\overline{W}_{lx}^2 + \overline{W}_{px}^2\right)} \sqrt{\left(\overline{W}_{ly}^2 + \overline{W}_{py}^2\right)} \quad (8.1)$$

Where all variables are as defined earlier (section 7.6.2).

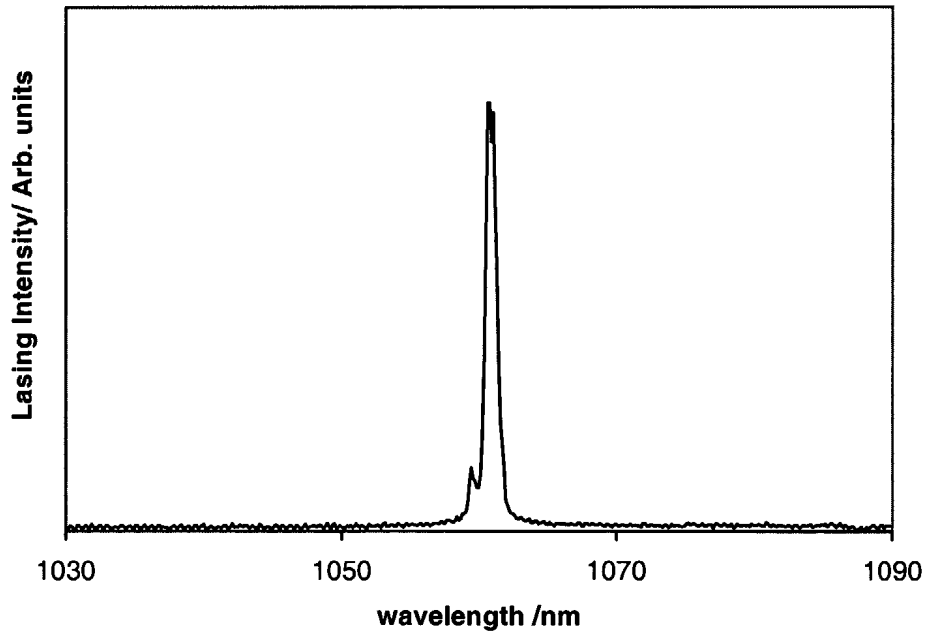

Figure 8.9: Typical lasing spectrum of a waveguide.

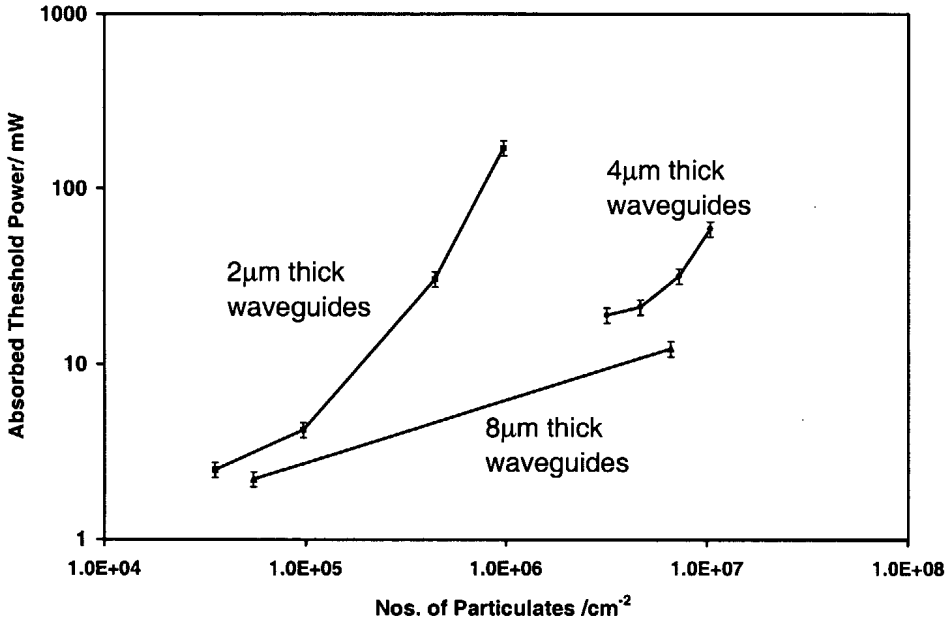

Figure 8.10: Lasing threshold versus particulate density for films of different thickness.

Using measured spot sizes and threshold values we have estimated the loss in each guide. This is plotted against particulate density in figure 8.11. It can be seen that the effect of the particulates has a far more dramatic effect on those guides with increased confinement. An increase in particulate density from 3.5×10^4 to 9.7×10^5 particulates/cm^2 led to an increase in absorbed power threshold from 2.5mW to 167mW. A 4μm thick guide with a particulate density of 3.2×10^6 particulates/cm^2, however, lased easily at 19mW where as a 2μm thick waveguide could not be made to lase at the pump powers available. Even with an increase in particulate density up to 1×10^7 particulates/cm^2 (a very poor quality film) lasing was possible at around 60mW of absorbed pump power. The 8μm thick waveguide showed good waveguide performance regardless of particulate density, lasing at 2.2mw and 12.2mw with particulate densities of 5.5×10^4 cm^{-2} and 6.6×10^6 cm^{-2} respectively, a change in particulate density of over 2 orders of magnitude.

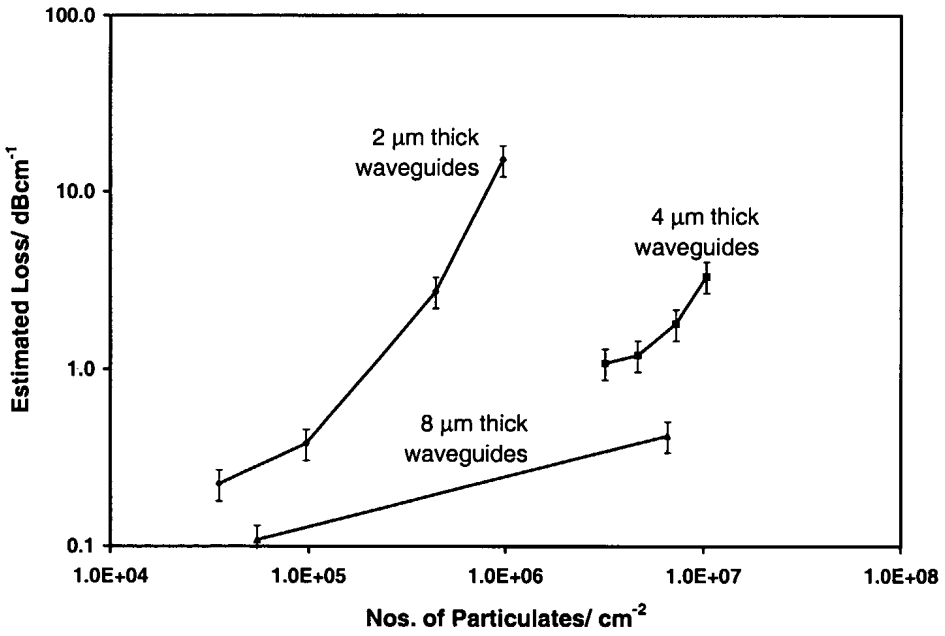

Figure 8.11: Estimated loss versus particulate density for films of different thickness.

In waveguides, the predominant cause of loss is believed to be largely

due to surface scattering, and not due to scattering from within the guide. The increased effect of particulates on the more confined waveguides (2μm thick) is possibly an example of this. As the size of particulates in a 2μm thick guide is of the order of the guide thickness itself then there is a higher probability of surface scattering, as most of the particulates will likely be protruding from the waveguide surface. In the larger guides there is more chance that the particulates will be enclosed within the guide and not contribute as significantly to the losses.

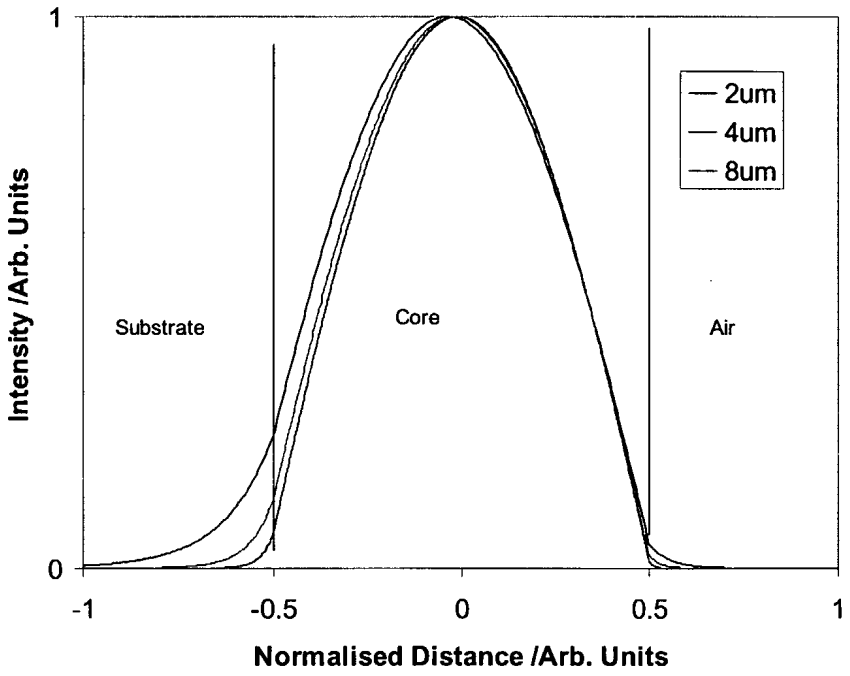

Figure 8.12: Mode profile of the fundamental mode of a laser for the 3 different thicknesses of waveguide studied.

Figure 8.12 shows the spatial mode profile of the fundamental mode in a three layer asymmetric waveguide as modelled from chapter 7. In this figure the spatial mode profiles of the waveguides, at the three different thicknesses studied, are plotted. The x-axis is normalised for each plot to the thickness of the active layer (i.e the distance across the core of each plot is set to '1'). This normalisation shows the *proportion* of the guided mode that interacts with the waveguide interfaces. It can be clearly seen that as the core dimensions are reduced the proportion of the mode that

exists as an evanescent field increases. It is this part of the mode that will see, proportionally, the highest scattering losses due to surface scattering. Therefore it would be expected that the 2μm guides will suffer more scattering when compared to thicker guides. This is possibly an alternative or additional reason why thicker waveguides appear to see proportionally lower scattering losses. It would agree with other reports of higher scattering losses seen in more confined waveguide structures [19].

The slight decrease in crystal quality, as observed via XRD, with increasing particulate density also contributes to the increase in threshold. This may partially account for the observed non-linear increase of threshold power with particulate density.

It should be noted that the particulate density counts given are taken from an optical microscope using particulate analysis software and so represent the particulate count throughout the entire guide per cm^2. Many reports take particulate counts from SEM data, which can only yield particulate counts for particulates that extend beyond the surface.

8.4 Conclusions

These results suggest that were particulates to remain an intrinsic problem in the fabrication of waveguide devices by PLD, the solution would be to move to thicker waveguides. The particulate density, in thicker guides, appears not to be such a critical factor in the performance of the resultant laser. Although this seems a relatively intuitive deduction it is in contrast to the accepted notion that lower thresholds can be attained with more confined waveguides structures.

The fabrication of thicker waveguides, however, is easily achieved with PLD. Deposition rates of up to 1μm /minute are achievable so there need not be a significant increase in fabrication time. Since high numerical aperture (NA) waveguides are also readily achievable with PLD, it would

suggest that thick, high NA, PLD fabricated waveguides are an attractive prospect for pumping with high power, high divergence sources. Finally it should be noted that proximity coupling has also been achieved with this kind of device [20].

8.5 References

[1] J. T. Cheung. History and fundamentals of pulsed laser deposition. In D. B. Chrisey and G. K. Hubler, editors, *Pulsed laser deposition of thin films*, pages 1–22. John Wiley and Sons, New York, 1994.

[2] A.A. Anderson, C.L. Bonner, D.P. Shepherd, R.W. Eason, C. Grivas, D.S. Gill, and N. Vainos. Low loss (0.5 db/cm) Nd:$Gd_3Ga_5O_{12}$ waveguide layers grown by pulsed laser deposition. *Optics Communications*, 144(4-6):183–186, 1997.

[3] F. Qian, R.K. Singh, S.K. Dutta, and P.P. Pronko. Laser deposition of diamond-like carbon-films at high intensities. *Applied Physics Letters*, 67(21):3120–3122, 1995.

[4] K. H. Wong, S. K. Hau, P. W. Chan, L. K. Leung, C. L. Choy, and H. K. Wong. XeCl excimer laser interaction with partially-stabilized zirconia target. *Journal of Materials Science Letters*, 10(14):801–803, 1991.

[5] S. Gaponov, J. Gavrilov, M. Jelinek, E. Kluenkov, and L. Mazo. YbACuO and ZrO_2 laser deposition on sapphire using 2 crossed laser-beams. *Superconductor Science & Technology*, 5(11):645–647, 1992.

[6] H. Sankur. Annual report no.2 air force office of sci. reseach. Technical report, 1986.

[7] D. Lubben, S. A. Barnett, K. Suzuki, S. Gorbatkin, and J. E. Greene. Laser-induced plasmas for primary ion deposition of epitaxial Ge and Si films. *Journal of Vacuum Science & Technology B*, 3(4):968–974, 1985.

[8] H. Kawasaki, K. Doi, S. Hiraishi, and Y. Suda. Effects of cross-magnetic field on thin film preparation by pulsed Nd:YAG laser deposition. *Thin Solid Films*, 374(2):278–281, 2000.

[9] E. Agostinelli, S. Kaciulis, and M. Vittori-Antisari. Great reduction of particulates in pulsed laser deposition of Ag-Co films by using a shaded off-axis geometry. *Applied Surface Science*, 156(1-4):143–148, 2000.

[10] D. W. Kim, S. M. Oh, T. W. Noh, and S. H. Lee. Epitaxial $LiNbO_3$ thin films grown by the "eclipse method". *Journal of the Korean Physical Society*, 32:S1408–S1410, 1998.

[11] D. W. Kim, S. M. Oh, S. H. Lee, and T. W. Noh. Structural and optical properties of $LiNbO_3$ films grown by pulsed laser deposition with a shadow mask. *Japanese Journal of Applied Physics Part 1-Regular Papers Short Notes & Review Papers*, 37(4A):2016–2020, 1998.

[12] K Murakami. Dynamics of laser ablation of high Tc superconductors and semiconductors, and a new method for growth of films. In E. Fogarassy and S. Lazare, editors, *Laser ablation of electronic materials: Basic mechanism and applications*, volume 4 of *European research society monographs*, pages 125–140. Elsevier Science, The Netherlands, 1992.

[13] P.K. Schenck, M.D. Vaudin, D.W. Bonnell, J.W. Hastie, and A.J. Paul. Particulate reduction in the pulsed laser deposition of barium titanate thin films. *Applied Surface Science*, 129:655–661, 1998.

[14] S.J. Field, D.C. Hanna, A.C. Large, D.P. Shepherd, A.C. Tropper, P.J. Chandler, P.D. Townsend, and L. Zhang. An efficient, diode-pumped, ion-implanted Nd-GGG planar waveguide laser. *Optics Communications*, 86(2):161–166, 1991.

[15] J. Geusic, H. M. Marcos, and L. G. Van Uitert. *Applied Physics Letters*, 4:182–184, 1964.

[16] Kh. Bagdasarov, G. A. Bogomolova, M. M. Gritsenko, A. A. Kaminskii, A. M. Kevorkov, A. M. Prokhorov, and S. E. Sarkisov. *Sov. Phys. Dokl*, 19:353, 1974.

[17] B. Comaskey, B. D. Moran, G. F. Albrecht, and R. J. Beach. Characterization of the heat loading of Nd-Doped YAG, YOS, YIF, and GGG excited at diode pumping wavelengths. *IEEE Journal of Quantum Electronics*, 31(7):1261–1264, 1995.

[18] W.A. Clarkson and D.C. Hanna. Effects of transverse-mode profile on slope efficiency and relaxation oscillations in a longitudinally-pumped laser. *Journal of Modern Optics*, 36(4):483–498, 1989.

[19] K. K. Lee, D. R. Lim, H. C. Luan, A. Agarwal, J. Foresi, and L. C. Kimerling. Effect of size and roughness on light transmission in a Si/SiO_2 waveguide: Experiments and model. *Applied Physics Letters*, 77(11):1617–1619, 2000.

[20] C. L. Bonner, T. Bhutta, D. P. Shepherd, and A. C. Tropper. Double-clad structures and proximity coupling for diode-bar- pumped planar waveguide lasers. *IEEE Journal of Quantum Electronics*, 36(2):236–242, 2000.

Chapter 9

Capped Nd:GGG waveguides

9.1 Introduction

As reported in chapter 3 the growth of optical waveguide devices by PLD is becoming more widespread with the recent successful fabrication of two waveguide lasers of Nd:GGG [1] and Ti:sapphire [2]. Complex stoichiometric crystal waveguide devices have also been fabricated, for example Nd,Cr:GSGG [3], $Ca_4GdO(BO_3)_3$ (GdCOB) [4], Cr^{4+}:YAG and Cr^{4+}:GGG [5]. These reports demonstrate that PLD is capable of controlling not just the stoichiometry of the film but also the valence states of dopants such as chromium and titanium. Fabrication of heterostructures by PLD has also been reported [6,7] demonstrating that PLD is capable of producing complex structures as well as stoichiometries. With the growth of more exotic non-linear, electro-optic and piezoelectric crystals such as $LiNbO_3$ more intricate devices are to be expected in the MEMS (micro-electro-mechanical systems) area.

However, the ability of PLD to grow complex stoichiometry heterostructures in order to fabricate a multilayer or *capped* waveguide laser has not, as yet, been utilised. In this chapter we report on the growth of YAG superstrate layers grown on Nd:GGG waveguides (as reported in chapter 8),

as a method of reducing loss in our waveguide device.

9.1.1 YAG overlayers

As described in chapter 7 the evanescent field in a waveguide extends beyond the active layer. Any imperfections on the top surface of the active layer are a source of loss due to scattering from the surface. The amount of scattering seen at the surface is a function of the refractive index difference between the two interfaces from which scattering occurs. This is due to the fresnel reflection at the interface which is given by:

$$R = 1 - \frac{4n_1 n_2}{(n_1 + n_2)^2} \tag{9.1}$$

Where R is the fraction of light reflected and n_1 and n_2 are the refractive indices either side of the interface.

By covering the active layer with another layer possessing a slightly lower refractive index the amount of scattering from the interface of the waveguide will be reduced. Such waveguides are known as capped or buried waveguides.

If capping can be performed *in situ* then it is not possible for contaminants to come into contact with the surface of the guiding layer therefore reducing the number of scattering sites on the waveguide interface.

Usually the most obvious choice of capping material for the waveguide is that used for the substrate. For GGG it is known that the lattice match between the substrate (YAG) and the active layer (GGG) is close enough to allow epitaxial growth of GGG on YAG [8]. Therefore, it follows that the lattice match will also be adequate for growth of YAG on GGG. Epitaxial growth of a YAG film on a GGG substrate has, in fact, already been reported [9].

9.2 Previous results of Nd:GGG waveguides

The Nd:GGG waveguides investigated in this chapter were fabricated using the growth conditions as described in chapter 8.

The target used for the work presented in this thesis has deteriorated over time. This has led to production of films that possess, on average, increasingly higher particulate densities with successive depositions. For these reasons some of the waveguides fabricated have much higher particulate counts than have been reported previously in this thesis and elsewhere [8] even though the same target and growth conditions were used. Although we have grown waveguide lasers with thresholds as low as those previously reported (i.e $\sim$2 mW absorbed power) the waveguides used in section 9.4 were all grown towards the end of the target's useful lifespan, and so thresholds as low as this are not to be expected. We believe, however, that capping of films plays a more important role in films with high particulate densities.

It was mentioned earlier in this report that the mechanism for particulate production in these waveguides is not clear and it is this deterioration in the target that clouds the issue. The particulates observed on these films are exclusively round features that have clearly solidified from a previously molten droplet. They would appear to a product of 'splashing' as detailed in chapter 8, but it is thought that high density dielectrics should not suffer from splashing [10] and there is no reason why this effect should be exacerbated over time. Exfoliation of the target is a mechanism by which dielectrics do produce particulates, but the particulates in this case have characteristic angular shaped fragments which are rarely observed in these experiments. Brief resurfacing of the target did not produce any noticeable effects in particulate production but this may be due to resurfacing for an insufficient time for the hardness of the target. Two mechanisms have been hypothesised for the increased production of particulates over time; increased degradation of the target composition due to

repeated ablation leading to increased splashing or, increased exfoliation due to surface quality deterioration, and subsequent melting of the characteristic particulates. More rigorous investigation into this phenomenon would have to be undertaken before either of these hypotheses could be confirmed.

9.3 Method of growing capped layers

We have utilised the geometry of the target holder/rotator as described in section 6.2.1 to construct a very simple system for growing capped layers *in situ*.

The target holder for the cylindrical Nd:GGG target is rotated on a threaded spindle. This allows the target to travel backwards and forwards during deposition permitting a greater surface area of the target to be used. By adhering a YAG target of similar dimensions on the end of the Nd:GGG rod we can now select our target by turning the spindle until the desired material is the target of the ablation laser. This is depicted in figure 9.1.

A Nd:GGG layer is first grown as described previously. The vacuum chamber is evacuated and back filled with oxygen to a pressure of $\sim 5 \times 10^{-2}$ mbar. The substrate is then heated using the scanning CO_2 laser as described in section 6.3 up to a temperature of ~750°C . A deposition time of ~15 mins is required for a ~5μm film.

Once a Nd:GGG layer is deposited the laser is turned off. The chamber is held at the same pressure whilst the temperature of the substrate is elevated to ~1000°C . This temperature elevation is required for the growth of crystalline YAG [11]. Deposition at lower temperatures leads to the YAG depositing as a white powder-like layer that does not adhere well to the substrate surface.

The target is then rotated in one direction until the YAG component is in

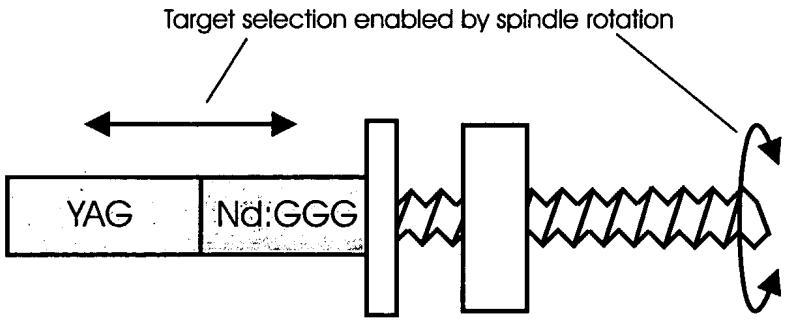

Figure 9.1: Details of target holder. Rotating the spindle causes the target to translate across the beam of the ablation laser radiation, allowing target selection during deposition.

line with the ablation laser radiation. Except for the substrate temperature the same laser ablation conditions are used for the deposition of the YAG on the Nd:GGG layer. The deposition rate for YAG is slower than for Nd:GGG, 15 mins are required for a 2-3μm layer.

After growth the sample must be cooled down over ~20 minutes to avoid 'micro-cracking'. This effect can just be seen in figure 9.2. Under high magnification (× 100) a fine network of cracks appear on the surface of the film. It is believed this fracturing of the film occurs due to the thermal stresses imposed on the film under rapid cooling. This cool down time appears to be only necessary for YAG crystal growth and not for Nd:GGG.

With the above technique both the capping layer and the active layer can be grown whilst under vacuum, ensuring very little contamination between the layers and hence good adhesion.

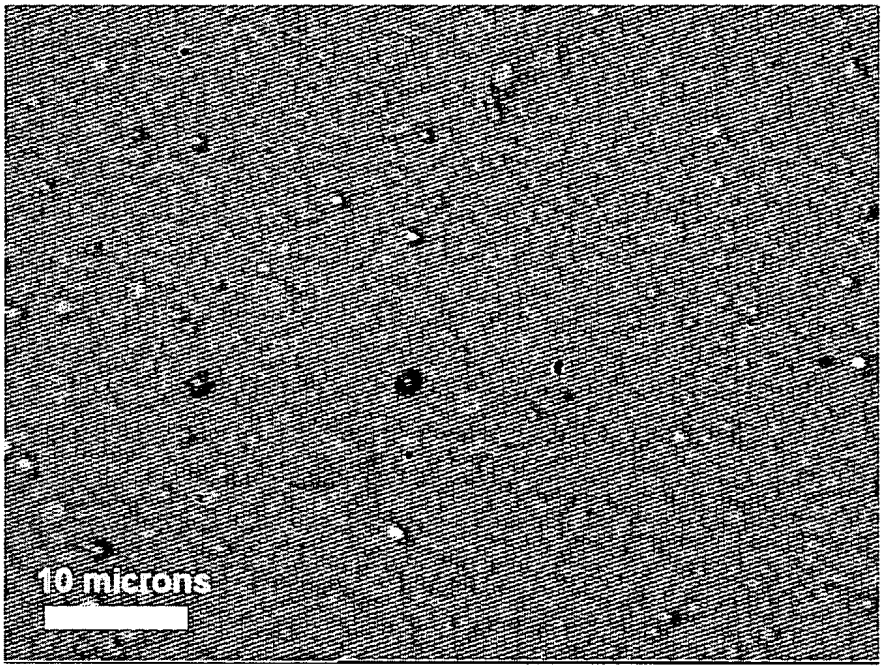

Figure 9.2: Optical Microscopy image of the cracked surface due to fast cooling.

9.4 Results of Nd:GGG layers capped with YAG

Figure 9.3 shows the XRD spectra for the YAG capped Nd:GGG film.

Comparison of this with figure 8.3 shows that there is no peak present corresponding to the YAG (400) plane. A large peak is seen in the the YAG (321) plane and other smaller peaks can be just observed overlapped with the YAG (321) and the Nd:GGG (400) peak. XRD spectra of similar samples have shown peaks from different YAG planes. It is clear that neither epitaxial nor textured growth of YAG has been achieved in these films. This is possibly due to the particular orientation of the Nd:GGG sub-layer or insufficient heating during deposition. As YAG is not the laser host, however, it is not believed to be essential to obtain single crystal growth. It is recognised, though, that a single crystal layer would produce less scattering due to an absence of grain boundaries.

The film grown is a 4μm Nd:GGG layer with a 2μm YAG capping layer.

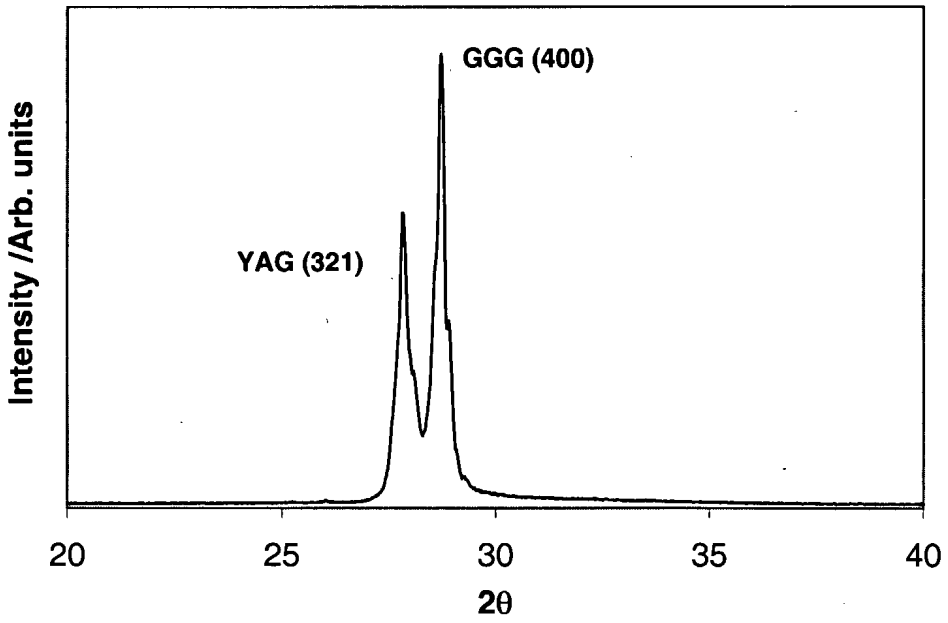

Figure 9.3: XRD of Nd:GGG film capped with YAG.

This can, therefore, be compared to the 4μm thick Nd:GGG films we have grown previously.

As with the previous devices the waveguide was end polished flat to an optical quality and its lasing threshold measured by the method described in section 8.3.

The particulate density of the capped layer is higher than that of the other 4μm unclad waveguides. The particulate density in the buried waveguide is $\sim 1.5 \times 10^7$ cm^{-2}. A film with such a high particulate density had been made in a 4μm unclad structure but did not lase at the incident laser pump powers available (~700mw @ 808nm). Figure 9.4 shows the results for the threshold of the buried waveguide laser compared to that of the uncapped layers.

The buried laser had a lasing threshold of 14.8 mW of absorbed power. For comparison laser action in an uncapped layer with a particulate density 4 times lower was observed at 19mW absorbed power.

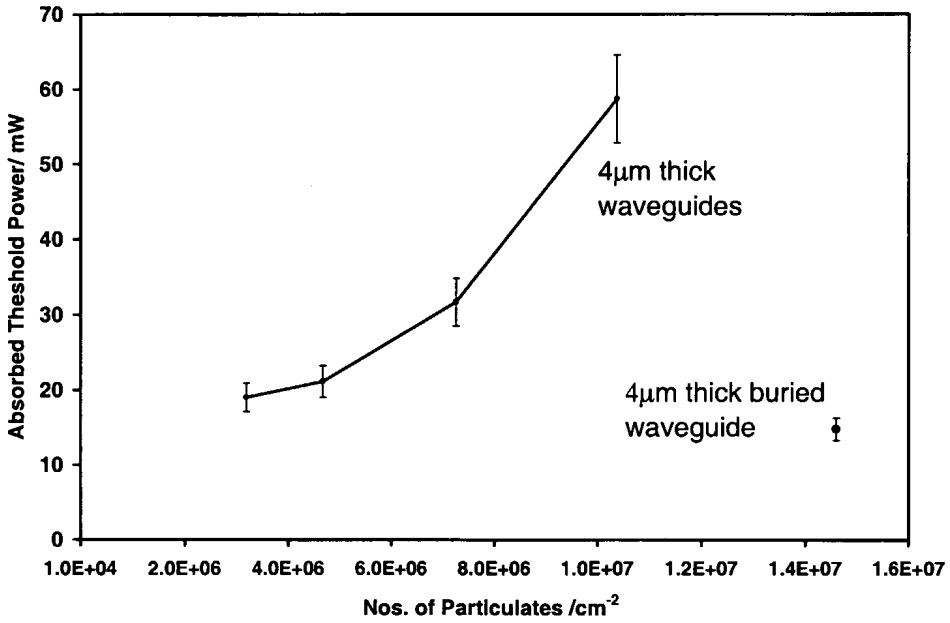

Figure 9.4: XRD of Nd:GGG film capped with YAG.

It could be argued that the increase in the number of particulates of the capped layer is largely due to the YAG capping layer and thus the real number of particulates on the film should be measured before the YAG layer is grown. It is not however possible to measure the particulate density without removing the sample from the vacuum chamber. Nor is it possible to gauge the number density from a film grown in similar conditions but without the YAG overlayer due to the large (upto ~1 order of magnitude), apparently random, fluctuation in particulate density from one film to the next.

We have, however, grown YAG films straight onto YAG substrates and measured the particulate density. Due to the YAG target being relatively unused compared to the Nd:GGG target, the particulate density is 2 orders of magnitude lower than for the Nd:GGG films. Particulate densities for the YAG layer are of order 10^4 cm^{-2}. This shows the increase in particulate density due to the YAG layer is negligible compared to the high (10^6 - 10^7 cm^{-2}) densities seen in the Nd:GGG Layer.

9.5 Conclusions

We have shown that the capping of a Nd:GGG waveguide *in situ* can greatly decrease the lasing threshold of the device when compared to a similar uncapped device. This implies that the capping of the Nd:GGG layer reduces the waveguide losses in the device. It must be noted that the most probable cause of loss within the guide is due to surface scattering from the particulates. Therefore it follows that although the capping layer appears to be of great benefit to these low quality films, should a higher quality film be grown (with particulate densities down to 10^3 - 10^4 cm^{-2} as is possible from an unused single crystal target) then the capping layer will be of less benefit.

9.6 References

[1] C.L. Bonner, A.A. Anderson, R.W. Eason, D.P. Shepherd, D.S. Gill, C. Grivas, and N. Vainos. Performance of a low-loss pulsed-laser deposited Nd:$Gd_3Ga_5O_{12}$ waveguide laser at 1.06 and 0.94μm . *Optics Letters*, 22(13):988–990, 1997.

[2] A.A. Anderson, R.W. Eason, L.M.B. Hickey, M. Jelinek, C. Grivas, D.S. Gill, and N.A. Vainos. Ti:sapphire planar waveguide laser grown by pulsed laser deposition. *Optics Letters*, 22(20):1556–1558, 1997.

[3] P. R. Willmott, P. Manoravi, and K. Holliday. Production and characterization of Nd,Cr : GSGG thin films on Si(001) grown by pulsed laser ablation. *Applied Physics A-Materials Science & Processing*, 70(4):425–429, 2000.

[4] R. Chety, E. Millon, A. Boudrioua, J. C. Loulergue, A. Dahoun, and J. Perriere. Growth of $Ca_4GdO(BO_3)_3$ thin films by pulsed-laser deposition for nonlinear optical applications. *Journal of Materials Chemistry*, 11(2):657–659, 2001.

[5] S Fukaya, K Adachi, M Obara, and H Kumagai. The growth of Cr^{4+}:YAG and Cr^{4+}:GGG thin films by pulsed laser deposition. *Optics Communications*, 187:373–377, 2001.

[6] J. T. Cheung and J. Madden. Growth of HgCdTe epilayers with any predesigned compositional profile by laser molecular-beam epitaxy. *Journal of Vacuum Science & Technology B*, 5(3):705–708, 1987.

[7] X. L. Guo, Z. G. Liu, S. N. Zhu, T. Yu, S. B. Xiong, and W. S. Hu. Pulsed laser deposition of c-oriented $LiNbO_3$ /$LiTaO_3$ optical waveguiding bilayered films on silicon wafers. *Journal of Crystal Growth*, 165(1-2):187–190, 1996.

[8] A.A. Anderson, C.L. Bonner, D.P. Shepherd, R.W. Eason, C. Grivas, D.S. Gill, and N. Vainos. Low loss (0.5 db/cm) Nd:$Gd_3Ga_5O_{12}$ waveguide layers grown by pulsed laser deposition. *Optics Communications*, 144(4-6):183–186, 1997.

[9] H. Kumagai, K. Adachi, M. Ezaki, K. Toyoda, and M. Obara. Epitaxial growth of Nd:YAG thin films by pulsed laser deposition. *Applied Surface Science*, 110:528–532, 1997.

[10] J. T. Cheung. History and fundamentals of pulsed laser deposition. In D. B. Chrisey and G. K. Hubler, editors, *Pulsed laser deposition of thin films*, pages 1–22. John Wiley and Sons, New York, 1994.

[11] N.A. Vainos, C. Grivas, C. Fotakis, R.W. Eason, A.A. Anderson, D.S. Gill, D.P. Shepherd, M. Jelinek, J. Lancok, and J. Sonsky. Planar laser waveguides of Ti : sapphire, Nd : GGG and Nd : YAG grown by pulsed laser deposition. *Applied Surface Science*, 129:514–519, 1998.

Chapter 10

Conclusions and future work

10.1 Introduction

This chapter presents a summary of work that has has been described within this thesis. It also suggests possible further work that would logically follow on from the work presented here. This thesis is intended to be a comprehensive study of using PLD to fabricate planer waveguide devices and has focussed largely on the effect that particulates generated by PLD have on the waveguide devices.

10.2 Conclusions of the introductory Chapters

A thorough review of the recent activities in the field of active optical waveguides fabricated by PLD was presented. This shows that PLD is capable of living up to its expectation of being able to fabricate materials in thin film form that cannot presently be fabricated by other processes. Of interest is the finding that nearly all of the reviewed work of active optical devices grown by PLD are thin $\lesssim 2\mu m$ devices and efficient lasing action in these reports has not been demonstrated. The two exceptions to this are the only two reports of thick film active optical waveguides [1, 2] where

efficient lasing is reported in both. This finding is important as it lends weight to the conclusions drawn in chapter 8.

10.3 Conclusions from Chapter 5

This represents the first report of growth of photosensitive lead germanate glass by PLD. It is also of special interest as the material is capable of exhibiting both positive and negative refractive index changes. The maximum index difference observed in this system was also the highest reported for a germanium based glass at -1.06 $\times$ 10^{-2} .

10.3.1 Future work

Lead germanate targets also have been fabricated, in house, with both Nd and Ce dopants. With Nd dopants it would be clearly possible to fabricate a Nd:lead germanate waveguide laser as lead germanate possesses many attractive properties of a glass laser host. Initially it is our intention to attempt to fabricate lead germanate films with a less discontinuous surface. Alternatively, methods of reflowing the film without compromising the photosensitivity could be investigated. The Ce dopant is believed to enhance photosensitivity in lead germanate and this would be another avenue of further work to explore.

Using lead germanate as a capping layer is a possible route of further work as described below.

10.4 Conclusions from Chapter 6

A versatile technique has been developed to efficiently and homogeneously heat substrates using a raster scanned CO_2 laser. This device has been

successfully utilised throughout the course of work presented in this thesis and so has also proven its practicality. The turn around time for depositions of crystalline films has been greatly reduced through two main factors: 1) Homogenous heating enables substrate temperatures to be elevated rapidly without substrate fracture occurring. 2) Efficient heating also prevents the chamber reaching temperatures too hot to touch, thus requiring a lengthly wait between depositions.

10.4.1 Future work

More intelligent and faster methods of raster scanning may help to to minimise cycle time. This would enable a greater resolution of heated points on the substrate and could in principle enable much higher levels of homogeneity in heating should this be required.

As mentioned earlier, efficient heating of rotating or moving substrates could be possible with this technique allowing deposition of a more uniform thickness profile when growing crystalline films.

For growth of Ti:sapphire (for example) the dopant concentration in the film is dependent on the temperature of the film during fabrication [3,4]. This heating technique could allow fabrication of a graded dopant level along the waveguide width, allowing rapid characterisation of optimal dopant levels.

10.5 Conclusions from Chapter 7

A generalised model for a five layer asymmetric waveguide was presented in chapter 7. This model was first derived by Bonner [5], but this is the first time that it has been numerically evaluated. The model has helped show how the spatial mode profile changes with waveguide geometry. It also demonstrates how the proportion of the spatial mode that interacts with

the waveguide surface, changes with waveguide thickness.

10.6 Conclusions from Chapter 8

Conclusions drawn from this chapter are: 1) The effect of particulates is detrimental to the lasing threshold of waveguide lasers and the threshold is seen to increase as particulate density increases. 2) This detrimental effect becomes less pronounced in thicker (~8μm) films.

10.6.1 Future work

Work is currently being undertaken to fabricate thick multilayer (up to five layer) waveguide lasers. The performance of these devices will be tested at thicknesses up to ~100μm . The high numerical aperture and high damage threshold of these devices perfectly suit the requirements for high power laser diode pumping by proximity coupling [5].

10.7 Conclusions from Chapter 9

It has been demonstrated that PLD is well suited to growing multilayer active optical waveguide devices. A buried Nd:GGG waveguide laser has been fabricated for the first time by PLD and lasing action was achieved at a threshold of 14.8 mW of absorbed pump power.

Comparison of the lasing threshold to that of similar uncapped devices demonstrates that the capped layer has a highly beneficial effect on the lasing threshold when the particulate density in the film is high.

10.7.1 Future work

As mentioned above, growth of thick, multilayer waveguide lasers is currently being investigated for high power devices.

It is also hoped that lead germanate, as grown in chapter 5, can be used as a thin *overlayer* on a waveguide laser. In recent work presented by Pissadakis [6] it has been shown that writing a relief grating in photosensitive overlayers will also effect the excited mode in the active layer and act as a Bragg reflector. Bragg reflectors in a waveguide lasers structure would be beneficial for two reasons. It would enable production of very narrow linewidth lasers and it would also remove the necessity to glue or deposit mirrors onto the end face of the waveguide. This would also eliminate the stringent requirement for parallelism between the two end faces that currently exists.

Fabrication of such a device could take two routes. Deposition of lead germanate onto a higher index guide like Nd:GGG would maintain confinement of the mode and so would require strong index (relief) gratings. Fortunately these gratings have been observed in lead germanate under UV exposure as shown in chapter 5. The other route is to deposit onto a lower index guide like Ti:sapphire. The higher index superstrate means the mode interacts more strongly with the lead germanate layer (due to the layer being thin, however, mode confinement is still maintained). Therefore a relief grating may not be necessary and a Bragg grating could be sufficient to reflect the waveguide mode. The disadvantage of the latter of these two methods is that interaction with the lossy lead germanate layers may cause unacceptable losses in the guide.

However, this is not a trivial project to undertake however and functioning waveguide devices by this route are not to be expected imminently.

10.8 References

[1] C.L. Bonner, A.A. Anderson, R.W. Eason, D.P. Shepherd, D.S. Gill, C. Grivas, and N. Vainos. Performance of a low-loss pulsed-laser deposited Nd:$Gd_3Ga_5O_{12}$ waveguide laser at 1.06 and 0.94μm . *Optics Letters*, 22(13):988–990, 1997.

[2] A.A. Anderson, R.W. Eason, L.M.B. Hickey, M. Jelinek, C. Grivas, D.S. Gill, and N.A. Vainos. Ti:sapphire planar waveguide laser grown by pulsed laser deposition. *Optics Letters*, 22(20):1556–1558, 1997.

[3] L. M. B. Hickey and J. S. Wilkinson. Titanium diffused waveguides in sapphire. *Electronics Letters*, 32(24):2238–2239, 1996.

[4] A.A. Anderson, R.W. Eason, M. Jelinek, C. Grivas, D. Lane, K. Rogers, L.M.B. Hickey, and C. Fotakis. Growth of Ti:sapphire single crystal thin films by pulsed laser deposition. *Thin Solid Films*, 300(1-2):68–71, 1997.

[5] C. L. Bonner, T. Bhutta, D. P. Shepherd, and A. C. Tropper. Double-clad structures and proximity coupling for diode-bar- pumped planar waveguide lasers. *IEEE Journal of Quantum Electronics*, 36(2):236–242, 2000.

[6] S. Pissadakis, L. Reekie, M. N. Zervas, J. S. Wilkinson, and G. Kiriakidis. Gratings in indium oxide film overlayers on ion-exchanged waveguides by excimer laser micromachining. *Applied Physics Letters*, 78(6):694–696, 2001.

Appendix A

Publications

List of journal and conference proceeding publications arisen from this work.

S Mailis, C Riziotis, J Wang, E.R. Taylor, A. Anderson, S.J. Barrington, and R.W Eason. Photosensitive lead germanate glass waveguides grown by pulsed laser deposition. In *CLEO Europe 98*, page CWF51, Glasgow, Scotland, 1998.

S.J. Barrington, S. Mailis, A.A. Anderson, W.S. Brocklesby, R. Greef, H.N. Rutt, and R.W. Eason. UV induced refractive index changes in lead germanate glass waveguides grown by pulsed laser deposition. In *Photosensitivity in Optical Waveguides and Glasses*, Lake Lucerne, Switzerland, 1998.

S. Mailis, C. Riziotis, J. Wang, E. Taylor, A.A. Anderson, S.J. Barrington, H.N. Rutt, R.W. Eason, N.A. Vainos, and C. Grivas. Growth and characterization of pulsed laser deposited lead germanate glass optical waveguides. *IOP meeting on Laser ablation*,The Institue of Physics, London ,1998.

S. Mailis, A.A. Anderson, S.J. Barrington, W.S. Brocklesby, R. Greef, H.N. Rutt, and R.W. Eason. Photosensitivity of lead germanate glass waveguides grown by pulsed laser deposition. *Optics Letters*, 23(22):1751–1753, 1998.

S. Mailis, L. Reekie, S. Pissadakis, S. J. Barrington, R. W. Eason, N. A. Vainos, and C. Grivas. Large photoinduced refractive index changes in pulsed-laser- deposited lead germanate glass waveguides with controllable refractive index sign change. In *5th International Conference on Laser Ablation COLA'99, ,* Goettingen, Germany, 1999.

S. Mailis, C. Riziotis, J. Wang, E. Taylor, A.A. Anderson, S.J. Barrington, H.N. Rutt, R.W. Eason, N.A. Vainos, and C. Grivas. Growth and characterization of pulsed laser deposited lead germanate glass optical waveguides. *Optical Materials*, 12(1):27–33, 1999.

S. Mailis, L. Reekie, S. Pissadakis, S. J. Barrington, R. W. Eason, N. A. Vainos, and C. Grivas. Large photoinduced refractive index changes in pulsed-laser- deposited lead germanate glass waveguides with controllable refractive index sign change. *Applied Physics a-Materials Science & Processing*, 69:S671–S674, 1999.

S.J. Barrington, T. Bhutta, D.P. Shepherd, and R.W. Eason. The effect of particulate density on performance of Nd : $Gd_3 3Ga_5O_{12}$ waveguide lasers grown by pulsed laser deposition. *Optics Communications*, 185(1-3):145–152, 2000.

S. J. Barrington and R. W. Eason. Homogeneous substrate heating using a co2 laser with feedback, rastering, and temperature monitoring. *Review of Scientific Instruments*, 71(11):4223–4225, 2000.

S. J. Barrington and R. W. Eason. The effect of particulate density on performance of waveguide lasers grown by pulsed laser deposition. In *CLEO 2000*, CWK36, San Francisco, 2000.

S. J. Barrington and R. W. Eason. Buried nd:gadolinium gallium garnet waveguide lasers grownby pulsed laser deposition. In *CLEO/Europe-EQEC*, To be published, Munich , Germany, 2001.